DONOR-ANION INTERACTIONS IN QUARTER-FILLED LOW-DIMENSIONAL ORGANIC CONDUCTORS

Jean-Paul Pouget

Laboratoire de Physique des Solides, Université Paris-Sud, CNRS UMR 8502, 91405 Orsay, France

ORCID: 0000-0002-6244-389X

Pere Alemany

Departament de Ciència de Materials i Química Física and Institut de Química Teórica i Computacional (IQTCUB), Universitat de Barcelona, Martí i Franquès 1, 08028 Barcelona, Spain

ORCID: 0000-0002-3139-6189

Enric Canadell

Institut de Ciència de Materials de Barcelona (ICMAB-CSIC), Campus de la UAB, 08193 Bellaterra, Spain

ORCID: 0000-0002-4663-5226

Abstract.

Anions have often been considered to act essentially as electron donors or acceptors in molecular conductors. However there is now growing evidence that they play an essential role in directing the structural and hence electronic properties of many of these systems. After reviewing the basic interactions and different ground states occurring in molecular conductors we consider in detail how anions influence the structure of the donor stacks and often guide them toward different types of transitions. Consideration of the Bechgaard and Fabre salts illustrates how anions play a crucial role in directing these salts through complex phase diagrams where different conducting and localized states are in competition. We also emphasize the important role of hydrogen bonding and conformational flexibility of donors related to BEDT-TTF and we discuss how anions have frequently a strong control of the electronic landscape of these materials. Charge ordering, metal to metal and metal to insulator transitions occurring in these salts are considered.

I. Introduction: the rich phase diagrams of D_2X quarter-filled molecular conductors

It has been commonly assumed that organic materials are good electrical insulators. This statement was, however, proven to be incorrect in 1954 when a metallic-type conductivity was observed when exposing perylene, a polycyclic aromatic hydrocarbon, to bromine.[1] About twenty years later, the unexpected discovery that the conductivity of semiconducting *trans*-polyacetylene could be raised by more than seven orders of magnitude when exposed to AsF_5 [2] revealed the key role of charge transfer to achieve a metallic state in organic systems. With the observation of the same effect through either electron or hole "doping" in other conjugated polymers such as poly(para-phenylene), polypyrrole and polyaniline, a completely new field of research with promising technological applications emerged. Presently, doped polymers have electrical conductivities approaching that of cooper. However, conducting polymers are poorly crystalline materials, exhibiting an inhomogeneous structural texture due to the flexibility of the polymeric chains and dopant position disorder, which prevent a precise control of the conduction process at a microscopic level.

Crucial steps towards the preparation of well crystallized highly conducting organic materials followed the synthesis in 1960 of the TCNQ (7,7,8,8-tetracyanoquinodimethane) [3] acceptor (A) and later, of the TTF (tetrathiafulvalene) donor (D) in 1970.[4] After the synthesis of the TCNQ molecule it was found that the association of this acceptor with quinoline (Qn) leads to the $Qn(TCNQ)_2$ salt with a sizeable metallic conductivity of 100 S/cm at room temperature (RT). [5] In this case, metallic carriers are obtained by the transfer of one electron from each Qn to two TCNQ molecules, resulting in an average of half an electron per acceptor. A few years later, in 1965, a similar RT conductivity was obtained in the NMP-TCNQ compound where NMP is N-methylphenazine, with a partial transfer of $\rho = 2/3$ electrons from the NMP donor to TCNQ. [6] Since in that case carriers are shared by both segregated A (TCNQ) and D (NMP) stacks, NMP-TCNQ can be considered as the first synthesized AD charge transfer salt. [7] After this, the association of TCNQ with TTF in 1972 opened a new route towards highly conducting charge transfer salts. [8-9] With a partial charge transfer of $\rho = 0.55$ electrons from the TTF donor to TCNQ, TTF-TCNQ exhibits not only a RT conductivity of 500 S/cm, significantly larger than those found for $Qn(TCNQ)_2$ and NMP-TCNQ, but also a metallic type behaviour on a larger temperature range than any of the previous salts, reaching a 10^4 S/cm conductivity around 50 K, just before suffering a drastic drop due to the occurrence of a Peierls metal-to-insulator transition. A common feature of all these A_2Y (where Y is a singly charged cation) or AD salts is their very anisotropic crystal structures where acceptors and/or donors form segregated stacks which facilitate a good overlap between the π type LUMOs (lowest unoccupied molecular orbital) of acceptor molecules and/or the HOMOs (highest occupied molecular orbital) of donor molecules along the direction of the stacks, leading to one-dimensional (1D) electronic properties, aspects that have been already reviewed. [10]

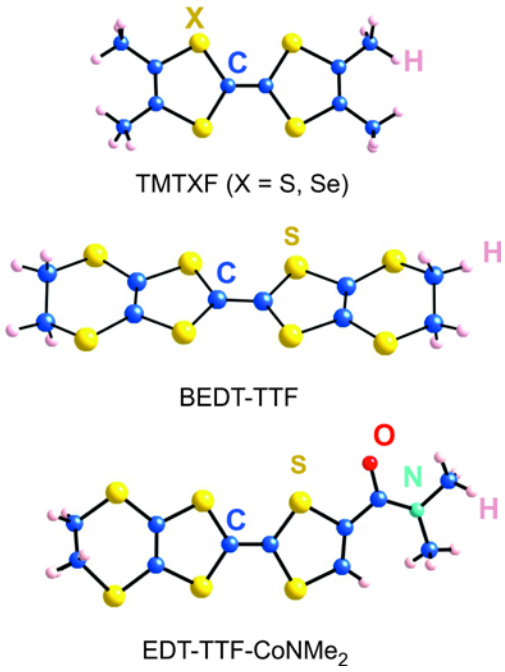

Figure 1. Some of the more commonly used donors in the preparation of molecular conductors discussed in this review: TMTTF/TMTSF, BEDT-TTF and EDT-TTFCONMe$_2$. EDT-TTF is a hybrid of TTF and BEDT-TTF.

The discovery of organic superconductivity at the beginning of the eighties in D_2X organic salts, where D is a TTF (or its Se analogue TSF) based donor and X a monovalent inorganic anion, boosted a whole new area of research. [11] With a transfer of an electron to the anion, D_2X salts are 1D or 2D metals where the carriers are holes located on the donor stacks or layers (on average one hole on every two donor molecules). The study of D_2X salts really started with the successive synthesis of two series of 1D conductors: the $(TMTTF)_2X$ series, now called Fabre salts [12] in 1977, and the isostructural series of Se analogues $(TMTSF)_2X$, now called Bechgaard salts, in 1980 [13] where TMTTF is tetramethyltetrathiafulvalene and TMTSF tetramethyltetraselenafulvalene (Fig. 1). Organic superconductivity was initially discovered in the Bechgaard salts with a critical temperature of T_S ~ 1 K in pressurized $(TMTSF)_2PF_6$ samples [11] and later with T_S ~ 1.4 K at ambient pressure in $(TMTSF)_2ClO_4$. [14] D_2X salts of the new BEDT-TTF (bis(ethylenedithio)tetrathiafulvalene – see Fig. 1) donor incorporating anions similar to those of the Bechgaard salts (ClO_4 and ReO_4) were prepared in 1982 [15] and superconductivity was observed in pressurized quasi-1D $(BEDT\text{-}TTF)_2ReO_4$ [16] with T_S ~ 2 K. In 1985 bulky linear anions such as I_3^- were used in the preparation of several families of $(BEDT\text{-}TTF)_2X$ salts which, due to the presence of donor layers, exhibited 2D (two-dimensional) metallic properties. Most of these salts were superconducting with T_S up to 8 K for slightly pressurized β-$(BEDT\text{-}TTF)_2I_3$.[17–18] At the end of the eighties, T_S values above 10 K were found at ambient pressure for several members of the κ polytype incorporating an insulating layer of polymeric chains built from the X = $Cu(SCN)_2$ [19-20] or $Cu[N(CN)_2]Br$ [21] anions sandwiched between two successive conducting BEDT-TTF layers. A review of these earlier studies can be found in ref. [22].

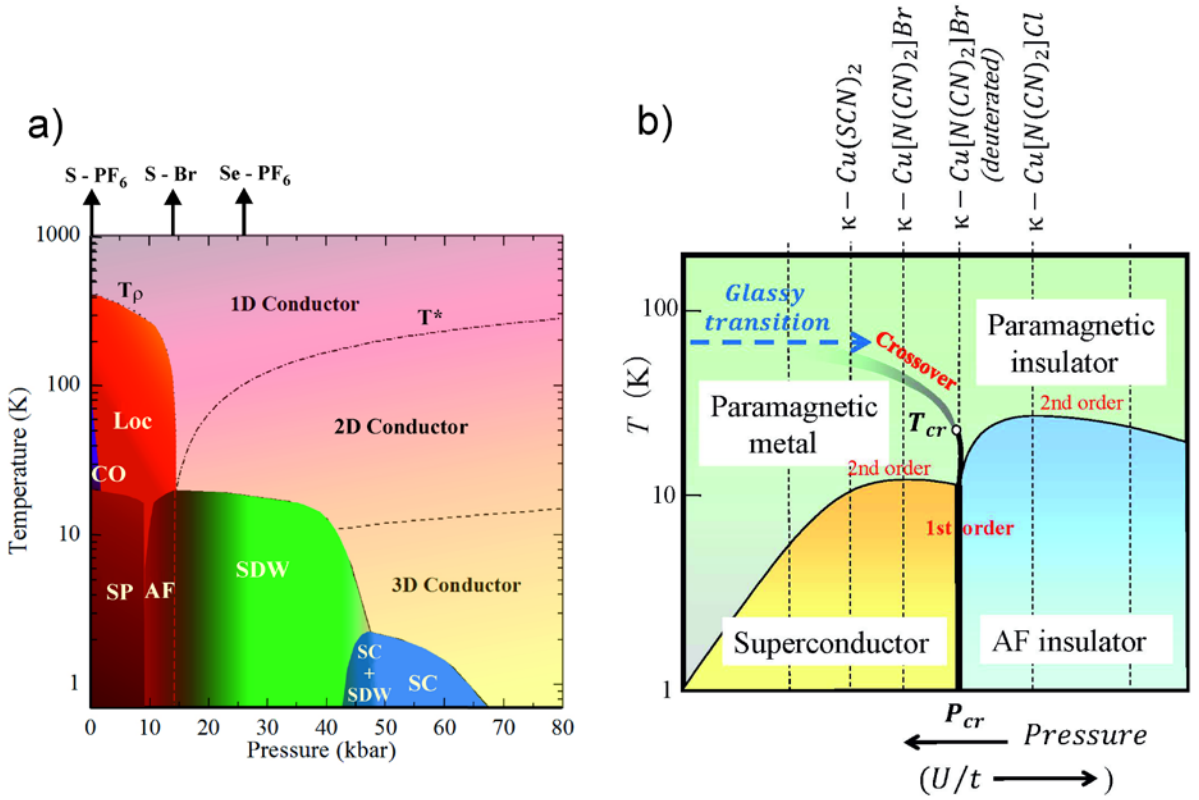

Figure 2. (a) (T-P) generalized phase diagram for Fabre (S-X) and Bechgaard (Se-X) salts where X is a centrosymmetrical anion. The pressure scale corresponds to $(TMTTF)_2PF_6$. Vertical arrows place $(TMTTF)_2Br$ and $(TMTSF)_2PF_6$ at atmospheric pressure in the phase diagram. CO, SP, AF, SDW and SC ground states introduced in the text are indicated. QCP is a quantum critical point between the SP and AF ground states. T_ρ indicates the onset temperature for charge localization as detected in the conductivity measurements of Fig. 3. T* is the crossover temperature from a 1D (in the stack direction, *a*) to a 2D (in the *ab* donor layer) delocalized electron gas. On the right scale there is also a crossover to a 3D delocalization regime along *c*, through the anion cavities, at lower temperature. (Adapted from a figure kindly provided by C. Pasquier) (b) (T, P) conceptual phase diagram of κ-$(BEDT\text{-}TTF)_2X$ salts (denoted κ-X) exhibiting a dimeric donor structure according to reference [23]. Vertical lines refer to various hydrogenated and deuterated (when indicated) salts at atmospheric pressure. The glass-like transition where the BEDT-TTF ethylene disorder freezes, according to reference [24], is indicated by the horizontal blue dashed line (Adapted from a figure kindly provided by H. Kanoda. Copyright 2004 by the American Chemical Society).

Metallic D_2X organic salts are not only interesting for their superconducting properties but also because of their complex temperature-pressure (T-P) phase diagrams exhibiting a large number of competing insulating ground states, where charge (hole) and/or spin (each hole bears a spin 1/2) degrees of freedom of the donor collectively order. [25] The phase diagram of D_2X salts changes also drastically with the chemical nature of both the donor and anion. An

important feature is that superconductivity emerges in close proximity to collective ground states where magnetic or charge degrees of freedom order. These collective states are spin- or charge-density wave (SDW or CDW) modulated structures for quasi-1D metals such as the Bechgaard or $(BEDT\text{-}TTF)_2ReO_4$ salts respectively. In the presence of strong Coulomb repulsions (see section II.B below), each hole becomes localized. There is a spin-charge decoupling and the ordering of the spin degrees of freedom occurs at low temperature, either into an antiferromagnetic (AF) ground state or, in presence of a sizeable magneto-elastic coupling, into a spin-Peierls (SP) ground state where the spins are paired via a stack dimerization (i.e. a dimerization of the stack of dimers in the case of the Fabre salts) into a magnetic singlet. Charge ordered (CO), AF and SP ground states are observed in Fabre salts as well as in some $(BEDT\text{-}TTF)_2X$ salts. The phase diagrams of two of the most studied series of 1D and 2D D_2X organic salts shown in Fig. 2 illustrate the richness of such phase diagrams.

The generalized temperature-pressure (T-P) phase diagram of the isostructural Fabre (S-X) and Bechgaard (Se-X) salts incorporating a centrosymmetrical anion X such as PF_6 or Br is shown in Fig. 2a. [26] Fabre salts with X= PF_6 or AsF_6, which are poor conductors at ambient pressure, exhibit a progressive charge localization (Loc. phase in Fig. 2a) of one hole per donor dimer (every dimer is built from two successive TMTTF in the stack direction, see section II.A) with the opening of a (half-) gap of charge, Δ_ρ (Δ_{BOW} in the inset of Fig. 3), below $T_\rho \sim 230$ K, when conductivity becomes thermally activated (see Fig. 3). T_ρ significantly decreases to ~100 K in the X = Br salt. In the PF_6 and AsF_6 salts a charge disproportion inside each dimer transforms the bond localized state (BOW charge modulation – see section II-C) into a CO/ferroelectric phase below $T_{CO} \approx 70$ and 100 K, respectively (see Fig. 3). This leads to an enhancement of the activation energy (or half-gap of charge) Δ_ρ of the conductivity (from Δ_{BOW} to Δ_{CO} in the inset of Fig. 3). At lower temperature the spin 1/2 of each localized hole orders either into an AF (S-Br salt) or SP (S-PF_6 and S-AsF_6 salts) commensurate structure.

Under application of a modest pressure the phase diagram is completely modified: the CO phase vanishes and then, the non-magnetic SP ground state transforms into a magnetic AF ground state (as for S-Br salt). At higher pressures the charge localization completely disappears and a metallic behavior is recovered. Then, the commensurate AF structure due to the exchange interaction between localized spins transforms into an incommensurate magnetic structure via a metal-insulator transition driven by the SDW instability of the quasi-1D metallic structure. The SDW ground state is observed in $(TMTSF)_2PF_6$ at ambient pressure (Se-PF_6 in Fig. 2a). In pressurized $(TMTSF)_2PF_6$, the insulating SDW ground state vanishes and, with the restoration of a metallic state down to low temperature, superconductivity (SC) is observed exhibiting the highest T_S value at the SDW phase boundary. Note also that superconductivity is observed at ambient pressure in the anion ordered (AO) phase of $(TMTSF)_2ClO_4$ (Fig. 4).

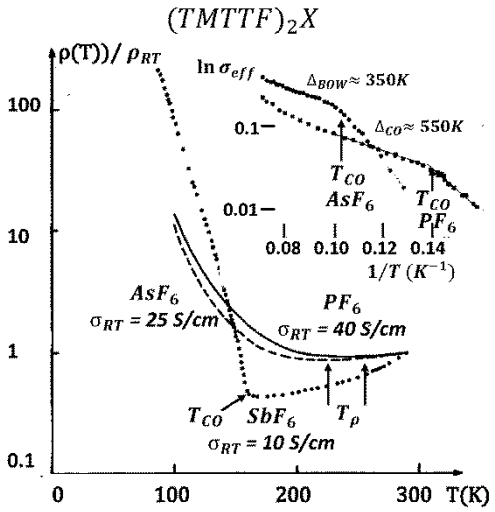

Figure 3. Thermal dependence of the normalized electrical resistivity of $(TMTTF)_2MF_6$ salts with M = P, As and Sb at ambient pressure (adapted from ref. [27] Copyright 1984 by EDP Sciences). The RT resistivity is indicated. The insert gives the thermal dependence of the half-gap of charge obtained from ESR measurements in the $4k_F$ BOW charge localisation regime, Δ_ρ^{BOW}, and in the CO phase, Δ_ρ^{CO}.[28] This figure defines also the critical temperatures T_ρ and T_{CO} of the phase diagram shown in Fig. 2a.

Fig. 2b is the conceptual (T, P) phase diagram for the κ-$(BEDT\text{-}TTF)_2X$ salts incorporating polymeric anionic chains, according to Kanoda. [29] As κ-phases are characterized by the formation of layers of BEDT-TTF dimmers (Fig. 7) where strong Coulomb repulsions (see section II.b), tend to localize one hole on each dimer. A crude description of the phase diagram is obtained assuming that each dimer is equivalent to a single site occupied by one hole. In this framework when the Coulomb repulsion increases, a metal to insulator Mott-Hubbard transition occurs between a strongly correlated paramagnetic metal and a Mott paramagnetic insulator. These two phases are separated by a first order transition line which ends in a critical point (T_{cr}, P_{cr}) above which one proceeds continuously from a bad (i.e. strongly correlated) metal to the Mott insulator through a crossover line. In the Mott insulating phase, achieved in κ-$(BEDT\text{-}TTF)_2X$ for X = $Cu[N(CN)_2]Cl$ (i.e. κ-Cl), there is charge localization of one hole per dimer and at T_N = 25 K the spin ½ of the hole localized in each dimer orders into an AF way. The correlated metallic state is observed for the X = $Cu[N(CN)_2]Br$ and $Cu(NCS)_2$ salts which also become superconducting above 10 K at ambient pressure. The fully deuterated κ-$(BEDT\text{-}TTF)_2Cu[N(CN)_2]Br$ salt is just located in the critical region. The phase boundaries sketched in Fig. 2b have been more accurately determined using κ-$(BEDT\text{-}TTF)_2Cu[N(CN)_2]Cl_xBr_{1-x}$ alloys, deuterated salts and through application of modest pressures (κ-$(BEDT\text{-}TTF)_2Cu[N(CN)_2]Cl$ becomes a superconductor under 300 bars). [24]

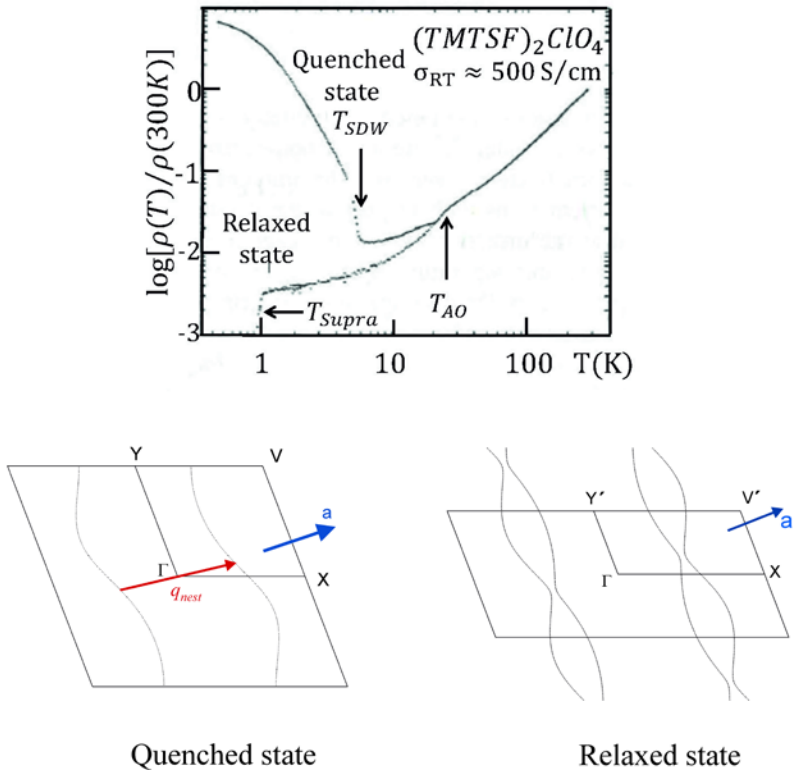

Figure 4. (Upper part) Normalized longitudinal resistivity of $(TMTSF)_2ClO_4$ for quenched and relaxed samples at ambient pressure (adapted from ref. [25] Copyright 1998 by Springer Nature). Relaxed samples exhibits superconductivity at $T_S \approx 1K$ while the quenched ones lead to an SDW insulating ground state at $T_{SDW} \approx 6K$. Note the slope anomaly at the $T_{AO} = 24$ K transition. (Bottom part) Two sheets and one sheet Fermi surfaces of relaxed and quenched $(TMTSF)_2ClO_4$ respectively, according to ref. [30] (Copyright 2014 by the American Physical Society). In quenched samples the SDW ground state is stabilized by the nesting through q_{nest} of one sheet of the Fermi surface into the other, as indicated.

The parameter controlling the phase diagram of a Mott-Hubbard metal-insulator phase transition is *U*/*t*, where *U* is the effective intra-dimer Coulomb repulsion and *t* the inter-dimer transfer integral. For the κ-$(BEDT\text{-}TTF)_2X$ series it is assumed that *t* increases under pressure or by replacing Cl by the bulkier Br atom in the polymeric anionic chains controls the phase diagram. However recent studies of κ-$(BEDT\text{-}TTF)_2Cu[N(CN)_2]Cl$ show that the (T, P) phase diagram is also controlled by lattice effects [31]. Lattice plays a crucial role in the Mott-Hubbard transition since there is a considerably extended range of "critical elasticity" around the critical endpoint (T_{cr}, P_{cr}), where the lattice goes soft. As a result of the long-range shear forces of the lattice, the universal behavior of the transition changes from Ising-type (for a pure electronic system) to a mean-field one for an electronic system coupled to a compressible lattice. Also a fine tuning of the κ-$(BEDT\text{-}TTF)_2X$ phase diagram is achieved by the cooling rate through the ~70 K glass transition (shown in Fig. 2b) which changes the

amount of static disorder between ethylene group conformations of BEDT-TTF (see section V.A.2) [32-33]

In addition, recent studies show also that the physics is not so simple and that one has to go beyond the single-site Mott description to understand the physical properties of κ-(BEDT-TTF)$_2$X. Firstly the occurrence of a structural transition at ≈200K in both hydrogenated and deuterated κ-(BEDT-TTF)$_2$Cu[N(CN)$_2$]Br [34] induces an incommensurate modulation of electronic density, [35] which renders the dimers non-equivalent at low temperature. Secondly, from the observation of a mutiferroicity phenomenon in κ-(BEDT-TTF)$_2$ Cu[N(CN)$_2$]Cl around T_N [36], and the recent report of a ferroelectric instability around 10K in some samples [37], it appears that charges are not frozen at low temperature, in contradiction with the use of a localized Mott-Hubbard phase diagram.

The phase diagrams in Fig. 2 could endorse the idea that organic superconductivity arises in close proximity of magnetically modulated phases. This is, however, not true when one considers the phase diagram of other superconducting (BEDT-TTF)$_2$X salts. Indeed superconductivity is close to charge modulated phases such as a Peierls insulator in (BEDT-TTF)$_2$ReO$_4$, [38-39] a CDW order in the α-(BEDT-TTF)$_2$MHg(SCN)$_4$ series where M = NH$_4$, K, Rb, or even a CO ground state in α-(BEDT-TTF)$_2$I$_3$ and the θ-(BEDT-TTF)$_2$X series (α and θ phases are explicitly considered in section V).

Phase diagrams such as those of Fig. 2 show that temperature and hydrostatic pressure and the nature of the anion and polymeric chains exert a fine tuning on the nature of the ground state. Since organics are quite soft materials, lattice parameters, especially those in the stacking direction, are sizeably modified under pressure and thermal contraction [40]. In this framework can be viewed as exerting an internal pressure. Thus, it is generally understood that pressure and anion size should simply modify the interatomic distances which control the electronic interactions (see sect. II). Lattice parameters are also sensitive to deuteration of the donor [40].

In fact, the situation is somewhat more delicate when there are chemical species presenting some internal structural degrees of freedom. This is particularly the case for anions and methyl/ethylene groups of the donors, as illustrated by the following examples:

- For non-centrosymmetrical anions such as X = ReO$_4$ and ClO$_4$, the “generalized” phase diagram of the Bechgaard salts (Fig. 2a) is completely modified. The reason is that anions which exhibit orientation disorder at RT should order for entropy reasons upon cooling. This is achieved via the stabilization of various superstructures below T_{AO} (177 K and 24 K for (TMTSF)$_2$ReO$_4$ and ClO$_4$ respectively), which drastically change the electronic structure (see section III.C). Also, the nature of the ground state of (TMTSF)$_2$ClO$_4$ depends upon the cooling rate across its AO transition. Figure 4 shows that superconductivity at T_S ~ 1K is obtained in relaxed samples while quenched samples, where a complete AO cannot be achieved, exhibit a SDW ground state below ~6 K as for Se-PF$_6$ at ambient pressure.
- Change of the conformational order of the ethylene groups of the BEDT-TTF together with the associated kinetics, control the electronic phase diagram of (BEDT-TTF)$_2$X

salts. This is well illustrated in β-(BEDT-TTF)$_2$I$_3$ where different superconducting phases (with T_S=1.5 K or 8 K) can be reached by varying the (T, P) cooling path through the ethylene group modulated phase diagram (see section V.A.3). [49-50]

Sensitivity of the phase diagram to deuteration (see for example Fig. 2b) points out the influence of the hydrogen bond network located at the interface between the donor and anion layers. In addition, most D_2X salts exhibit a significant dielectric charge response which, for some of them, leads to electronic ferroelectricity.[51] However since anions are charged entities, the 3D dielectric response, even if it has a primarily 1D or 2D electronic origin, should be controlled by the ionic response of the anion sublattice and various types of anion and H-bond disorders. Also CO transitions (i.e. T_{CO} for the Fabre salts [27]) seen to be controlled by the nature of the anions and its coupling with donors; such a coupling allowing to stabilize the 3D CO ground state.

Here we review structural aspects which control the stabilization of various electronic states in D_2X organics. We pay a special attention to structural degrees of freedom such as those of anions and donor side groups which modulate the electronic interactions and whose interaction with the π hole donor's HOMO, already considered long time ago [52], has not been fully analysed until recently. In this respect our review completes recent monographs on D_2X quarter-filled organic metals. [24-25,53-56].

We describe basic interactions occurring in molecular metals in section II. In section III we consider the archetypal D_2X 1D conductors: the Bechgaard and Fabre salts. In section IV we analyze the interplay of structural degrees of freedom with localized charges in the CO superstructure of δ-(EDT-TTF-CONMe$_2$)$_2$Br and show the crucial role of hydrogen bonding in CO transitions. In section V we consider at some length the role of ethylene groups in structural and electronic instabilities exhibited by several (BEDT-TTF)$_2$X salts. Finally in section VI we conclude the review by emphasizing the importance of donor-anion interactions for the chemical and physical properties of molecular conductors.

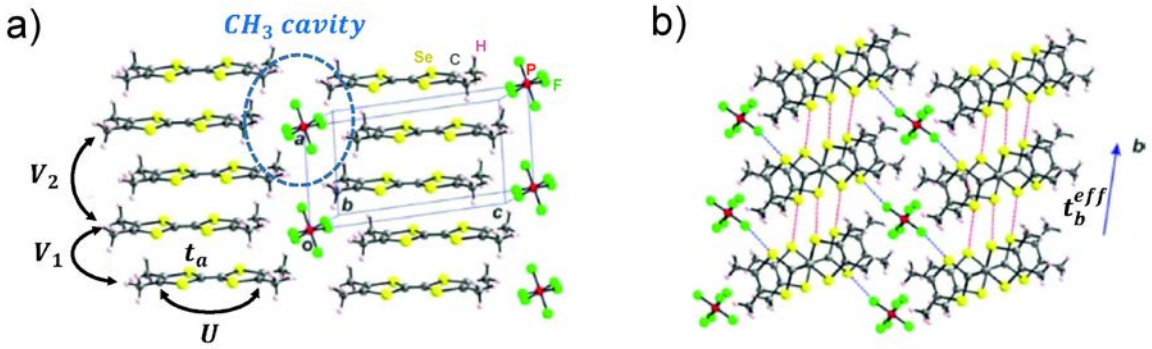

Figure 5. Crystal structure of the (TMTSF)$_2$PF$_6$ Bechgaard salt. (a) Quasi-planar organic molecules form stacks along the *a* axis that are separated by PF_6 anions occupying methyl cavities formed between neighboring stacks along the *c** direction. (b) Projection of the structure along the stack direction. $Se_{donor}\cdots Se_{donor}$ inter-stack donor interactions are shown as red dashed lines and short $Se_{donor}\cdots F_{anion}$ donor-anion interactions as blue dashed lines. The different interdonor electronic interactions defined in Hamiltonian (1) are indicated.

II. Relevant aspects of D_2X molecular metals

A. Anisotropic crystal structure. The crystal structures of two prototypical molecular metals, the Bechgaard salt $(TMTSF)_2X$ with the centrosymmetric anion X = PF_6 and α-$(BEDT\text{-}TTF)_2X$ with X = $KHg(SCN)_4$ are shown in Figs. 5 and 6, respectively. In $(TMTSF)_2X$ and $(TMTFF)_2X$, donors form slightly dimerized zig-zag stacks running along the *a* direction that pack into layers along the *b*-direction (or *b'*- the direction perpendicular to *a*). Anions are located in centrosymmetrical cavities delimited by methyl groups of the neighboring donors along the *c**-direction (i.e. the perpendicular to the (*a*,*b*) donor layers) The room temperature (RT) crystal space group of all these salts is $P\bar{1}$ [57-58], impliying that non-centrosymmetric anions must be disordered in their cavity in order to restore, on average, an inversion center. These salts are quasi-1D metals with the strongest electronic coupling along *a* (t_a), the direction of the stacks. The anisotropy of resistivity (ρ_a: $\rho_{b'}$: ρ_{c^*} ~ 1:10^2:10^5; see Fig. 19b below) follows the structural anisotropy. Note that the coupling along the inter-stack *b*-direction (t_b^{eff}) is stronger for the Bechgaard than the Fabre salts because of the closest $Se_{donor}\cdots Se_{donor}$ distances (shown in Fig. 5) are smaller than the sum of the van der Waals radii, while the corresponding $S_{donor}\cdots S_{donor}$ distances in the Fabre salts are not.

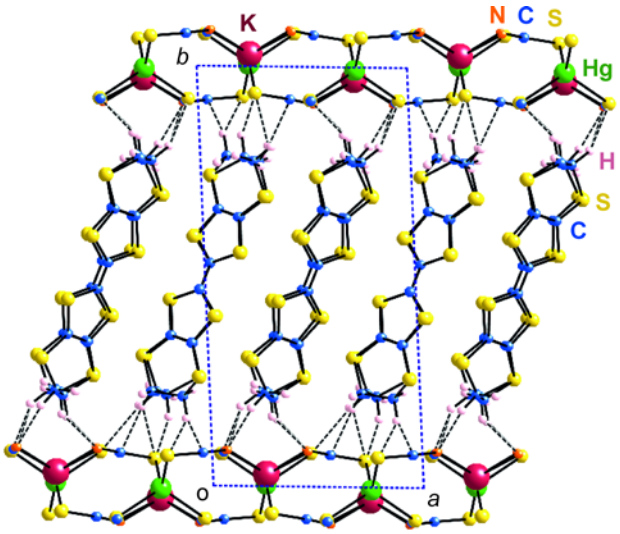

Figure 6. Projection of the crystal structure of α-$(BEDT\text{-}TTF)_2KHg(SCN)_4$ along the *c* direction showing the alternation of donor and anion polymeric chain layers along the *b* direction and the hydrogen bonding network between the BEDT-TTF ethylene and SCN groups (dotted black lines) at the interface between these layers.

In most of the $(BEDT\text{-}TTF)_2X$ salts, donors are packed into layers alternating along the third direction with layers of anions or polymeric anionic chains or networks. These salts are usually quasi-isotropic 2D metals with a typical intra- to inter-layer resistivity ratio $\rho_{//}$: $\rho_{\perp}$ of about 1:10^3. [22] The interface between layers is controlled by a hydrogen bonding network established between the ethylene groups of the BEDT-TTF molecules and some constituents

(SCN group, I_3 ….) of the anion layer (see Fig. 6 for instance). This explains the existence of polymorphism for the (BEDT-TTF)$_2$X salts which crystallise in different structural types mainly characterized by the different types of packing of the BEDT-TTF molecules. The more common packings, identified by Greek letters α, β, θ, κ, etc… are represented schematically in Fig. 7.[22] The 2D electronic structure of (BEDT-TTF)$_2$X strongly depends on the packing mode which thus, controls the electronic properties, which will be analysed in more detail in section V.

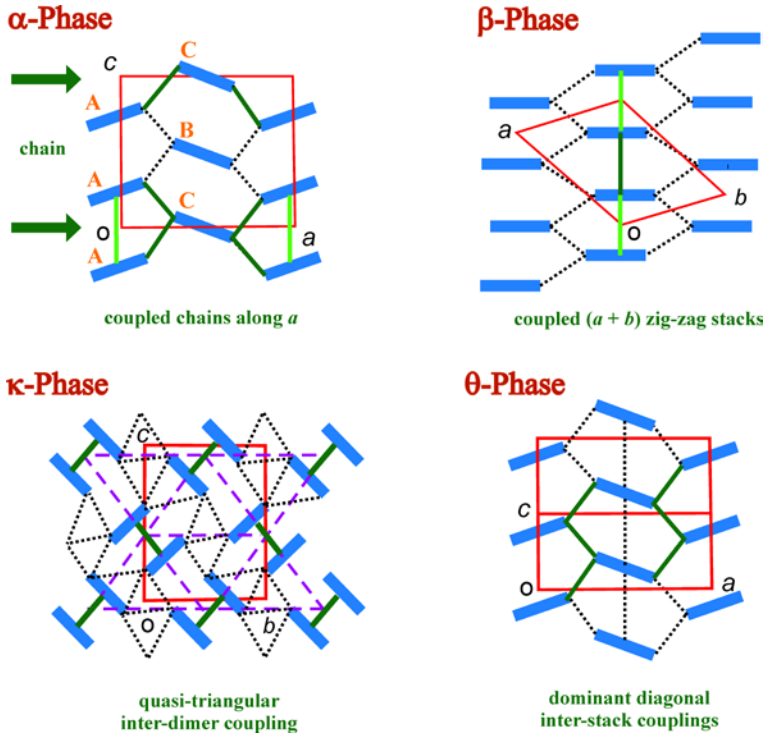

Figure 7. Schematic representation of the BEDT-TTF layer present in the α, β, θ and κ polytypes of (BEDT-TTF)$_2$X salts. Only the strongest inter-donor interactions are indicated. Note that the lattice of the κ-phases can be considered as an effective triangular lattice of dimeric units (the dashed purple lines indicate the effective interactions between dimers)

B. Inter-donor coupling energies. Let us consider the Fabre/Bechgaard salts. The main intermolecular electronic interactions are labeled in Fig. 5. Since TMTSF is an electronic donor, the relevant part of the band structure is that of its HOMO bands. DFT (density functional theory) calculations and plasma edge measurements give an intra-stack transfer integral between donor HOMOs (t_a) ≈ 0.20/0.25eV for the Fabre/Bechgaard salts, respectively. Plasma edge measurements for the Bechgaard salts led to an effective inter-stack transfer integral t_b^{eff} ~ 25meV along the *b*' direction for Bechgaard salts. Because of the thermal broadening of the electronic structure in the vicinity of the Fermi level, the inter-chain coupling is only relevant in the temperature range $k_BT < t_b^{eff}/\pi$. [59] Above the 1D to 2D crossover condition $T^{el}_{1D\rightarrow 2D} = t_b^{eff}/\pi$ (~ 100K for the Bechgaard salts), the thermal broadening of the Fermi surface is larger than its warping so that the electron wave function is coherent only in the direction of the stack. Above $T^{el}_{1D\rightarrow 2D}$ the electron gas is really 1D. In contrast,

below $T^{el}_{1D\rightarrow 2D}$ the electron gas is coherently delocalized on neighboring stacks and is thus 2D. In this situation, the electron gas exhibits a warped Fermi surface (FS) open in directions perpendicular to the chain direction like that shown in the lower part of Fig. 4b. Materials with open FS are refereed as quasi-1D in the literature. $T^{el}_{1D\rightarrow 2D}$ defines an important crossover line that really tunes the electronic properties. Such a line, which can be determined experimentally, for example by the observation of a transverse plasma edge below $T^{el}_{1D\rightarrow 2D} \equiv T^*$ [60], is indicated at the right side of the phase diagram in Fig. 2a. This figure shows that the enhancement of t_b^{eff} under pressure leads to an increase of T^*. In the Fabre salts, where no transverse plasma edge is detected, t_b^{eff} is not a relevant. Thus Fabre salts are 1D metals. The intra-layer transfer integrals are much smaller in the $(BEDT\text{-}TTF)_2X$ salts. For instance, in β-$(BEDTTF)_2I_3$ the average intra-layer transfer integral is $\langle t \rangle \sim 12$meV from plasma edge measurements. Due to the same type of side by side overlap between HOMOs in $(BEDTTF)_2X$, the magnitude of $\langle t \rangle$ am,ounts to the average *transverse* transfer integral t_b^{eff} of the Bechgaard salts.

The interactions U and V_m (m = 1, 2), defined in Fig. 5 for a 1D system, are respectively the intramolecular and m^{th} neighbor Coulomb repulsion terms. With comparable inter- and intramolecular distances, U and V_m (generally for $m \leq 3$) interactions should be considered. Since U and V_m are estimated to be significantly larger than the first neighbor transfer integral t, the electron gas of organic conductors is often described by the extended Hubbard Hamiltonian [61]:

$$H_{el} = \sum_i \varepsilon_i n_i + \sum_{i,j} t_{ij} \left(c^+_{i,\sigma} c_{j,\sigma} + h.c. \right) + \sum_i U n_{i\uparrow} n_{i\downarrow} + \sum_{i,j} V_{ij}\ n_i\, n_j \qquad (1)$$

where ε_i is the HOMO energy of the donor located on site i, t_{ij} is the hopping term from site i to site j, $c^+_{i,\sigma}$ the creation operator for an electron (with spin σ) on site i and $c_{j,\sigma}$ the corresponding annihilation operator. U is the on-site Coulomb repulsion term and V_{ij} the Coulomb repulsion between electrons located on sites i and j ($|j\text{-}i| = m$ in Fig. 5). In (1) $n_{i\uparrow}$ and $n_{i\downarrow}$ refer to the count operator for electrons with spin-up and spin-down, respectively so that $n_{i\sigma} = c^+_{i,\sigma} + c_{i,\sigma}$, and $n_i = n_{i\uparrow} + n_{i\downarrow}$.

Quantum chemistry calculations for stacks of TTF molecules [62] and layers of BEDT-TTF molecules [63] show than V_m (V_{ij}) basically decay as $\sim 1/m$ ($\sim 1/|j\text{-}i|$). When the screening due to the molecular polarizability is considered, the following values are obtained for the TTF stack of TTF-TCNQ: $U \sim 2$ eV, $V_1 \sim 1$eV, $V_2 \sim 0.55$ eV and $V_3 \sim 0.4$ eV, where the donor-donor transfer integral is $t \sim 0.15$ eV. V_3 is also comparable to the first neighbor interstack Coulomb repulsion energy [64]. It is expected that screening in the solid should still reduce these values. In κ-$(BEDT\text{-}TTF)_2X$ salts *ab-initio* calculation for the screened Coulomb interaction leads to $U \sim 0.8$eV (i.e. $U/t \sim$ 12-15) [65]. From the analysis of the optical conductivity in the Bechgaard salts the following values have been estimated: $U/V_1 \sim$ 2.5 and $U/t \sim$ 5-7 (i.e. $U \sim$ 1.2-1.5eV).[66]

Important additional interactions in organic conductors arise also from coupling of electrons to lattice vibrations (phonons), modulating the different energy terms in the Hamiltonian (eq. 1). Intramolecular (optic) phonons modulate site energies ε_i and U while

intermolecular (acoustic) phonons modulate the inter-site energies t_{ij} and V_{ij}. Acoustic phonons play in important role in 1D organic conductors since their coupling to electrons drives the Peierls instability observed in DA charge transfer salts. [67] Using the mean-field theory of the Peierls transition the electron-phonon coupling constant for acoustic modes can be estimated from the magnitude of the Peierls gap (see subsection *C* below). For instance, an electron-(acoustic) phonon coupling energy of $g_{ep} \approx 7.5$ meV has been estimated for the quarter-filled 1D conductor TMTSF-DMTCNQ, whose donor stacks have essentially the same electronic structure as the Bechgaard salts. Interestingly, g_{ep} is comparable to the spin-phonon coupling energy, g_{sp}, driving the SP transition of the Fabre salts, for instance $g_{sp} \sim$ 8.5meV in $(TMTTF)_2PF_6$. [68]. Note that the electron-phonon coupling interaction can be directly probed by Resonant Inelastic X-ray Scattering (RIXS).[69]

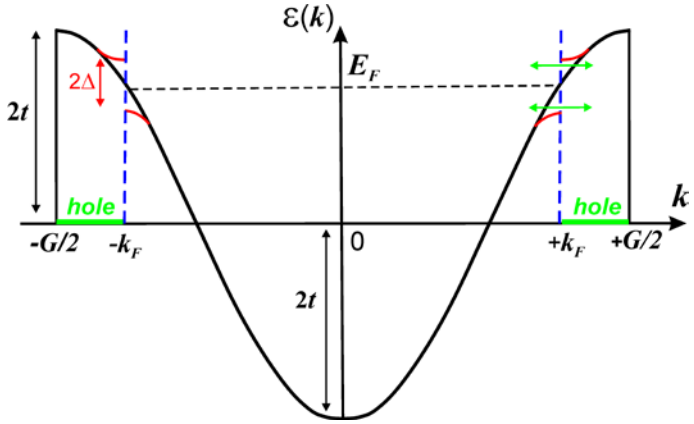

Figure 8. Schematics of a 1D band filled from $-k_F$ to $+k_F$ and how it is modified as a result of a $2k_F$ stack modulation. Since the band dispersion should reach all zone boundaries with a zero slope (see the green double arrows), the modulation opens a gap 2Δ at the Fermi energy E_F.

C. Main manifestations of charge and spin instabilities. Let us first consider the band structure for a 1D non-interacting electron gas with one available HOMO per donor in a stack with periodicity *a* (Fig. 8). If the transfer integral between the HOMOs is noted as *t*, the tight-binding energy band runs from $-G/2$ to $+G/2$, where $G = 2\pi/a$ is the reciprocal wave vector of the stack and the bandwidth is $4t$. This band is completely filled when there are 2 electrons per HOMO ($\rho = 2$) while with $\rho < 2$ the band is partially filled and the system is metallic. The electronic states are filled from $-k_F$ to $+k_F$ and the linear relation $2k_F = (\rho/2)\, G$ holds for 1D systems. In D_2X salts, the average charge transfer of one electron from two donors to the anion leads to an occupation of the HOMO bands with $\rho = 2-1/2 = 3/2$ electrons or 1/2 hole per donor. Thus, as shown in Fig. 8, the band is three-quarter-filled with electrons ($2k_F^e = 3G/4$) or one quarter-filled with holes ($2k_F^h = G - 2k_F^e = G/4$).

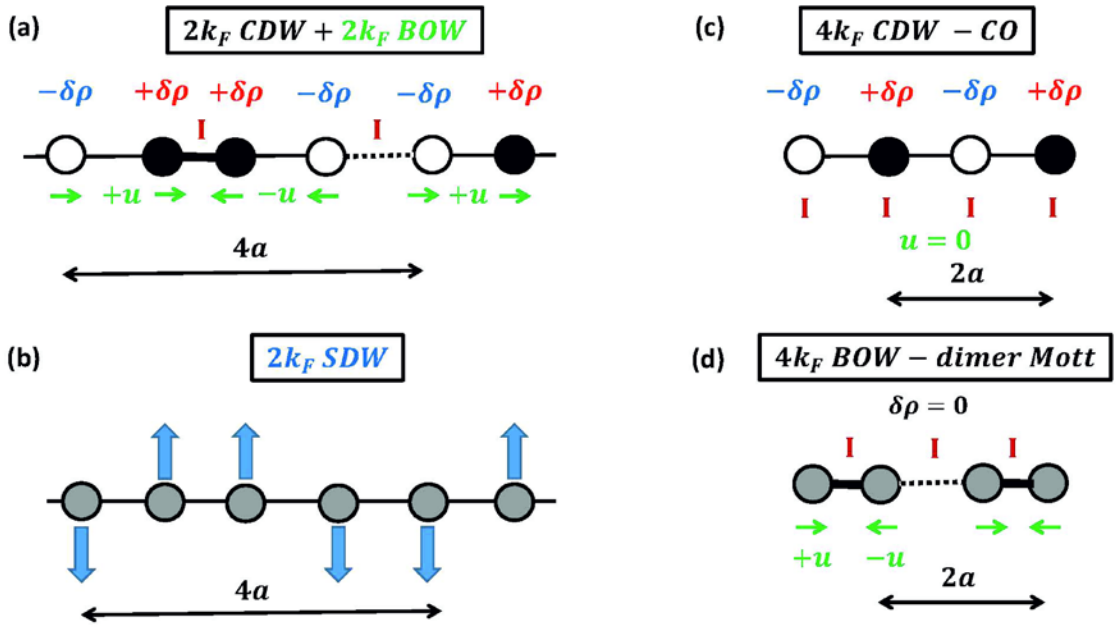

Figure 9. Schematic representation of (a) a $2k_F$ CDW+BOW modulation, (b) a $2k_F$ SDW modulation, (c) a $4k_F$ CDW-CO modulation, and (d) a $4k_F$ BOW dimer-Mott modulation for a quarter filled 1D band. The charge modulation, +δρ and – δρ, of the CDW is indicated by empty and black filled circles, respectively. The absence of charge modulation is indicated by grey filled circles. Green arrows represent the shift of molecules in the BOW states. The blue vertical arrows represent the spin orientation in the SDW. Inversions centres (I) of the modulated chains are also indicated.

Such a 1D system can gain electronic energy if a new periodicity with $2k_F$ wave number develops along the chain introducingl new zone boundaries at ± k_F in addition to those at $\pm G/2$ due to the initial stack periodicity. Since the band dispersion must exhibit a horizontal slope at these new zone boundaries, the energy of filled (emptied) states in the vicinity of ± k_F will be lowered (raised) as illustrated in Fig. 8. Consequently, a gap 2Δ opens in the conduction band at the Fermi energy (± k_F). In 1D systems, this process is accompanied by a metal to insulator transition and the electronic energy of the occupied states always overcomes the energy cost needed to set-in the $2k_F$ modulation. The gap opening process is thus achieved by the setting of a modulation with the $2k_F = 3/4G \equiv G/4$ wave number (Fig. 8) corresponding to a $4a$ wavelength. The modulation may be:

(i) A $2k_F$ periodic lattice modulation coupled to the 1D electron-gas through the electron-phonon coupling g_{ep} (Peierls mechanism). In this case the ground state consists of a $2k_F$ modulation of the electronic density (a charge density wave, CDW) accompanied by a bond order wave (BOW) modulation of the bond distances if g_{ep} is due to the coupling to acoustic phonons (see Fig. 9a).

(ii) A $2k_F$ magnetic modulation driven by the exchange potential arising from the intrasite U Coulomb term (Slater mechanism). In this case the ground state consists of a $2k_F$ modulation of the spin-density (a spin-density wave, SDW, see Fig. 9b).

These two kinds of density wave modulations (see the left part of Fig. 10), are both driven by a $2k_F$ electron-hole instability of the 1D electron gas (for a recent review see [70]).

According to the mean-field approximation, for an electron-phonon coupled system in the adiabatic limit, half of the amplitude of the Peierls gap at 0 K is given by the BCS-like equation [70]:

$$\Delta_0 = C E_F e^{-1/\lambda_{ep}} \qquad (2)$$

with $C = 4$ for a parabolic band dispersion. In (2) the reduced electron-phonon coupling constant λ_{ep} is related to the electron-phonon coupling constant g_{ep} by the expression:

$$\lambda_{ep} = \frac{{g_{ep}}^2 N(E_F)}{\hbar\Omega_{ph}} \qquad (3)$$

where $N(E_F)$ is the 1D electronic density of states at the Fermi energy, E_F, for the two spin directions ($i.e.\ N(E_F) = \frac{2\pi a}{\hbar v_F} = \frac{\pi\sqrt{2}}{t}$ for a quarter-filled band) and Ω_{ph} is the frequency of the critical acoustic mode ($\hbar\Omega_{ph} \approx 5meV$ in TTF-TCNQ). For instance, in the case of TMTSF-DMTCNQ, which is a quarter-filled 1D conductor (whose donor band parameters are t = 0.23 eV and $E_F = \sqrt{2}\,t$) undergoing a Peierls transition at 42 K, one obtains, by including the Peierls gap ($\Delta_0 \approx 12.5$ meV [71]) in expression (2), a reduced electron-phonon coupling constant $\lambda_{ep} \approx 0.22$. Using expression (3) an electron-(acoustic) phonon coupling energy of $g_{ep} \approx 7.5$ meV can be estimated.

The same BCS-like expression (2) holds for a SDW gap with a reduced magnetic coupling constant

$$\lambda_{mag} = N(E_F)\,U/2 \qquad (4)$$

instead of λ_{ep}.

The Peierls/Slater transition observed in true materials is a second-order phase transition with a 3D order between the $2k_F$ 1D modulations. In crystalline systems made of a collection of weakly coupled chains, the 3D CDW/BOW Peierls transverse order is generally achieved by the Coulomb coupling between CDWs on neighboring stacks (the minimization of the inter-chain Coulomb repulsion imposes an out of phase transverse order where an excess of charge is in front of a defect of charge) as schematically shown in Fig. 11a. The 3D SDW transverse order is usually attained through inter-chain exchange coupling.

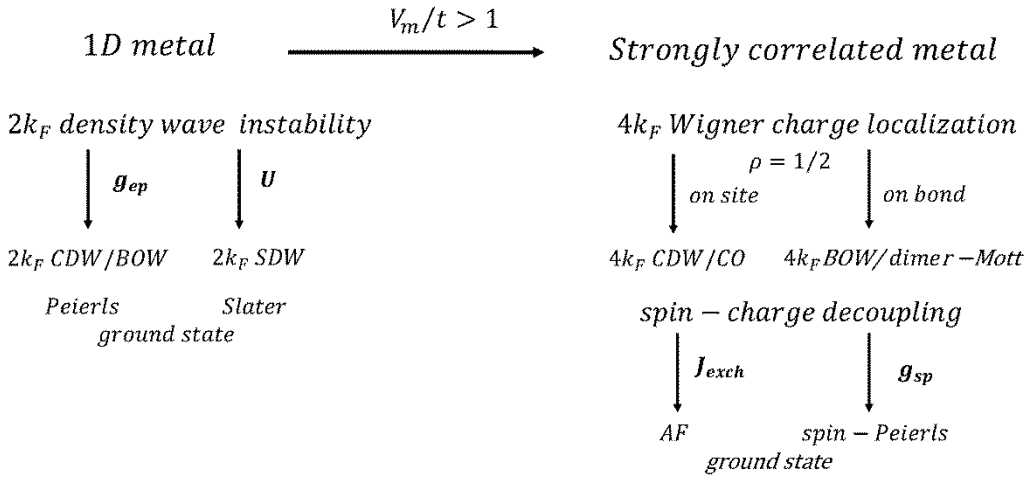

Figure 10. Different ground states of the 1D Hamiltonian (eq. 1) when coupled to a phonon field. Some of these ground states are represented in Fig. 9.

When long range Coulomb repulsions (i.e. the $V_{i,j}$ terms in the Hamiltonian) are relevant compared to t the electron gas tends to undergo a Wigner charge localization [61] (see left part of Fig. 10). Since the average distance between localized charges is $1/\rho = 2\pi/4k_F$, amounting to $2a$ for a quarter-filled electronic system, the periodic charge localization stabilizes the critical $4k_F$ wave number. If there is localization of one charge on one site out of two, one gets a $4k_F$ CDW or CO ground state (Fig. 9c), which can be favored by the electron-phonon coupling to intramolecular modes. In the presence of an electron-phonon coupling to acoustic phonons there is localization of one charge in one bond out of two, leading to a $4k_F$ BOW or Mott-dimer ground state (Fig. 9d). The $4k_F$ CDW and $4k_F$ BOW instabilities are common in DA charge transfer salts [73].

The Wigner charge localization achieves a spin-charge decoupling. The spin 1/2 of each localized charge may couple either in an AF manner via the exchange coupling J_{exch}, or in a non-magnetic singlet. In the presence of a sizeable spin-phonon coupling g_{sp} the magnetic singlet is stabilized through a stack dimerization into a SP ground state. These two magnetic-like ground states are respectively illustrated in Figs. 12a and 12b. Note that if AF occurs whatever the spatial dimension of the spin lattice it is, the SP instability requires the presence of well-decoupled spin 1/2 AF chains. The reason is that the SP instability is driven by the S=0 component of spin 1/2 AF quantum fluctuations which are picked out of the continuum of magnetic fluctuations by the spin-phonon coupling. In Fig. 12b the dimerization of a chain of dimers (each bearing a localized spin 1/2) brings into close contact two neigbouring dimers out of two between which the magnetic singlet is formed.

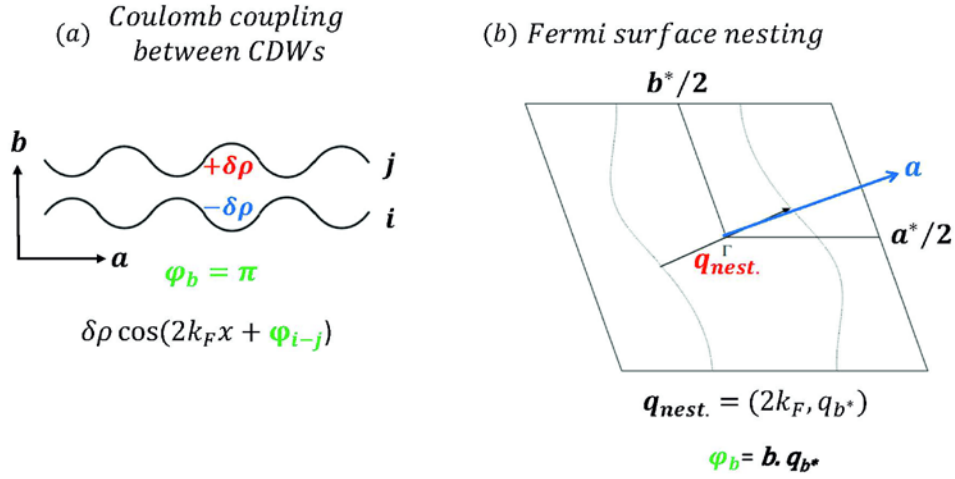

Figure 11. Main mechanisms of transverse coupling for $2k_F$ density waves: (a) Coulomb coupling between 1D CDWs whose minimization leads to an out of phase transverse ordering with a phase shift $\varphi_b = \pi$; (b) Best nesting mechanism of the Fermi surface as illustrated for the 4 K warped FS of $(TMTSF)_2PF_6$ calculated by DFT.[72] The transverse component q_{b*} of q_{nest} defines the phase shift φ_b between first neighbour $2k_F$ CDWs or SDWs. Note that in the oblique Brillouin zone of the Bechgaard salts q_{nest} is nearly aligned with the stack direction a (this is also the case for q_{nest} of the warped FS of quenched $(TMTSF)_2ClO_4$ – see Fig. 4).

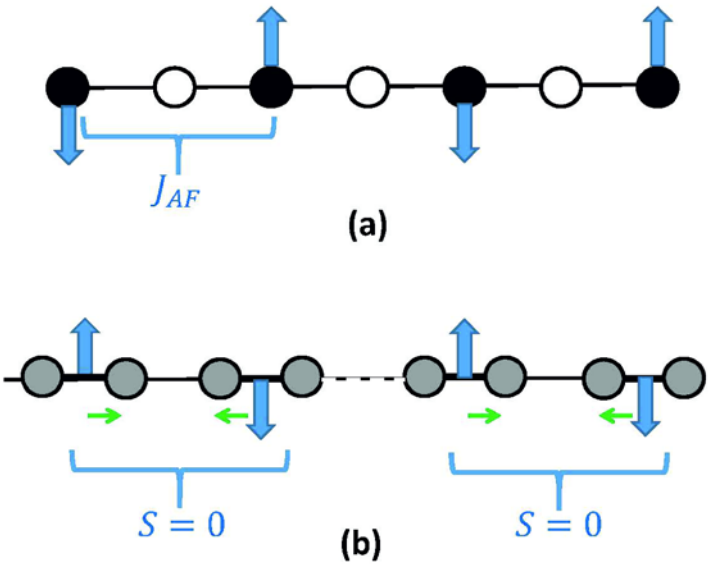

Figure 12. (a) AF and (b) SP orders arising from the coupling of S = 1/2 in the CO and dimer-Mott chains shown in Figs. 9c and d respectively. In (a) the magnetic order is due to AF exchange coupling (J_{AF}) between S = 1/2 spins localized on one site out of two. In (b) the S = 0 pairing between individual S=1/2 localized on neigbouring dimers is stabilized by the dimerization (green arrows) of the chain of dimers.

A 2D electron gas can exhibit CDW or SDW instabilities if important portions of the 2D FS can be nested by a well-defined wave vector q_{nest}. In the case of quasi-1D systems exhibiting a warped FS, such as that shown in Fig. 11b where $q_{\text{nest}} = (2k_F, q_{b^*})$, the interstack q_{b^*} component sets the transverse phase shift φ_b between neighboring density waves.

In the case of a strongly interacting 2D electron gas, ground states consisting on a Wigner charge localization are obtained. Various charge patterns depending on the relative values of the different microscopic parameters have been obtained by solving Hamiltonian (1) in the Hartree approximation. [74] Fig. 13 shows typical CO patterns obtained in the case of an anisotropic triangular lattice of sites, an idealized representation of BEDT-TTF layers (see Fig. 7).

(P, T) phase diagram of D_2X salts, as that shown in Fig. 2a, involes a sequence of several competing electronic ground states. The condition of stability of these phases depends upon the relative values of the electron interactions entering in the Hamiltonian (1) (for recent reviews see [75-77]). More recent works include the effect of the electron-phonon coupling in the stabilization process (for a recent review see [55]). However, at the exception of few works [59, 78-81], the coupling of the electron gas with the anion subsystem is generally ignored. Below we show that spectacular effects arise from such a coupling.

D. Basic interactions with the anion subsystem. The anion sub-lattice of 1D or 2D D_2X organic conductors lies outside the donor stacks or layers (see Figs. 5 and 6) exerting a Coulomb interaction over the hole-cloud located on the donor sub-lattice. This interaction, with the periodicity of the anion sub-lattice, can lead to an important charge response of the delocalized holes for 1D or quasi-1D metallic systems that will be enhanced if the wave number of the anion periodicity coincides with the critical $2k_F$ or $4k_F$ wave vectors for which the 1D electron-hole response function exhibits maxima (the relative importance of the $2k_F$ vs. $4k_F$ maxima depends upon the values of the electronic parameters in the Hamiltonian (eq. 1) (see for example [55,73]). There are many examples where the $2k_F$ potential of the anion sub-lattice helps stabilizing a Peierls ground state.[82-83] Here we note that the $4k_F$ potential of the anion sub-lattice plays an important role in the physics of the Fabre salts as we shall see below.

In 1D and 2D correlated electron systems, the anion Coulomb potential adds to the V_{ij}'s considered in the extended Hubbard Hamiltonian. In 1D conductors such as the Fabre salts, the anion sub-lattice potential plays a very subtle role because its inverse periodicity along the direction of the stacks corresponds to the critical $4k_F$ wave vector of the electron-hole response of the strongly interacting electron gas. The reason, initially developed in ref. [78-79] is the following. For a regular quarter-filled band, the $4k_F$ BOW response of the electron gas to a $4k_F$ anion potential leads to a $4k_F$ BOW modulation of the stack (i.e. a stack dimerization of amplitude u) and to a $4k_F$ modulation of the carrier density, with an excess of one hole per dimer, see Fig. 9d). One thus gets a $4k_F$ Wigner-type charge localization due to the $4k_F$ BOW response of the 1D correlated electron gas to the anion potential. The charge localization opens a gap of charge, $2\Delta_\rho^{\text{BOW}}$, which explains the thermally activated conductivity below T_ρ in the Fabre salts (see Fig. 3).

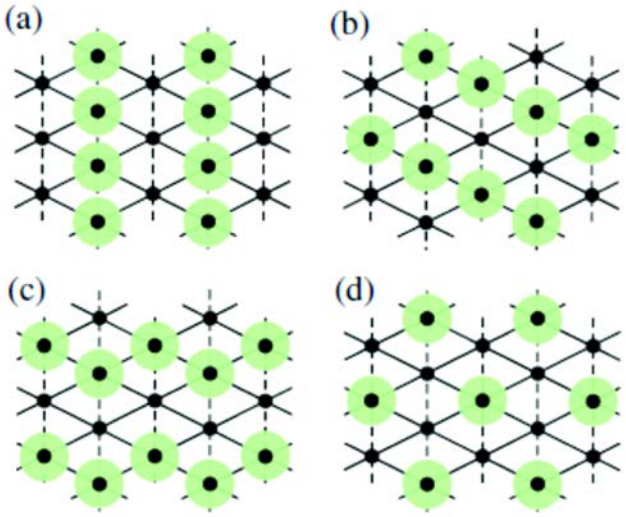

Figure 13. CO pattern in the quarter-filled extended Hubbard model for anisotropic triangular lattices: (a) vertical, (b) diagonal and (c) horizontal stripe arrays; (d) represents a threefold state. Sites with/without coloured circle represent charge rich/poor occupancies, respectively.[75] (Copyright 2006 by the Physical society of Japan)

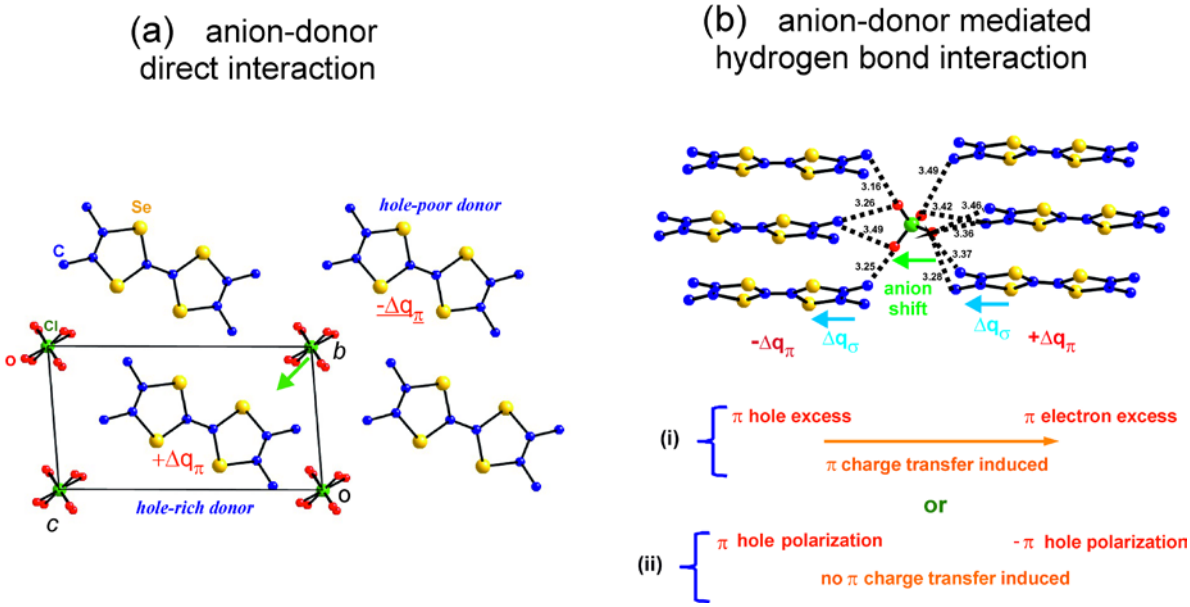

Figure 14. (a) Direct and (b) mediated methyl group interactions between anion and donors, inducing a differentiation of the π hole density on donors. Part (b) of the figure shows the establishment below T_{AO} of short contacts between outer O atoms of the anion and C atoms of the methyl groups located at the left side of the anion cavity for $(TMTSF)_2ClO_4$. [30] (Copyright 2014 by the American Physical Society)

It is also interesting to go beyond the electrostatic considerations and to analyze the microscopic interaction between anions and donors in the Fabre and Bechgaard salts. Fig. 14 shows that, there is either a direct interaction between the outer atoms of the anion and the S/Se atoms of the donor core (Fig. 14a), or an indirect (mediated) interaction with the core of the donor via a polarization effect of the σ electron cloud resulting from the interaction of atoms of the anion with terminating methyl groups of the donor (Fig. 14b). [84] When anions and methyl groups order at low temperature, the latter interaction becomes more effective by establishing hydrogen bonds between donors and anions. Such a coupling is frequently present in $(BEDT\text{-}TTF)_2X$ salts where anion-donor interaction occurs essentially through the hydrogen bond network linking the anions and ethylene groups at the periphery of the donors (dashed lines in Fig. 6). This indirect (mediated) interaction mechanism, first proposed for α-$(BEDT\text{-}TTF)_2I_3$ (see Fig. 34b) [85] and analysed in section V, will be more explicitely considered below in the case of Fabre/Bechgaard salts.[30]

In short, when anions located in centrosymmetrical cavities shift towards a given donor the inversion symmetry breaks. The donor towards whom the anion moves becomes hole-rich while the donor left from it becomes electron-rich. In a *direct* donor-anion interaction, the anion shift modifies the Hartree potential polarizing the π hole in the inner core of the donor. In addition, the anion displacement may also distort the donor stack with the subsequent changes in the transfer integrals. The *indirect* interaction is more subtle. An increase in strength of the hydrogen bonds between the terminal methyl groups of the donor molecules and a neighboring anion makes the hydrogen atoms of the methyl group more positively charged, inducing a negative σ charge shift towards the inner part of the donor (see Fig. 14b). Consequently, a larger hole density is stabilized in the inner π system. This hydrogen bond mediated process induces either a charge transfer or a molecular polarization depending on the existence or not of a sizeable transfer integral with the neighboring donors of the chain (see Fig 14b).

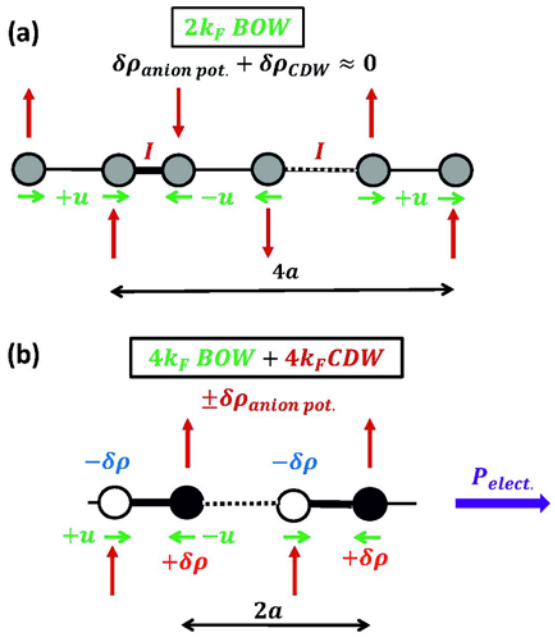

Figure 15. (a) $2k_F$ bond modulation wave resulting from the superimposition of a standard Peierls distortion of the stack with an induced $2k_F$ CDW set by the 4*a* periodic anion potential. The induced $2k_F$ anion CDW, $\delta\rho_{\text{anion pot}}$, is out of phase with the $2k_F$ Peierls CDW, $\delta\rho_{CDW}$, leading to a cancellation of the total CDW modulation. (b) Superimposition of the $4k_F$ BOW modulation of the stack with an induced $4k_F$ staggered CDW, $\pm\delta\rho$, set by the 2*a* periodic anion potential. The resulting modulation is no longer centrosymmetric so that the stack should exhibit an electronic polarisation. Red arrows mimic either an anion displacement or an anion orientation (if the anion is non centrosymmetric) wave.

The anions, through the interactions with the donors, should contribute to the stabilization of collective CDW or CO ground state originating from the $2k_F$ or $4k_F$ instability of 1D donor subsystem (section II.C). An important source of coupling is provided by the setting of an anion superstructure with the 4*a* or 2*a* periodicity (i.e. $2k_F$ or $4k_F$ wave length) along the stack direction. At the beginning of this section we already mentioned the effect of the anion periodicity on the $4k_F$ BOW charge localization process of the Fabre salts. Below, in Fig. 15 we schematically illustrate two other important examples:

(a) In Fig. 15a a modulated anion displacement or anion orientation wave (red arrows) towards donor sites sets a 4*a* superlattice whose periodicity coincides with one of the $2k_F$ intrinsic instabilities of the quarter-filled donor stack. Thus, in addition to the intrinsic $2k_F$ BOW and CDW modulation of the donor stack (Fig. 9a), the anion 4*a* superstructure which modulates the environment of donor sites as schematically indicated in Fig. 15a, which will induce a $2k_F$ CDW response of the stack through the Hartree potential. The induced CDW (noted $\delta\rho_{\text{anion pot}}$) superimposes with the intrinsic $2k_F$ CDW stack modulation, $\delta\rho_{CDW}$. An interesting situation, depicted in Fig. 15a, occurs when because of a proper phasing of the 4*a* anion superstructure with respect to the intrinsic $2k_F$ stack modulation, $\delta\rho_{\text{anion pot}}$ and $\delta\rho_{CDW}$ cancel. Such a cancellation should minimize inter-chain CDW Coulomb interactions. In this case a pure $2k_F$ BOW Peierls ground state occurs. This situation is realized at the AO transition of some Bechgaard salts (see section III.C.1).

(b) In Figure 15b an anion displacement or orientation wave (red arrows) towards donor sites sets a 2*a* superstructure whose periodicity coincides with that of the $4k_F$ intrinsic instability of the quarter-filled donor stack. The 2*a* anion superstructure, which modulates the environment of donor sites, induces a $4k_F$ CDW or CO response of the stack (Fig. 9c) through the Hartree potential. If the stack in the Fabre salts already experiences a $4k_F$ BOW modulation or $4k_F$ Mott-dimer order, as represented in Fig. 9d, the setting of the new anion periodicity will superimpose with the $4k_F$ CDW and $4k_F$ BOW stack modulations, as indicated in Fig. 15b. Since the $4k_F$ CDW and $4k_F$ BOW (separately represented in Figs 9c and 9d) have different inversion symmetry in a quarter-filled band system, the resulting modulation breaks the inversion symmetry of the stack, which thus exhibits an electronic polarisation with important consequences for the Fabre salts (see section III.D.2)

Anion shift or anion orientation waves as a response to the charge instability of the organic stacks are also expected [86]. This is the case of electronic ferroelectricity which will be

considered in section III.D. It has also been proposed that the anion sublattice should participate in the magnetoelastic coupling involved in the SP instability of the Fabre salts [67]. If it is strong enough, the mediated electron-anion (hole-anion) interaction, g_{eA}, can also help localize the charge carriers through some kind of "polaronic" effect adding to those provided by pure Coulomb repulsion terms.

III. Bechgaard [$(TMTSF)_2X$] and Fabre [$(TMTTF)_2X$] salts as prototypes of 1D conductors

Several aspects of the relation between structural and electronic properties of the Bechgaard and Fabre salts have been covered in earlier reviews. [87-89] Here we present a more synthetic approach based on recent findings stressing the role of the donor-anion interactions.

A. Degrees of freedom of the anion cavity. The anion cavity plays an essential role in the physics of the Bechgaard and Fabre salts (Fig. 5) which has not been fully recognized in the past. At RT the anions are located in a soft cavity made of thermally disordered methyl groups. Because of their relatively weak interaction with donors, anions exhibit a considerable thermal motion inside these cavities. Irrespective of its centro- or non-centrosymmetric nature, the anion keeps, on average, a centrosymmetric position in the cavity and the space group of the average crystal structure is $P\bar{1}$.

Translational and rotational modes of the rigid anion within its cavity manifest through an anomalous thermal dependence of the uniaxial lattice expansion coefficients, which at high temperature decrease upon heating (Fig. 16). [89-91] The decrease rate is strongest for measurements along the c^* direction where donor layers and anion cavities alternate. The lattice contraction should be caused by a decrease of the cavities effective volume upon heating due to the thermal enhancement of the orientational disorder of methyl groups and the rotation and reorientation disorders of the anion. The anion's contribution seems to be the dominant one since the uniaxial thermal expansion coefficient is regular and nearly one order of magnitude smaller in $(TMTTF)_2Br$ where the anion has no orientation degrees of freedom. [92]

Fig. 16 reports also the complementary temperature ranges of anion reorientation jumps (above 140 K) and rotation movements (above 70 K) probed by ^{19}F NMR in $(TMTSF)_2PF_6$. [93] Note that the start of the PF_6 rotation is consistent with the determination of a characteristic anion libration energy θ_L = 76 K from an analysis of thermal expansion of $(TMTSF)_2PF_6$. [48] Similar effects were observed by ^{19}F NMR of the SbF_6 anion in $TMTTF)_2SbF_6$ [94-95].

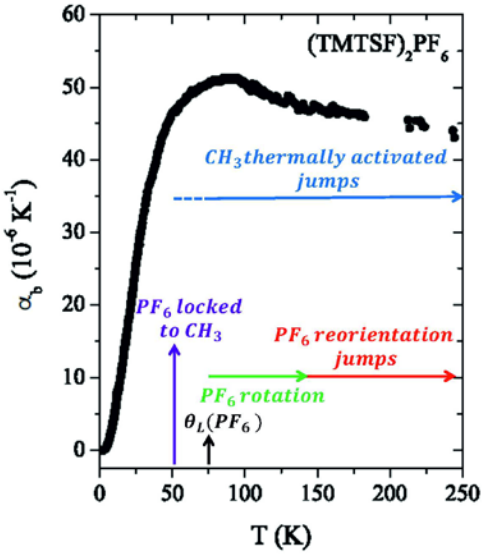

Figure 16. Coefficient of thermal expansion along the *b*'-axis for $(TMTSF)_2PF_6$ (adapted from a figure kindly provided by J. Müller and ref. [89] (Copyright 2004 by EDP Sciences)). The regimes of PF_6 rotation and reorientation jumps as well as CH_3 thermally activated jumps as probed by NMR have also been indicated. The libration energy of the PF_6 anion as well as the temperature at which the PF_6 locks to the methyl groups according to Fig. 17, has also been indicated.

Thermally activated jumps of methyl groups over finite energy potential barriers have also been probed by ^1H NMR T_1^{-1} measurements in $(TMTSF)_2PF_6$ revealing two activated processes above 55 K and 74 K. [96-99] When these activated (classical) methyl group motions cease, a sizeable enhancement of the intensity of some Bragg reflections (Fig. 17a) has been observed in deuterated $(TMTSF)_2PF_6$ below ~55 K (T_{link}) [48] that has been interpreted as a signature of the linkage of the anions to the methyl groups through the formation of hydrogen bonds. The hydrogen bonding network is revealed in the 4 K structure of both hydrogenated [41] and deuterated [48] $(TMTSF)_2PF_6$. The hydrogen bond linkages between anions and donors, which stiffen the structure, must be responsible for the enhancement of the longitudinal sound velocity observed below 55 K in $(TMTSF)_2PF_6$ (Fig. 17b). [100] The singular stiffening of the interlayer compressibility modulus observed below 40 K in both hydrogenated and deuterated $(TMTTF)_2PF_6$ is probably due to a similar hydrogen bond linkage of PF_6 anions to the methyl groups of the donor. [101] At this temperature (T_{int} in Fig. 22b) the thermal dependence of the uniaxial lattice expansion of $(TMTTF)_2PF_6$ exhibits a slope anomaly.

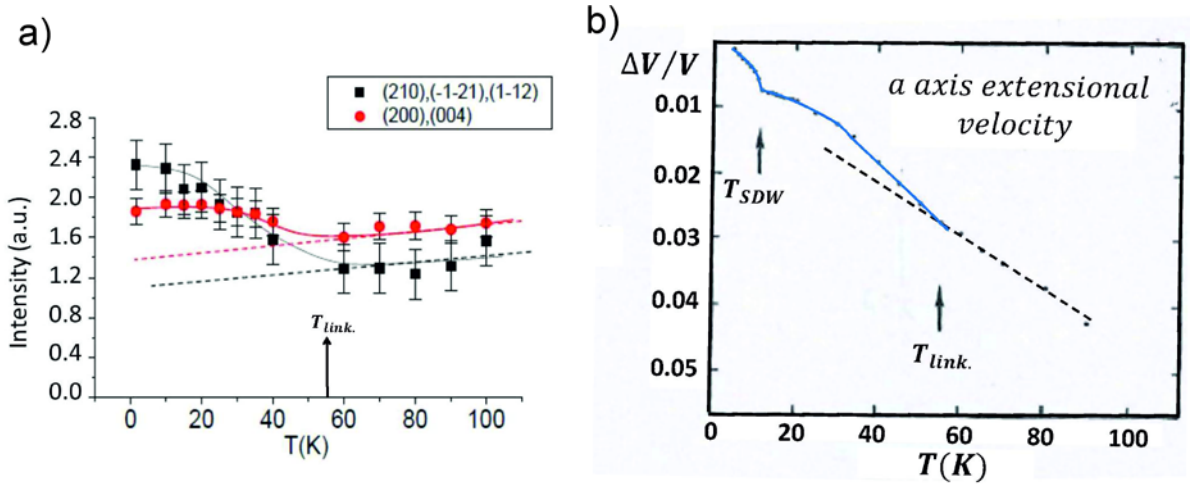

Figure 17. (a) Thermal dependence of the integrated intensity of two sets of Bragg reflections of deuterated $(TMTSF)_2PF_6$. The PF_6-CH_3 linkage temperature $T_{link.}$ is indicated (adapted from [48] (Copyright 2013 by the American Physical Society)). (b) Fractional change in the sound velocity of $(TMTSF)_2PF_6$ at low temperatures. The arrows indicate sharp changes in the slope at the PF_6-CH_3 linkage temperature (T_{link}) and at the metal-insulator SDW transition (T_{SDW}) (adapted from reference [100] (Copyright 1982 by Elsevier)). The blue line is just meant as a guide for the eyes.

When donors and anions of $(TMTTF)_2PF_6$ are linked by hydrogen bonds the ^1H NMR T_1^{-1} relaxation rate increases upon cooling below 45 K exhibiting a maximum around 20 K. [96-98] It was proposed that those features originate from quantum rotational tunneling effects, as directly evidenced at 1.2 K by ^1H NMR measurements in relaxed $(TMTSF)_2ClO_4$. [102] The presence of a residual methyl group motion at low temperatures is consistent with the observation of a sizeable and continuous thermal increase below 30 K of the intensity of several Bragg reflections located at low diffraction angles in deuterated $(TMTSF)_2PF_6$. [48]

B. The $2k_F$ density wave instabilities of the Bechgaard salts. As usual among 1D conductors studied so far, Bechgaard salts undergo a $2k_F$ density wave instability [103] associated to the nesting of the planar FS from $-k_F$ to $+k_F$. This longitudinal nesting process leads to a low temperature divergence of the 1D $2k_F$ CDW response function. A $2k_F$ CDW electronic instability driving a Peierls transition is commonly observed in charge transfer salts of the TTF-TCNQ family. [10,70] The $2k_F$ BOW response of the lattice coupled to the 1D $2k_F$ CDW electronic instability via electron-phonon coupling, leads to X-ray diffuse planes at the $\pm 2k_F$ reduced wave vectors in reciprocal space. [105] Fig. 18 shows the thermal divergence of the 1D $2k_F$ BOW response of the donor stack deduced from the peak intensity of such diffuse planes, in the quarter-filled TMTSF-DMTCNQ salt. The $2k_F$ BOW response grows over a large temperature range starting around ~225 K (T_{fl}), well above the Peierls critical temperature of T_P = 42 K. Similar features are commonly observed in other quarter-filled D_2X salts such as those built from derivatives of the perylene (Per) donor. [105]

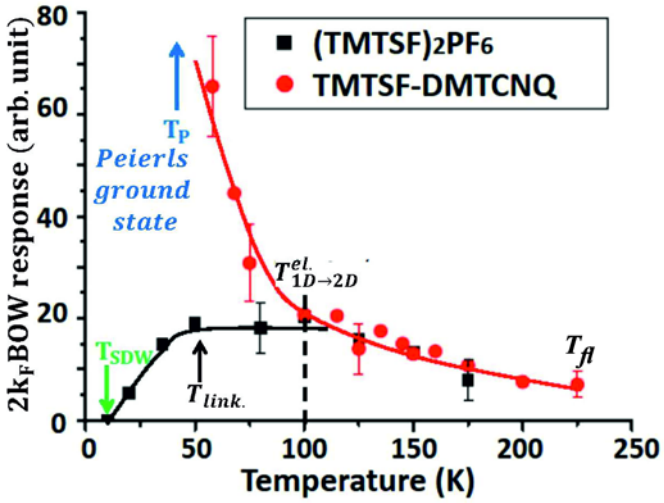

Figure 18. Thermal dependence of the $2k_F$ BOW response function of TMTSF-DMTCNQ and $(TMTSF)_2PF_6$, taken from the peak intensity of the $2k_F$ X-ray diffuse sheets, $I(2k_F, T)$, corrected by the thermal population factor: $\chi_{BOW}(2k_F, T) \propto I(2k_F, T)/T$ (adapted from [88]).

Fig. 18 shows, however, that the 1D $2k_F$ BOW response of $(TMTSF)_2PF_6$ behaves differently from that of TMTSF-DMTCNQ. At high temperatures (below $T_{fl} \sim 175$ K) the $2k_F$ BOW response behaves similarly to that in TMTSF-DMTCNQ. It saturates then below 100 K before decreasing below 50 K. The saturation occurs at the temperature $T^{el}{}_{1D\rightarrow 2D}$ at which the FS warping becomes relevant. Thus, below $T^{el}{}_{1D\rightarrow 2D}$ the high temperature longitudinal $-k_F$ to $+k_F$ FS nesting process stops. Then except for the best nesting wave vector of the FS (q_{nest} shown in Fig. 11b for the FS of $(TMTSF)_2PF_6$) any general $2k_F$ FS nesting process becomes imperfect, killing the 1D divergence of the CDW electronic response [59], and as shown in Fig. 18 the $2k_F$ BOW response saturates below $T^{el}{}_{1D\rightarrow 2D} \approx 100$ K. Finally at temperatures below the linkage temperature of the anion to the methyl groups, $T_{link} \approx 50$ K, the $2k_F$ BOW response decreases because the lattice becomes more rigid (this induces a lowering of the reduced electron-phonon coupling λ_{ep}). The $2k_F$ BOW response vanishes around T_{SDW} (= 12 K) when the metal-insulator transition stabilizing a SDW ground state occurs.

NMR line shape analysis has shown that the SDW modulation of $(TMTSF)_2PF_6$ stabilizes the best nesting wave vector q_{nest} of its low temperature FS shown in Fig. 11b. [88, 92], The SDW ground state of $(TMTSF)_2PF_6$ is in fact quite subtle because, in addition to the q_{nest} SDW, the modulated phase exhibits q_{nest} and $2q_{nest}$ structural modulations, which respectively correspond to $2k_F$ and $4k_F$ CDWs along the stack direction. [87,106] This means that $(TMTSF)_2PF_6$ exhibits more likely a mixed $2k_F$ SDW-CDW modulation. This modulation can be achieved for instance by superimposing the $2k_F$ CDW and $2k_F$ SDW shown respectively in Figs. 9a and 9b, and shifted by $\pi/2$. [88,106] The $4k_F$ CDW may be due to some kind of "magneto-elastic" effect induced by the $2k_F$ mixed density wave or to Wigner-like charge correlation effect. The magnetic ground state of $(TMTSF)_2PF_6$ undergoes also a sub-phase

transition (T_{sub}) around 4 K below which there is coexistence between incommensurate and commensurate SDW modulations. [107] Interestingly, the $2k_F$ and $4k_F$ CDW modulations are no longer observed below T_{sub}. [108-109] Thus, the vanishing of the charge modulation could be due either to a change of nature of the modulated state or to a drastic limitation of its spatial extend (inhomogeneous modulation [107] or glassy behavior [54]) affecting primarily the charge order.

At this point an important question remains to be answered: why the FS nesting process of $(TMTSF)_2PF_6$ does not stabilize a BOW with the q_{nest} ctitical wave vector since it has been established that such a nesting mechanism is at work in other D_2X salts such as α-$(BEDT\text{-}TTF)_2KHg(SCN)_4$ (see section V.C)? One possible explanation relies on the observation that q_{nest} is nearly aligned with the stack direction (see Fig. 11b). This means that such a nesting process would stabilize a superstructure made of longitudinal $2k_F$ BOW/CDW ($2k_F$ being the modulus of q_{nest}), where the modulation is in phase in the direction perpendicular to q_{nest} (i.e. between neighboring stacks in the inter-stack direction *b*' perpendicular to a). The CDW counterpart would thus exhibit maxima of charge along *b*' which corresponds to a maximum of inter-chain Coulomb repulsion. This certainly explains why SDWs, which are not sensitive to inter-chain Coulomb interactions, are stabilized by the q_{nest} FS nesting process. However, one should note that with $2k_F$ SDW modulation aligned with the stack direction, the in-phase inter-chain coupling between SDW along *b*' is ferromagnetic! Such a situation has never been considered in the literature. Note that a similar situation occurs for the SDW ground state of quenched $(TMTSF)_2ClO_4$ (see Fig. 4).

Under pressure the insulating charge and spin modulated ground state vanishes and with the restoration of the metallic phase, superconductivity is achieved. [11] However, Fig. 2a shows that the maximum T_S occur at the boundary with the SDW-like ground state and it has been argued that $2k_F$ SDW fluctuations should mediate the formation of Cooper pairs in the superconducting state. [110]

C. Influence of the anion ordering transitions on the electronic structure of the Bechgaard salts.

The discussion in section A applies to $(TMTSF)_2X$ Bechgaard salts with centro-symmetric anions. These salts keep the $P\bar{1}$ space group symmetry of the RT structure over all the temperature range: there is no change of symmetry associated with the freezing and linkage of the anion within its methyl group cavity [41,48] (see section III.A). The situation is different for Bechgaard salts with non centro-symmetric anions, either with tetrahedral (ReO_4, ClO_4, BF_4) or triangular (NO_3) shape. At RT these anions are disordered within their methyl group cavities but restore the inversion symmetry by averaging their orientation. However, for entropy reasons their orientation should freeze and collectively order when cooling. Such orientation ordering breaks the inversion symmetry of each individual methyl group cavity (but not necessarily the inversion symmetry of the structure because two neigbouring orientations can be related by such a symmetry). This is achieved in a collective way through a structural phase transition which stabilizes superstructures with a well-defined staggered

anion order. [87,111] The mechanism of such transitions, called anion ordering (AO) transition in the literature, is in fact quite subtle because the staggered order depends both of the shape of the anion and of its interactions with the electronic state of the donor stack. AO is a general phenomenon observed both in Bechgaard and Fabre salts.[87] as well as in other series of D_2A 1D conductors incorporating RT disordered non-centrosymmetric anions such as $(DMEDO\text{-}TTF)_2X$ ($X = ClO_4$ and BF_4) [112] and $(o\text{-}DMTTF)_2NO_3$.[113]

In the following we will just consider two representative examples of Bechgaard salts with the ReO_4 and ClO_4 anions, both of them exhibiting superconducting properties. The AO transition occurring in the Fabre salts will be briefly considered in part E.

$(TMTSF)_2ReO_4$. In addition to the entropy driven orientation ordering process of the ReO_4 anions (AO) upon cooling, other interactions should be considered in order to understand the complex behavior of this salt:

(i) First, there is a sizeable interaction of the anion with donor molecules (involving an electron-anion coupling, g_{eA}): in the RT average structure the $O_{anion}\cdots Se_{donor}$ short distance, 3.16 Å, is smaller than the sum of Se and O van der Waals radii (3.4 Å);

(ii) Second, the AO transition occurs at T_{AO} = 177 K when the donor electron gas is 1D. [114] In such 1D regime the metallic stack should exhibit a $2k_F$ CDW/BOW instability as observed in $(TMTSF)_2PF_6$ for the same temperature range (Fig. 18).

Below T_{AO} the ReO_4 anions order with an alternate orientation along the three unit cell directions. This staggered order, characterized by the q_{AO}^1 = (1/2,1/2,1/2) reduced wave vector, is stabilized through a first-order phase transition. [111,115] Fig. 19a shows the thermal dependence of the intensity of satellite reflections due the development of the $2a\times2b\times2c$ superstructure below T_{AO} (a, b and c are the unit cell parameters of $(TMTSF)_2ReO_4$ at RT). The $a^*/2$ component of the q_{AO}^1 modulation corresponds to the $2k_F$ wave vector of the 1D electron gas. The AO transition is thus accompanied by a Peierls metal-insulator transition (Fig. 19b) with the subsequent opening of a conductivity gap, $\Delta_{AO} \approx 86$ meV in the insulating phase [116,117] also detected in photoemission measurements [114] as well as an optical gap of $2\Delta_{AO} \sim 200$ meV. [114]

The q_{AO}^1 AO transition involving both interacting anions and donors, is in fact quite complex. Fig. 20a shows that the staggered orientation order of the ReO_4 anions is accompanied by a shift of the anion towards one donor out of two (as schematically illustrated in Fig. 14a). This structural feature leads to two non-equivalent sets of donors: A type donors, with a short $Se_{donor}\cdots O_{anion}$ contact of 2.99 Å, and B type ones, with no $Se_{donor}\cdots O_{anion}$ short contacts. As shown in Fig. 20b anions also establish within their cavity short $C_{methyl}\text{-}O_{anion}$ contacts smaller than the sun of van der Waals radii (3.22Å). However, these contacts are practically the same for A and B type donors and do not really allow to differentiate between the two types of donors (this is an expected result because donors A and B are similarly charged [118]).

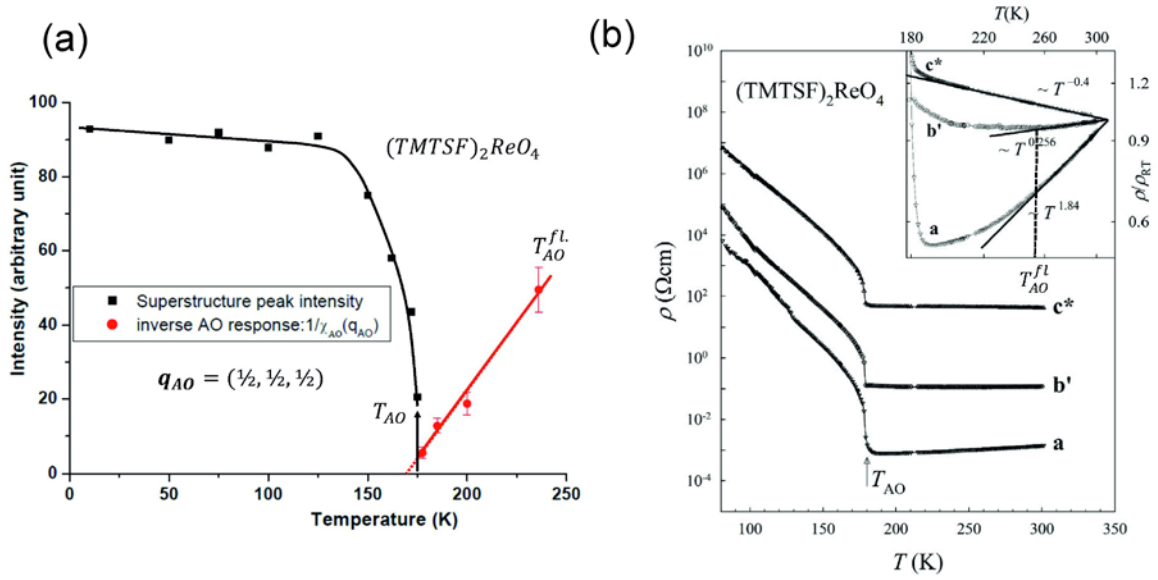

Figure 19. (a) Thermal dependence of the intensity of the q_{AO} superstructure reflection, I_{super}, below T_{AO} and of the inverse of the AO response function $\chi_{AO}(T)^{-1}$ below T_{AO}^{fl} in $(TMTSF)_2ReO_4$. Note that the small jump of I_{super} at T_{AO} and the vanishing of the Curie-Weiss behavior of $\chi_{AO}(T)^{-1}$ below T_{AO} make the first-order nature of the AO transition clear (taken from the data of ref. [115]). (b) Thermal dependence of the resistivity of $(TMTSF)_2ReO_4$ along the *a*, *b*' and *c** directions. The insert magnifying the measurements in the metallic phase show the upturn of the resistivity measured in the (*ab*') donor layer at around T_{AO}^{fl} (adapted from [117] (Copyright 2003 by the American Physical Society)).

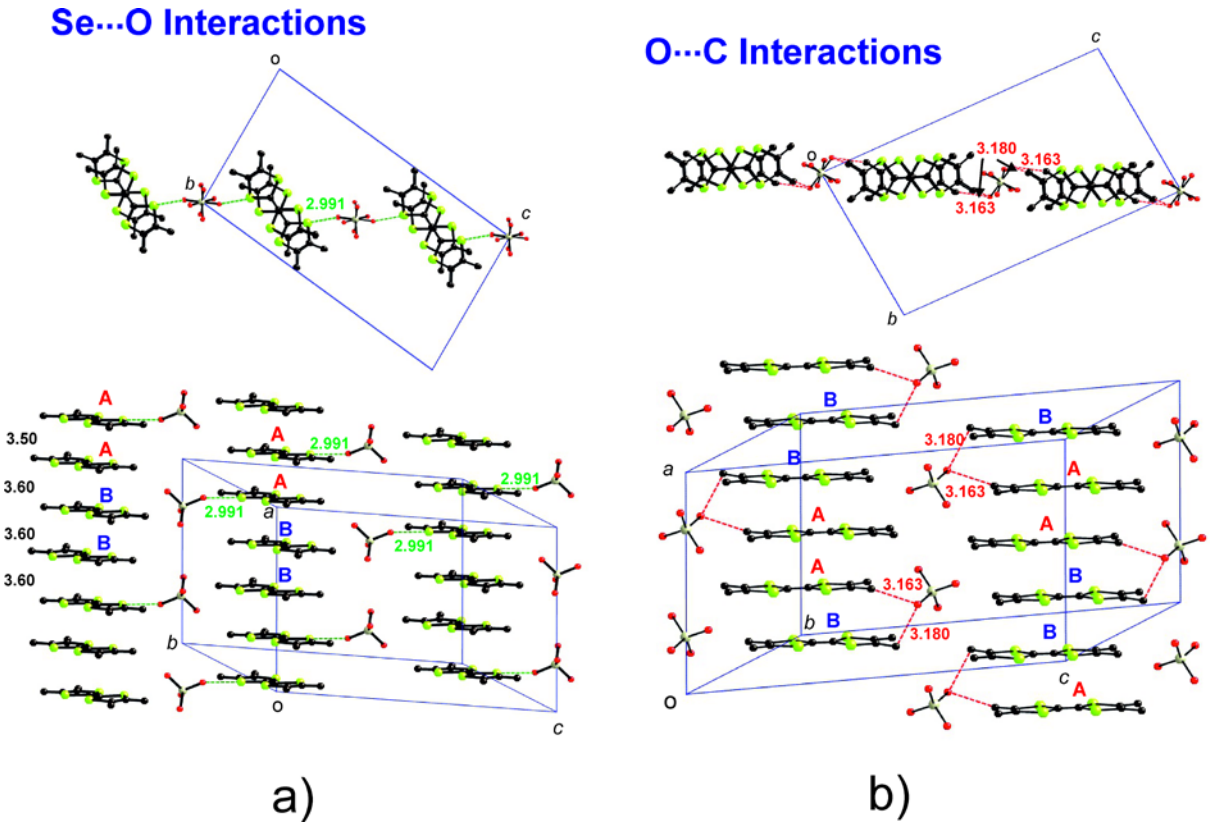

Figure 20. $2a\times2b\times2c$ AO superstructure of $(TMTSF)_2ReO_4$ at 120 K viewed with two different orientations. (a) A single (a,b-c) anion-donor layer with the strongest $Se_{donor}\cdots O_{anion}$ interactions shown. (b) A single (a,b+c) anion-donor layer with the strongest $C_{methyl}\cdots O_{anion}$ interactions indicated. Inter-planar distances between TMTTF donors are indicated on the left stack of (a). Note that in the two representations AB dimers face the individual anions. Figure drawn using the atomic coordinates of ref. [121].

Now let us concentrate on the donor stacks with an AABB donor sequence along the stack direction corresponding to the $2k_F$ wavelength. $(TMTSF)_2ReO_4$ exhibits also an acoustic-like $2k_F$ modulated shift of the position of donors (0.02 Å and 0.06 Å along the a and c directions, respectively [121-122]) of amplitude comparable to that of the $2k_F$ BOWs in the Peierls ground state of TTF-TCNQ. In $(TMTSF)_2ReO_4$, the TMTSF shifts modulate the inter-dimer distances into a short A-A (3.5 Å) and a long B-B (3.6 Å) inter-planar distances (the inter-planar distance of the AB dimer is 3.6 Å). These shifts significantly modulate the inter-dimer transfer integral, of 0.25 meV in the average structure, to $t_{AA}\approx 0.28$ meV and $t_{BB}\approx 0.20$ meV in the AO structure, while the AB dimer transfer integral remains of $t_{AB}\approx 0.27$ meV in both the average and the AO structures. [123-124]

Thus, the anion ordering and shift leads to a strongly modulated donor-anion interactions along the stack direction, with only one $Se_{donor}\cdots O_{anion}$ short contact with A type donors. Due to the $Se_{donor}\cdots O_{anion}$ contact modulation, the anion develops a Hartree potential acting on the 1D electron gas, which should induce a $2k_F$ CDW with a hole excess on type A donors and an

electron excess on B type ones along the stack direction. The surprising result is that this induced CDW is out of phase with the $2k_F$ CDW associated with the $2k_F$ BOW stack modulation in which there is an excess of holes on the longer B-B contact where the transfer integral (t_{BB}) is the smallest one and an excess of electrons on the shorter A-A contact where the transfer integral (t_{AA}) is the largest one.[86] As schematically indicated in Fig. 15, there is a near cancellation of the two charge modulation waves such that the stacks basically exhibit only a $2k_F$ BOW modulation. This near charge cancellation, which agrees with the observation of similar intra-molecular distances for A and B molecules [118], should minimize the Coulomb interactions. In agreement with this finding it appears also that the Peierls gap which opens below T_{AO} is basically due to the $2k_F$ BOW modulation of the intra-stack transfer integrals [124]. Note that a majority BOW modulation apparently occurs in the metal-insulator AO phase transition of $(DMEDO\text{-}TTF)_2X$ (X = ClO_4 and BF_4) which stabizes a staggered anion order along the stack direction below ~200 K. [112]

If one assumes that the AO gap of $(TMTSF)_2ReO_4$, $2\Delta_{AO} \approx 180$ meV, is given by the same weak coupling BCS type expression as for a standard Peierls transition (eq (2)) one obtains an effective donor-anion coupling constant of $\lambda_{DA} \approx 0.38$, nearly two times larger than the electron-phonon coupling constant $\lambda_{ep} \approx 0.22$ estimated for TMTSF-DMTCNQ in section II.C. The sizeable value of λ_{DA} implies a stronger coupling than for a simple Peierls transition, in agreement with the observation of a 1st order AO transition (Fig. 19a). Indeed, λ_{DA} should include both the electron-anion coupling λ_{eA} (variation of anion potential induced by the staggered ordering of the ReO_4 [116,125]) and the electron-phonon coupling λ_{ep} involved in the BOW deformations of the TMTSF stacks which is comparable to the ones of AD charge transfer salts.

The AO transition of $(TMTSF)_2ReO_4$ is announced by pre-transitional q_{AO}^1 lattice fluctuations starting around $T_{AO}^{fl} \sim 250$ K (Fig. 19a). At ambient pressure the AO transition occurs in the temperature range where the electron gas is 1D (above $T^{el}_{1D\rightarrow 2D} \sim 100K$). Thus, the 1D stacks should exhibit $2k_F$ CDW/BOW diverging fluctuations below T_{AO}^{fl}. These $2k_F$ fluctuations, which modulate the molecular positions, should open a pseudo-gap in the electronic density of states at the Fermi energy (the pseudo-gap is the precursor of the Peierls gap which opens below T_{AO}). The formation of a pseudo-gap below T_{AO}^{fl} is revealed by an upturn in the thermal dependence of the resistivity (Fig. 19b). Such features are commonly observed in standard Peierls systems. [70]

Under pressure the enhancement of the FS warping increases drastically the 1D to 2D crossover ($T^{el}_{1D\rightarrow 2D}$) of the electron gas. Then, $T^{el}_{1D\rightarrow 2D}$ should reach a temperature comparable to T_{fl} around 10 kbar. [60] Consequently, at this pressure the 1D $2k_F$ instability should stop its divergence and $2k_F$ electronic processes should not contribute anymore to the AO. Thus, a new AO superstructure, characterized by the $q_{AO}^2 = (0,1/2,1/2)$ wave vector, which does not involve any more the $2k_F$ component of the modulation, is stabilized. [126] Since there is no opening of a Peierls gap for the q_{AO}^2 AO process, $(TMTSF)_2ReO_4$ remains metallic under such circumstances. In addition, with the restoration of a metallic ground state down to low temperatures, superconductivity is observed with a $T_S \sim 1.5$ K. [127-128]

$(TMTSF)_2ClO_4$. The coupling between anion and donor stacks is weaker than in $(TMTSF)_2ReO_4$ as shown by the fact that in its RT average structure the shortest $Se_{donor}\cdots O_{anion}$ contact is considerably closer (3.34 *vs*. 3.16 Å) to the sum of Se and O van der Waals radii (3.4Å). As a consequence, even if a q_{AO}^1= (1/2,1/2,1/2) short range anion order develops below ~ 250 K, [129] it is never stabilized into the q_{AO}^1 superstructure observed in $(TMTSF)_2ReO_4$. Furthermore the q_{AO}^1 short range order vanishes below 50 K and a new q_{AO}^3 = (0,1/2,0) short range anion order develops critically below 40 K, and is ultimately stabilized as an $a\times 2b\times c$ superstructure below T_{AO} = 24 K if the sample is slowly cooled (relaxed samples). [130] This AO order which does not involve the $2k_F$ wave vector component keeps the metallic state, and even achieves a better conducting state below T_{AO} (Fig. 4) since the scattering process of carriers due to the presence of disordered anions is suppressed.

The q_{AO}^3 AO of $(TMTSF)_2ClO_4$ is also noticeably different from the q_{AO}^1 AO of $(TMTSF)_2ReO_4$ in what concerns the displacement direction of the anions: the anions shift now away from the Se atoms of the closest donor molecules, increasing the $Se_{donor}\cdots O_{anion}$ short contacts, and move along a perpendicular direction towards some of the methyl groups (Fig. 14b). [131] The anion shift within its cavity differentiates two kinds of TMTSF stacks along the 2*b* direction of the superstructure. The TMTSF stack towards which the ClO_4 moves is deformed, while the other TMTSF stack, away from the ClO_4 anions, remains regular. The shift induces strengthened anion-methyl group interactions, leading to a hole-rich TMTSF stack (see Fig. 14b), while the other TMTSF stack becomes electron rich. This process is associated with a charge transfer of about 0.025 holes between the two non-equivalent TMTSF stacks. [30,131] The two kinds of TMTSF stacks, having different band filling, lead to two sets of quasi-1D bands with different k_F wave vectors.[30] The FS of relaxed $(TMTSF)_2ClO_4$ is thus composed of four warped open FS sheets as shown at the right-hand part of Fig. 4. As each ($-k_F$, $+k_F$) pair of FS sheets concerns mainly one given stack that is spatially decoupled from the other one, there is no possibility in achieving a single $2k_F$ SDW modulation in the system below T_{AO}. As a consequence, $(TMTSF)_2ClO_4$ remains metallic below T_{AO} and becomes a superconductor below T_S ~ 1.4 K (left-hand part of Fig. 4) [14]. There is thermodynamic evidence that with the presence of nodes in the superconducting gap the superconductivity of $(TMTSF)_2ClO_4$ should be unconventional. [132]

To get the right anion orientation to achieve the q_{AO}^3 periodic order from a high temperature disordered state, anions must overcome a potential barrier of ~ 240 K, one order of magnitude larger than T_{AO}. Thus, kinetic effects control the perfectness of the AO superstructure. Consequently, the spatial extent of AO domains and the texture of the superstructure [88,133] depend very sensitively on the cooling rate through the AO transition. At the extreme limit of a very fast cooling (quenched sample) a very large fraction of the sample remains disordered holding embedded small AO domains which had no time to grow. In the absence of a long range superstructure a quenched sample keeps basically the typical band dispersion of Bechgaard salts with centrosymmetric anions. In particular its FS is made up of two sheets and can be nested, as for $(TMTSF)_2PF_6$ (see the right-hand part of Fig. 4). Consequently, quenched $(TMTSF)_2ClO_4$ stabilizes an insulating q_{nest} SDW ground state below ~ 6 K, whose T_{SDW} depends on the cooling rate (left part of Fig. 4). An interesting

question concerns the evolution of the nature of superconductivity as a function of the cooling rate [134] when the microstructure texture of the AO domains changes [88].

D. Role of anions in the charge localized and charge ordered phases of the Fabre salts.

1- General aspects

The $(TMTTF)_2X$ Fabre salts exhibit a very rich sequence of phase transitions whose critical temperatures depend upon the type of anion and of the nature (hydrogenated vs. deuterated) of the methyl groups forming the cavity. At ambient pressure all $(TMTTF)_2X$ salts exhibit a progressive $4k_F$ BOW/dimer-Mott charge localization (Fig. 9d) resulting in an activated conductivity with a well-defined energy Δ_{BOW} below T_ρ ~ 200-300 K (Fig. 3). [12,27,135] In fact as Δ_{BOW} is comparable to T_ρ, each hole remains weakly localized on the dimers. [136] However, the amplitude of the $4k_F$ BOW charge modulation increases upon cooling as revealed by the enhancement below T_ρ of the integrated intensity of vibronic absorption lines in $(TMTTF)_2PF_6$. [137] The charge localization on the dimers keeps the $P\bar{1}$ crystal symmetry. The inversion symmetry is lost in all the Fabre salts, except perhaps $(TMTTF)_2ClO_4$, at a lower temperature when a $4k_F$ CDW/CO modulation is set (Fig. 9c) after a second order phase transition whose critical temperature T_{CO} strongly depends upon the nature of the anion. The CO transition of the SbF_6 salt is really a metal-insulator phase transition, whereas the CO transition of the other salts occurs in the charge-localized state. [27] In the $(TMTTF)_2SCN$ salt the CO and AO transitions coincide.

Table I: Transition temperatures (K) of the CO (T_{CO}), AO (T_{AO}), SP (T_{SP}) and AF (T_N) phase transitions in various Fabre salts in function of the anion X and of the hydrogenated ($X\text{-}H_{12}$) or deuterated ($X\text{-}D_{12}$) nature of the donor. T_ρ is the charge localization crossover temperature.

Salt	T_ρ	T_{CO}	T_{AO}	T_{SP}	T_N
$PF_6\text{-}H_{12}$	250	67 (local measure)	/	16.4	/
$PF_6\text{-}D_{12}$	?	87	/	13	/
$AsF_6\text{-}H_{12}$	230	102	/	11.1	/
$AsF_6\text{-}D_{12}$	250	117	/	?	/
$SbF_6\text{-}H_{12}$	/	154	/	/	8
$SbF_6\text{-}D_{12}$	/	168	/	/	?
$ReO_4\text{-}H_{12}$	RT	230	155	/	/
$ReO_4\text{-}D_{12}$	?	237	155	/	/
$BF_4\text{-}H_{12}$	200	85	40	/	/
$ClO_4\text{-}H_{12}$	230	/	76	/	/
$SCN\text{-}H_{12}$	250	160	160	/	7

Below T_{CO} local probes such as NMR [94,138] and infrared adsorption [139-140] reveal the presence of two types of differently charged TMTTF molecules. A recent X-ray determination of the valence electron density distribution [141] shows that the charge poor molecule (with on average 0.5 - δρ holes) and charge rich molecules (with on average 0.5 + δρ holes) alternate along the stack direction (with an intermolecular charge difference of 2δρ ≈ 0.4 holes for the PF_6 salt), a charge pattern expected for a $4k_F$ CDW/CO modulation (Fig. 9c).

The symmetry breaking at the CO transition opens a $4k_F$ CDW-CO gap, $2\Delta_{CO}$, which adds in quadrature with the $4k_F$ BOW-Mott dimer gap, $2\Delta_{BOW}$, already present above T_{CO} (Fig. 3). The amplitude of intermolecular charge disproportion δρ increases almost linearly with Δ_{CO}. [120] As the charge disproportion superimposes a $4k_F$ CDW-CO modulation on a $4k_F$ BOW/dimer-Mott modulation, the resulting charge pattern has no inversion symmetry as shown in Fig. 15b, the donor stack is polar and since the modulations for all neighboring stacks are in-phase, the CO structure should be ferroelectric (the only exception is the SCN salt where the inter-chain staggered q_{AO}^2 AO [142] coinciding with the CO imposes an antiferroelectric order). Although ferroelectricity has not yet been confirmed by polarization measurements, the dielectric constant exhibits a divergence at T_{CO} [143-144] (as a matter of fact such dielectric divergence was first observed many years before by microwave measurements.[145]) The real part of the dielectric constant measured in the stack direction reaches giant values (ε_a ranging between $2\cdot10^6$ [144] - $3.5\cdot10^4$ [146] at 100 KHz for the AsF_6 salt), while the quasi-static dielectric constant measured along the interlayer c^* direction, including the anions and their interaction with the methyl groups, is about three orders of magnitude smaller, $\varepsilon_{c^*} \sim 250$ [147]. Such a strong anisotropy shows that ε_a mostly probes the charge response due to the electronic CO while ε_{c^*} probes the charge response of the anion sublattice.

2- Influence of anions through the S···F interaction in the charge localization process.

The charge localization phenomenon in the Fabre salts is not surprising because the closely related quarter-filled system TMTTF-DMTCNQ exhibits a dominant $4k_F$ BOW instability.[86] Also as pointed out in section II.D, the $4k_F$ BOW modulation or stack dimerization, which can be viewed as stabilizing the above quoted $4k_F$ instability as a response to the $4k_F$ anion lattice potential, is accompanied by a $4k_F$ charge localization on the dimers below T_ρ. [78-79]

The direct role of anions in the charge localization process has been recently demonstrated by means of an X-ray absorption fine structure (NEXAFS) investigation of $(TMTTF)_2AsF_6$. [148] Fig. 21 left and center shows the F1s and S2p NEXAFS spectra of this salt as a function of the temperature. Upon cooling, the F1s spectra of the AsF_6 salt shifts downward in energy while the S2p spectra of the TMTTF shifts upward. The increase of separation between the S and F levels directly shows the occurrence of a strengthening of $F_{anion}\cdots S_{donor}$ electronic interactions. Such an effect is not due to lattice thermal contraction because no thermal shift of the F1s spectra is observed in $(TMTSF)_2PF_6$ (Fig. 21 right). [149-150] Consequently, the

increase of the $F_{anion}\cdots S_{donor}$ electronic interaction in $(TMTTF)_2AsF_6$ detected in these NEXAFS experiments must to be linked to the charge localization.

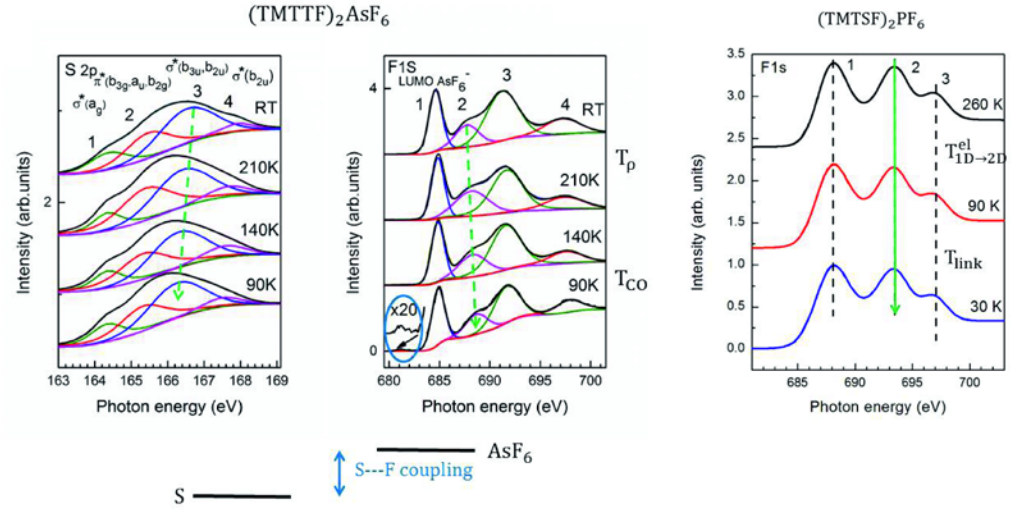

Figure 21. Thermal dependence of the sulfur and fluorine NEXAFS spectra of $(TMTTF)_2AsF_6$ (left and center) and of the F NEXAFS spectra of $(TMTSF)_2PF_6$ (right). The green arrows indicate the direction of energy shift in the spectra. The T_ρ ~ 230 K and T_{CO} = 102 K for $(TMTTF)_2AsF_6$ are indicated as well as $T^{el}_{1D\rightarrow 2D}$ ~ 100 K and T_{link} ~ 55K for $(TMTSF)_2PF_6$. The blue ellipse in the middle figure shows the onset of an additional fluorine transition in the CO phase of $(TMTTF)_2AsF_6$ (Figures adapted from [148] (Copyright 2015 by the Royal Society of Chemistry) and [149] (Copyright 2016 by the American Chemical Society)).

3- Structural aspects of the CO transition.

The CO transition in Fabre salts with centrosymmetric anions is accompanied by a symmetry breaking transition removing all the inversion centers of the $P\bar{1}$ high temperature structure. [141] This is associated with a $4k_F$ disproportion charge pattern alternating charge-rich and charge-poor TMTTF donors in the dimerized stack direction. [138-139] Since the $4k_F$ CDW-CO and the $4k_F$ BOW-Mott-dimer order parameters, which are of different symmetry (see Figs. 9c and 9d), are competing, a relative decrease of the $4k_F$ BOW stack dimerization of ~ 2% is observed below T_{CO} in in $(TMTTF)_2PF_6$ [141] (this quantity is defined here by the ratio between intra- to inter-dimer transfer integrals).

The 3D CO phase transition keeps the same unit cell volume. The intra unit cell structural deformation accompanying the CO is evidenced by a weak change of the intensity of Bragg reflections up to ~15% for $(TMTTF)_2PF_6$-D_{12}. [151] Furthermore, lattice expansion coefficients, exhibit anomalies at T_{CO} related to the specific heat anomaly expected for a second-order phase transition. [91] The CO transition of the SbF_6 salt exhibits a giant lambda type critical anomaly (Fig. 22a) [92] while the CO transition of the AsF_6 and PF_6 salts exhibit a mean-field jump. These effects are more visible for the lattice expansion coefficient measured in the interlayer c^* direction (Fig. 22b).[90]

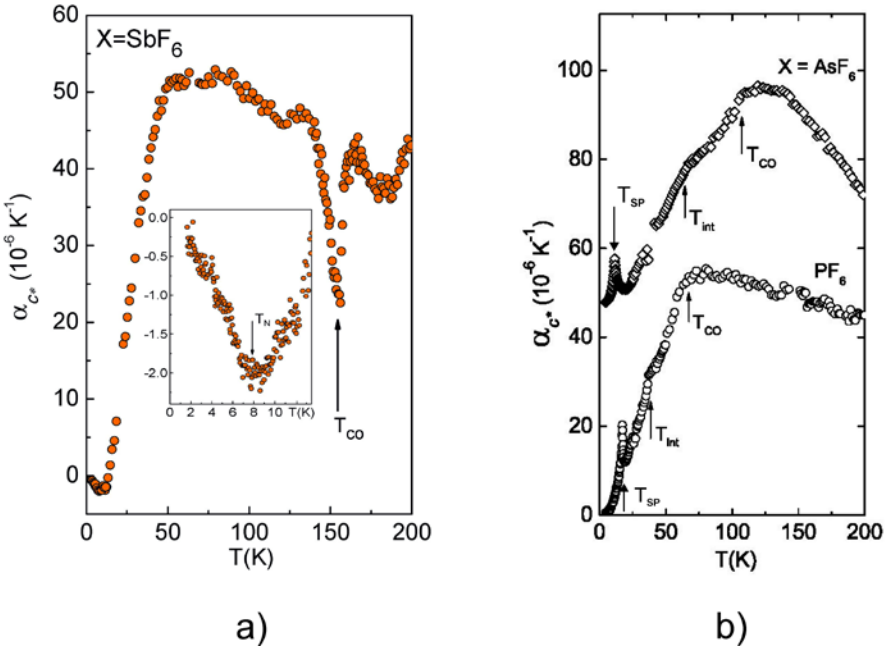

Figure 22. Thermal dependence of the uniaxial lattice expansion along the *c**-axis in (a) $(TMTTF)_2SbF_6$ (from the data of ref. [91] (Copyright 2013 by IOP Publishing), and (b) $(TMTTF)_2AsF_6$ and $(TMTTF)_2PF_6$ (from the data of ref. [152] (Copyright 2009 by Elsevier)). The T_{CO} and T_{SP} values of $(TMTTF)_2AsF_6$ and $(TMTTF)_2PF_6$ as well as the T_{AF} value of $(TMTTF)_2SbF_6$ are indicated. In $(TMTTF)_2AsF_6$ and $(TMTTF)_2PF_6$, T_{int} probably corresponds to the temperature of linkage of the anions to the methyl groups.

a. Specific role of the anions. Anions must play a specific role during the lattice deformation process consisting in the stabilization of a 3D structure built from a 1D (i.e. stack) donor charge pattern. One expect in particular that anions should interact with the π hole charge disproportion pattern on the donor stacks. In this respect a downward energy shift of the F1*s* core level in the photoemission spectra is observed when crossing the CO transition of $(TMTTF)_2SbF_6$ (Fig. 23).[153] The increase of the binding energy of the F1s core level spectra should be caused by the shift of the anion towards the hole-rich donor. In addition, the strengthening of the donor-anion interaction is probably responsible for the presence of an additional F1*s* peak in the NEXAFS spectra of $(TMTTF)_2AsF_6$ below T_{CO} (blue ellipse in Fig. 21) [148] It has been suggested that such peak originates from the hybridization between the anion LUMO and the unoccupied part of the donor's HOMO conduction band.

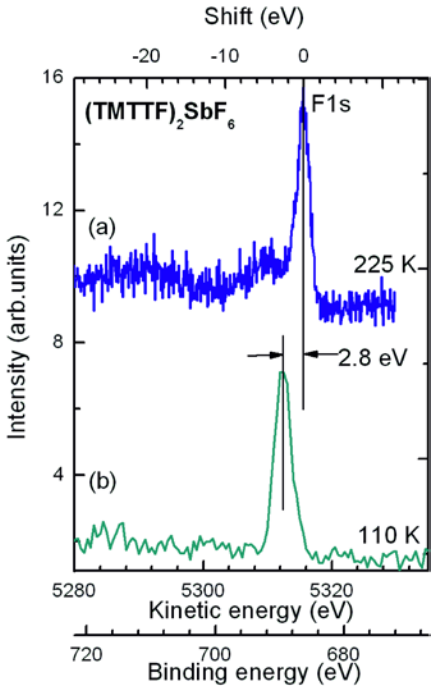

Figure 23. Fluorine 1s core level spectra of $(TMTTF)_2SbF_6$ above and below its CO transition at T_{CO}= 154 K (from reference [153] (Copyright 2014 by EDP Sciences)).

The collective role of anions in the ferroelectricity mechanism is assessed by the divergence of the transverse dielectric constant ε_{c*} at T_{CO} [147]. Observation of the strongest anomaly of the lattice expansion coefficient along c* as well as of the critical divergence of ε_{c*} means that anions participate in the ferroelectric phase transition through the breaking of the inversion symmetry via a reorganization of the interactions in the methyl group cavity (see below). The resulting modulation pattern including a phenomenological anion displacement below T_{CO} is schematically represented in Fig. 15b. Such a CO ground state can be obtained by minimization in the adiabatic approximation of the 1D correlated electron gas Hamiltonian incorporating the Coulomb coupling between anions and holes on the donor stacks. [81]

b. Lattice deformation below T_{CO}. On a local scale each anion can move inside its own methyl group cavity (Fig. 5) (i) either toward the S atom of one close donor (Fig. 14a) or (ii) towards the methyl groups of another set of donors (Fig. 14b). These two displacements are different so that the location of the hole-rich donor depends upon which shift (or combination of shifts) really occurs.

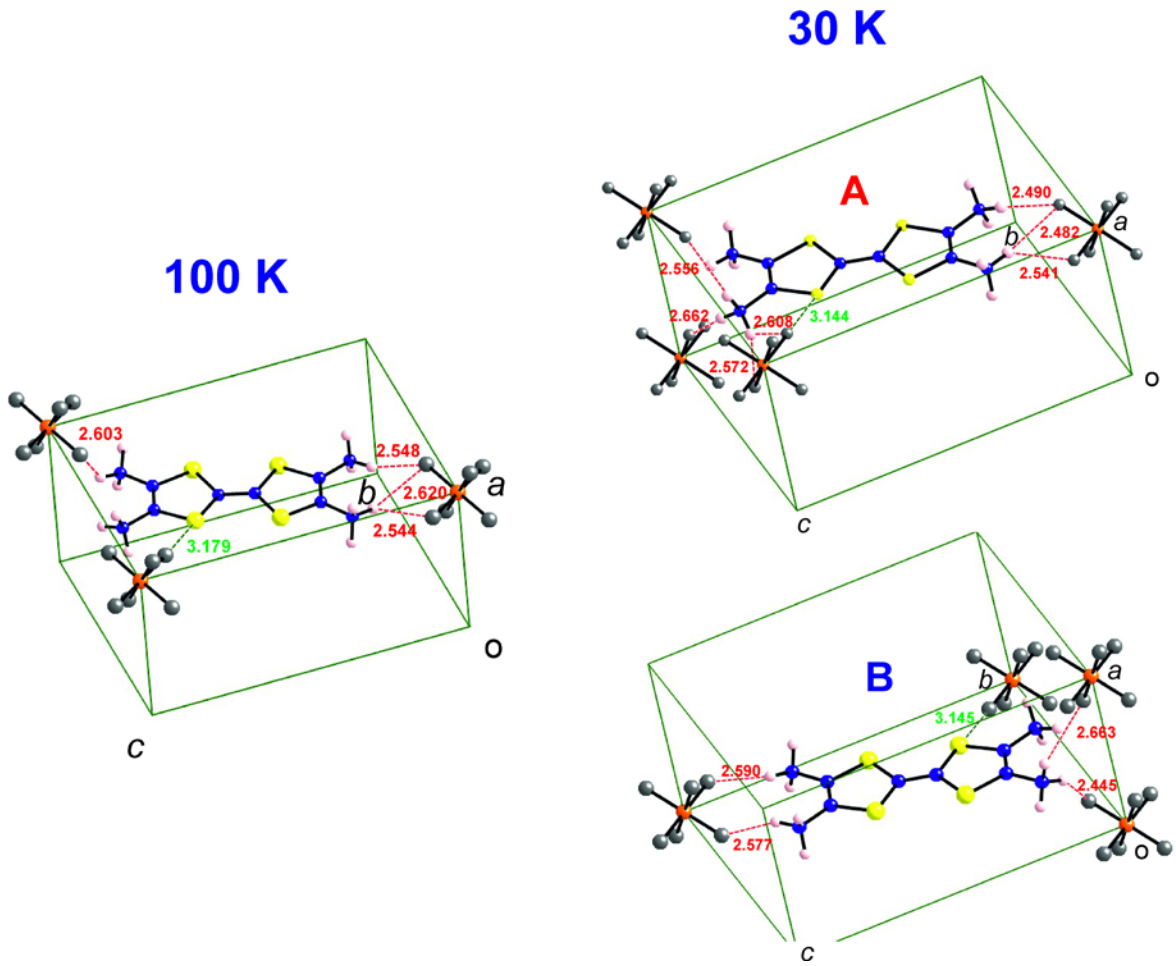

Figure 24. Structure of $(TMTTF)_2PF_6$ at 100 K, in the charge localized state, and at 30K, in the CO state. At 100 K only one of the two TMTTF molecules related by inversion symmetry is represented with its PF_6 environment. At 30 K environments of the hole-rich TMTTF molecule (A) and of the hole-poor one (B) are represented separately. The C-C central bond length as well as the shortest $S_{donor}\cdots F_{anion}$ and $F_{anion}\cdots H_{donor}$ distances are indicated in black, green and red, respectively (drawn from the structural refinement of ref [141] with atomic coordinates kindly provided by H. Sawa).

The $P1$ structure of the CO ground state of $(TMTTF)_2PF_6$ has been recently refined at 30 K, i.e. below T_{int} when the thermally activated motion of methyl groups is frozen. [141] Fig. 24 compares this structure with the $P\bar{1}$ structure of the charge localized state at 100 K above T_{CO}. Although there is a global shortening of the $S_{donor}\cdots F_{anion}$ distance by 0.034 Å between the two temperatures, $S_{donor}\cdots F_{anion}$ contact distance does not really differentiate type A (hole-rich) and type B (electron-rich) donors below T_{CO}. This means type (i) shift is not relevant for the CO transition while, type (ii) shift, i.e. anion displacement towards the methyl groups, should be the pertinent one. Indeed, there are seven $F_{anion}\cdots H_{donor}$ short contacts towards the hole-rich molecule A but only four towards the hole-poor molecule B (see Fig. 24). In addition, the average $F_{anion}\cdots H_{donor}$ contact distances between the left and right sides of

TMTTF are more differentiated for type A molecules (2.60 Å *vs*. 2.50 Å) than for type Bones (2.55 Å *vs*. 2.58Å) leading to a larger polarization for A than for B. In fact, Fig. 25 shows more precisely that the lattice deformation at the CO transition (as determined for $(TMTTF)_2PF_6$ [141]) is quite subtle because the establishment of the $F_{anion}\cdots H_{donor}$ short contacts originates basically from rotations of the methyl groups.

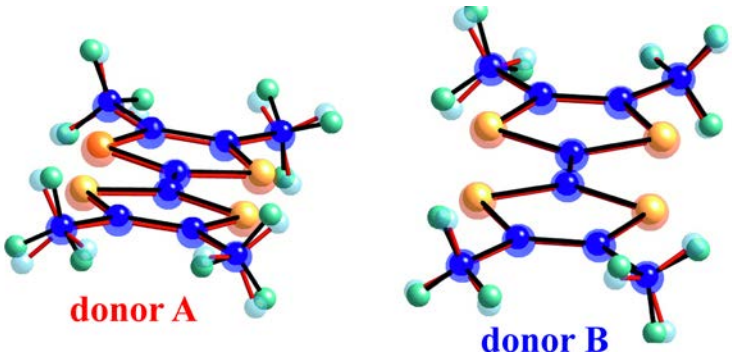

Figure 25. Modification of the shape of the donor molecules in $(TMTTF)_2PF_6$ between 100 K and 30 K (drawn from the structural refinement of ref [141], with atomic coordinates kindly provided by H. Sawa). For every donor molecule the structure at 100K and 30 K are superposed. The structure at 100 K is drawn with larger and more translucent atoms as well as with bonds in red.

The importance of the anion-methyl group interactions for the occurrence of the CO transition is also inferred from:

(i) The strong variation of T_{CO} with deuteration of the methyl groups (see Table I), and

(ii) The very strong sensitivity of the CO transition to X-ray irradiation damages affecting primarily the more mobile species. [154-155]

c. Anion-donor interaction. In fact the interaction of the anion with the methyl groups is not clearly defined as Fig. 24, suggests because T_{CO} occurs in the temperature range where SbF_6, AsF_6 and PF_6 anions are not yet linked to the methyl groups (T_{CO} is above T_{int}, see Fig. 22a). In addition the CO transition occurs in the temperature range where the anomalous behaviour of the lattice expansion (Fig. 22) indicates either that the reorientation jump of SbF_6 anions is still activated or that the rotation movement of AsF_6 anions just starts to freeze. Also in the case of non-centrosymmetric anions, T_{CO} occurs in the temperature range where the orientation of the ReO_4 or BF_4 anions is still disordered (i.e. $\underline{T}_{CO}$ is above T_{AO}, see table I). However, far infrared measurements show that there is a modification of the C-C-H and H-C-H methyl bending modes in the vicinity of T_{CO} which could rely on a modification of the coupling with the anions. [140] Also several H-C-H methyl bending modes become Raman active below T_{CO} where the inversion symmetry is broken, indicating some kind of ordering of the methyl groups due to their interaction with the anions.

In the temperature range where neither the methyl groups nor the anions are completely ordered the anion-donor interaction can be quantified by the misfit of the anion in its cavity. For octahedral and orientationally disordered tetrahedral anions whose shape can be approximated by a sphere in presence of thermally disordered methyl groups, this can be simply defined as the radii difference: [156]

$$\Delta R = R_C - (R_a + R_{Me}), \qquad (5)$$

where R_C is the cavity radius (the distance between the central atom of the anion located on the inversion centre of its cavity and the C atom of the nearest methyl group), R_a is the anion radius (approximated by its van der Waals radius) and R_{Me} is the van der Waals radius for a methyl group (≈ 2 Å). ΔR is a negative quantity which basically decreases when the size of the anion increases. Fig. 25 shows that T_{CO} increases as ΔR becomes more negative. The only exception is $(TMTTF)_2ClO_4$ where in contrast with the ReO_4 and BF_4 salts incorporating also tetrahedral anions, the CO/ferroelectric transition is not observed. [157-158] The reason for the absence of CO effects is not clear. A possible explanation could be that the AO transition first occurs in this salt (red segment in Fig. 26).

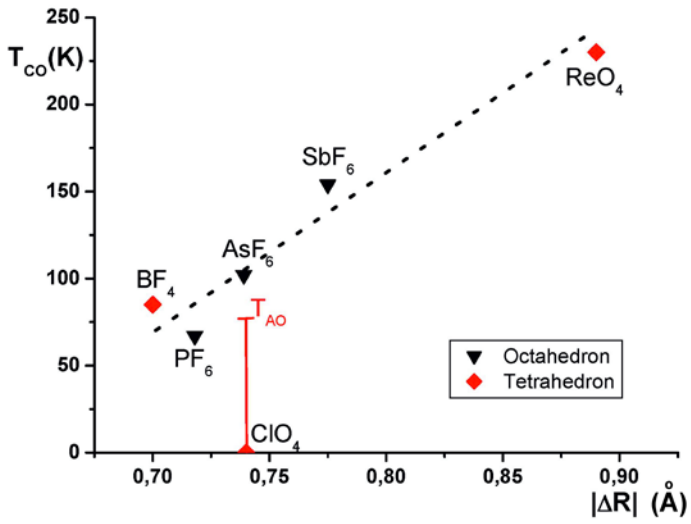

Figure 26. Variation of T_{CO} for the Fabre salts at ambient pressure as a function of the modulus of the anion misfit radius |ΔR| in its methyl group cavity.

d. Phenomenological model

Table I shows that T_{CO} strongly depends upon the size of the anion and the nature of its interface with donors via the hydrogenation or deuteration of the methyl groups. This means that these structural degrees of freedom should control the mechanism of the CO transition.

T_{CO} can be qualitatively accounted for [28] if one considers the CO transition as resulting from the $4k_F$ Peierls-like transition of a strongly correlated fermion gas in interaction with the

anions. If one assumes that the $4k_F$ CDW or CO instability is that of a gas of spin-less fermions, in the adiabatic limit and using the mean field approximation, an expression for T_{CO} [159] similar to the BCS-type expression found the $2k_F$ Peierls transition (see eq. (2)):

$$T_{CO} = C' E_F^* e^{-1/2\lambda_{eA}} \quad (6)$$

where the reduced electron-anion coupling constant λ_{eA}replaces the electron-phonon coupling constant of the Peierls transition. Assuming that there is a coupling g_{eA} to the anion whose vibration mode in its cavity is of frequency Ω_{anion}, one gets:

$$\lambda_{eA} = \frac{{g_{eA}}^2 N_{SL}(E_F^*)}{\hbar\Omega_{anion}}, \quad (7)$$

where $N_{SL}(E_F^*)$ is the density of states of spin-less fermions of Fermi energy E_F^*. In the following we assume that anion vibration modes are described by an Einstein oscillator of frequency:

$$\Omega_{anion} \propto \sqrt{\frac{V''}{M_X}}, \quad (8)$$

where M_X is an effective anion mass depending of the type of vibration and *V''* is the curvature of the potential experienced by the anion in its cavity.

In this crude model two parameters control the value of λ_{eA} given by expression (7) and thus the value of T_{CO} in expression (6):

(i) the electron-anion coupling g_{eA} that increases with $|\Delta R|$, as given by expression (5),

(ii) the anion vibration frequency Ω_{anion} that increases with the potential curvature *V''* according to eq. (8) i.e. when the misfit parameter of the anion in its cavity (also expressed by eq. (5), see also ref. [160]) becomes larger.

These two parameters act in opposite directions in the expression of λ_{eA} when $|\Delta R|$ varies. With the increase of the misfit parameter, $|\Delta R|$, g_{eA} increases as well as *V"* (Ω_{anion}). However Fig. 25 shows that at ambient pressure λ_{eA} and thus T_{CO} increases with $|\Delta R|$ whereas under pressure, when $|\Delta R|$ should increase, T_{CO} significantly decreases [88,161-162]. Thus, the decrease of T_{CO} under pressure should be attributed to the large increase of *V''* (Ω_{anion}) caused by the squeezing of the methyl group cavity which limits the volume needed to achieve the symmetry breaking of its structure.

An interesting peculiarity of the half-filled spin-less fermion model coupled to Einstein phonons is that the $4k_F$ Peierls transition can be suppressed by quantum fluctuations if the reduced electron-phonon coupling constant (λ_{eA} here) is not strong enough. [159,163]. This possibility could also explain the rapid vanishing of T_{CO} under pressure.

In this framework, the enhancement of T_{CO} upon deuteration (Table I) can be due either to an increase of the mediated electron-anion coupling by a modification of the cavity interface or by an increase of the potential curvature (deuteration is equivalent to a negative pressure in

the Bechgaard salts [48]; however such a finding is not confirmed by structural measurements performed in deuterated SbF_6 and ReO_4 Fabre salts [95]).

E. Additional low temperature phase transitions in the charge localized regime of the Fabre salts.

When the charges become localized below T_ρ and T_{CO}, the S = 1/2 spin degree of freedom on each hole remains active to promote a collective magnetic-like state at low temperature. In the case of salts with non-centrosymmetric anions, ordering effects also involve the anion's orientation degrees of freedom which add their effect to those of the spin degrees of freedom.

1- Fabre salts with centro-symmetric anions.

Fabre salts with centro-symmetric anions exhibit low temperature magnetic-type transitions towards either a spin-Peierls (SP) ground state, stabilizing a magnetic singlet below T_{SP}, or towards a more conventional AF order (Figs. 10 and 12). Note that the critical wave vector of the SP transition q_{SP} = (1/2,1/2,1/2) [164] is identical to that of the q_{AO}^1 AO transition, so that the same type of stack distortions are expected in both cases. A recent structural refinement of the SP distortion in $(TMTTF)_2PF_6$ reveals a tetramerization of the donor stack along the *a* and *c* direction, as found for $(TMTSF)_2ReO_4$, but with an amplitude of $\sim 2 \cdot 10^{-3}$ Å, [141] thirty times smaller than in $(TMTSF)_2ReO_4$ (see section III.C). This is in agreement with the very small intensity of the SP superstructure reflections. [164] Table I shows that these magnetic-type transitions occur at quite low temperatures. In particular, the SP transition (involving the $2k_F$ BOW order parameter, see Figs. 12b and 9a) is destabilized by the CO transition (involving the $4k_F$ CDW order parameter, see Fig. 9c). [161] Conversely, the SP transition should destabilize the CO one. In this respect, microwave dielectric measurements show a decrease of the CO gap by ~1 % at the SP transition of $(TMTTF)_2PF_6$-D_{12}. [165]. The anti-correlation effect between T_{SP} and T_{CO} has been rationalized by a Landau theory of phase transitions. [88] Also when T_{CO} is too large, as in the SbF_6 and SCN salts, the SP ground state, which cannot be stabilized, is replaced by an AF ground state (Fig. 12a). Under a modest pressure the CO state rapidly vanishes while T_{SP} is enhanced [161]. Under larger pressure the SP ground state vanishes at a quantum critical point (Fig 2a) [166], whose unexpected behavior is probably a consequence of (lattice and spin) quantum fluctuations not considered in this review. [67]

2- Fabre salts with non-centrosymmetric anions.

Non-centrosymmetric anions in Fabre salts order for entropy reasons at T_{AO} (Table I) as it is the case of Bechgaard salts. Among the Fabre salts with non-centrosymmetric anions, the SCN compound is particularly interesting because the AO transition, below which a huge gap of charge develops, [134,155], stabilizes the q_{AO}^2 = (0,1/2,1/2) superstructure. [142] Such structural instability enhances, for a strongly correlated system, the $4k_F$ CDW instability of the TMTTF stack as a response to the q_{AO}^2 anion potential (note that this potential caused by the staggered shift of the SCN anions towards the S atoms of the donors. [119] The q_{AO}^2 AO ground state thus coincides with the opening of a large CO gap in the charge degrees of

freedom. Since the AO transition of $(TMTTF)_2SCN$ stabilizes a CO ground state of $4k_F$ CDW symmetry below T_{CO} (Fig. 9c), there is a decrease of ~ 8% of the stack dimerization involving the competing $4k_F$ BOW order parameter (Fig. 9d). [119] Note also that the superimposition of the $4k_F$ CDW and $4k_F$ BOW modulations renders the stack polar as in the Fabre salts with octahedral anions below T_{CO} (see Fig. 15b). However, in contrastwith the later salts the staggered stack modulation and anion shift along transverse directions stabilizes an anti-ferroelectric ground state below T_{AO}.

In the salts with tetrahedral anions such as ReO_4, BF_4, and ClO_4, the AO transition stabilizes the q_{AO}^1 superstructure doubling the unit cell in all lattice directions. As q_{AO}^1 coincides with q_{SP}, an important consequence is the opening of a spin gap Δ_σ. In this respect the AO transition breaks the spin-charge decoupling of the CO transition. However as charges are not completely frozen (i.e. localized) at T_{AO}, the $2k_F$-type AO transition opens an additional gap of charge $2\Delta_{AO}$ that adds in quadrature to the $4k_F$ CO and BOW gaps already developed at T_{AO}. [144,155,157] However, since Δ_{AO} is comparable to Δ_σ [155] one should treat charge and spin degrees of freedom on the same footing in the mechanism of the AO transition. Finally, it is interesting to remark that AO and SP transitions are not necessarily coupled. In salts such as $(TMTSF)_2NO_3$ [155] and $(o\text{-}Me_2TTF)_2NO_3$ [113] incorporating the NO_3 anion which orders with a q_{AO} different from q_{AO}^1, the SP instability occurs below T_{AO}.

From the structural point of view the AO transition differs also from the CO transition. The q_{AO}^1 AO transition of the ReO_4 Fabre salt corresponds to an anion shift toward the S atom of a neighboring donor resulting in a shortening of the $S_{donor}\cdots F_{anion}$ contact as in the case of Bechgaard salts. [119] This anion shift occurs along a direction different from that of intra-cavity structural modifications associated with the CO transition (see section III.D). In contrast with the CO transitions, the methyl groups do not seem to be primarily involved in the AO transitions, as assessed by the observation that T_{CO} is not very sensitive to deuteration (see Table I) or to the presence of irradiation defects. [155]

Since CO and AO structural modifications add up their effects, a large enhancement of the gaps of charge and of charge disproportion below the AO transition are found for $(TMTTF)_2ReO_4$.[120,144,155,157] Interestingly one obtains $2\Delta_{AO} \approx 200$ meV for $(TMTTF)_2ReO_4$ [144,155] which is comparable to the AO gap that opens at T_{AO} for $(TMTSF)_2ReO_4$. However the q_{AO}^1 AO transition of the Fabre salts exhibits a substantial difference with the q_{AO}^1 AO transition of the Bechgaard salts: while in the latter the q_{AO}^1 anion potential induces a CDW which nearly cancels the $2k_F$ CDW modulation associated with the $2k_F$ BOW stack modulation (see section III.C), the Fabre salts experience a net charge modulation due to the supeposition of the $2k_F$ CDW modulation due to the q_{AO}^1 AO and the $4k_F$ CDW due to CO [119,120].

Finally, the important role of anion in these phase transitions has to be quantified by introducing explicitly the anion-electron Coulomb interaction in electronic Hamiltonian. This statement relies on two complementary observations:

(i) The total (half-) gap of charge $\Delta_{AO} \approx$ 135-175 meV that opens after the successive CO and AO transitions of $(TMTTF)_2ReO_4$ is comparable to the half-gap of charge which opens at the simultaneous CO-AO transition of $(TMTTF)_2SCN$. [144]

(ii) These two (half-) gaps which open after the AO transition are about three times larger than the (half-) gap of charge $\Delta_{CO} \approx$ 40-65 meV which opens at the individual CO transition of the Fabre salts with PF_6, AsF_6 and SbF_6 octahedral anions. [27,144,157]

IV. Charge ordering in δ-(EDT-TTF-CONMe$_2$)$_2$Br: The concerted action of anion shifts and hydrogen bonding modulation.

In section II we have explored the rich phase diagram of systems with three-quarter filled (or equivalently, one-quarter empty) 1D bands. We noted that one of the possible states is a $4k_F$ CDW leading to a doubling of the periodicity with charge ordering (CO), i.e. donors with an excess (+δρ) and deficit (-δρ) of charge alternating along the chain (Fig. 9c). Later, in section III, we have examined how these CDW/CO states are important in understanding the low-temperature behavior of the Fabre salts and the structural basis for their occurrence. In particular, we have shown the importance of the anion movements and the concomitant variation in the donor···anion connection through hydrogen bonding in stabilizing such CDW/CO states. The concerted action of anion shifts and hydrogen bonds is especially clear in the case of the δ-(EDT-TTF-CONMe$_2$)$_2$X (X= Br, AsF_6) salts [167]. EDT-TTF-CONMe$_2$ is a substituted derivative of EDT-TTF (see Figs. 1 and 27a) which is a hybrid of the TTF and BEDT-TTF donors.

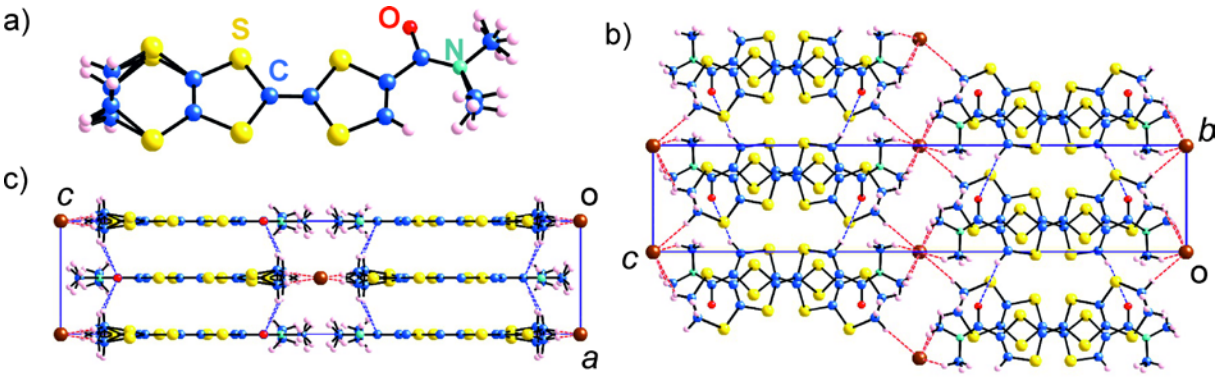

Figure 27. Room temperature *Pmna* average structure of the δ-(EDT-TTF-CONMe$_2$)$_2$Br salt: (a) EDT-TTF-CONMe$_2$ donor, (b) projection of the structure along the *a* axis showing the crisscross type of donors overlap and (c) projection of the structure along the *b* axis showing the uniform chains along *a*. Red and blue dashed lines refer to Br···H-C and O···H-C hydrogen bonds, respectively.[167] (Copyright 2009 from by The Royal Society of Chemistry)

The isostructural three-quarter filled δ-(EDT-TTF-CONMe$_2$)$_2$X (X= Br, AsF_6) salts exhibit room temperature activated conductivity and are Mott insulators. [167-169] However the Mott gap decreases under hydrostatic pressure and at 20/13 kbar the AsF_6/Br salts become

metallic. The contraction induced by the smaller anion Br^- is thus equivalent to a "chemical pressure" of approximately 7 kbar in stabilizing the metallic state. The room temperature *Pmna* average structure of δ-(EDT-TTF-$CONMe_2$)$_2$Br is shown in Fig. 27. [167] The unit cell contains one bromine ion and one independent donor. Note that in this average structure both the methyl groups of the NMe_2 group and the C_2H_4 fragment of the six-membered ring exhibit disorder. The bromine ion is connected to four donors in the same *bc* plane through hydrogen bonds with the ethylene groups of the six-membered rings (C_{Et}-H···Br) and with four donor molecules in planes above and below through longer hydrogen bonds (not shown in Fig. 27c) with methyl groups of the NMe_2 substituent (C_{Met}-H···Br). The donor stacks along *a* are completely uniform and adjacent donors exhibit a criss-cross type overlap (Fig. 27b). There are C_{Et}-H···O hydrogen bonds within the stacks and coplanar donors of adjacent stacks are also connected through C_{sp2}-H···O hydrogen bonds.

To further characterize the nature of the room temperature δ-(EDT-TTF-$CONMe_2$)$_2$X (X= Br, AsF_6) salts, ^{13}C NMR measurements were carried out in ^{13}C enriched single crystals. The variation of the spectra and the spin-lattice relaxation rate with temperature provided compelling evidence that both salts are in a charge ordered state already at room temperature. [167-169] The charge ordering appears to be exceptionally strong: the charge ratio (ρ_A/ρ_B) between the two non equivalent donor sites, A and B, is approximately 9:1, i.e. there is a localization of nearly one electron on every two donors. Thus, in chemical terms we can consider that these salts contain pairs of neutral/ionic donor molecules. Compared with the charge ordering phenomena of the TMTTF Fabre salts discussed above we emphasize the considerably larger charge imbalance in the present case, suggesting a strong coupling of the CDW/CO instability with the anion sublattice.

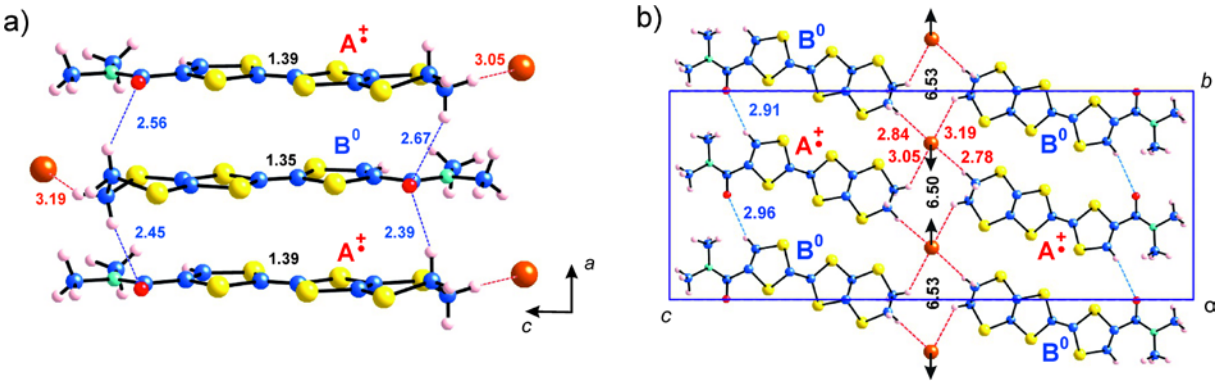

Figure 28. Room temperature *P2nn* structure of the δ-(EDT-TTF-$CONMe_2$)$_2$Br salt: (a) projection of the structure along the *b* axis showing one of the stacks; and (b) projection of the structure along the *a* axis showing one single *bc* layer. Red and blue dashed lines and distances refer to Br···H-C and O···H-C hydrogen bonds, respectively. The *cationic* and *neutral* donor molecules are labeled A^+ and B^0, respectively.[167] (Copyright 2009 from by The Royal Society of Chemistry)

As a consequence of these findings, the room temperature structure was reexamined using single crystal synchrotron X-ray measurements leading to a new structure (Fig. 28) based on the acentric *P2nn* group where two independent donors exhibit structural variations consistent with a large charge difference. The cell has doubled along the interstack *b*-direction (Fig. 28b) and the stacks along *a* are no longer uniform (Fig. 28a). The most outstanding difference with the average structure is the large difference in the inner C=C bond lengths of the TTF core, 1.354 vs 1.392 Å (see Fig. 28a), is in complete harmony with the above ^{13}C NMR results and suggesting a succession of neutral and positively charged donors along the *a*-direction. It is worth noticing that although the *P2nn* group allows any degree of dimerization along the stack direction, in practice, the dimerization is apparently quite small, i.e. the separation between planes along *a* amount to 3.550 and 3.563 Å. However, the difference in C_{Et}-H···O hydrogen bonds is significant (Fig. 28a). An important observation is that the C_{Et}-H···Br hydrogen bond is shorter for the donor molecule exhibiting the longer central C=C bond (Fig. 28a). As discussed in several parts of this work (see Figs. 14b or 34b for instance) an increase of the hole density is generally related to an increase in the hydrogen bonding strength of a given donor molecule through a subtle polarization mechanism which is also at work here. Thus, even if the interplanar spacing is very similar, the stacks along *a* exhibit a clear dimerization in contrast with the average structure.

Let us consider the structure within a *bc* layer (Fig. 28b). The dimerization along the *b*-direction is clearly seen when looking at the Br···Br distances, whose alternation leads to shorter C_{Et}-H···Br hydrogen bonds with the donor with the longer central C=C bond length, i.e. the formally cationic donor A^+. Again, the donor with the larger hole density is associated with the stronger hydrogen bonds. Still another aspect of the close relationship between hydrogen bonding and hole distribution appears when looking at the C_{sp2}-H···O hydrogen bonds at the other end of the donor. According to the polarization mechanism mentioned above, the donor with a C_{sp2}-H associated with the *stronger hydrogen bond* with the carbonyl group of the nearest donor must be associated with the *larger hole density*. Looking at Fig. 28b it is clear that this is indeed the case: donor A^+ is associated with the shorter (2.91 vs 2.96 Å) C_{sp2}-H···O hydrogen bond.

Consequently, the anion and the $CONMe_2$ substituent act concertedly to induce an alternation of neutral and positively charged donor molecules along the *b*-direction also. At the same time the out-of-phase displacement of the anions along *b* leads to an in-phase ordering of cationic and neutral donors along the *c*-direction to optimize both hydrogen bonding and electrostatic interactions (Fig. 28b). As noted before, there is also an alternation of neutral and positively charged donors along the *a*-direction (Fig. 28a) which is possible because of the anti-phase anion displacement in successive *bc* layers (see Fig. 29) that is essential for the stabilization of the charge ordered phase. Starting from the high temperature fully delocalized metallic state, the delocalized holes must be relocated in alternating donor molecules through the direct interaction between the donor HOMOs along *a*. The cooperation of both anions and $CONMe_2$ substituents allows such relocation to be induced concertedly

along the whole crystal structure (Fig. 29) providing a strong driving force for the CDW/CO structure.

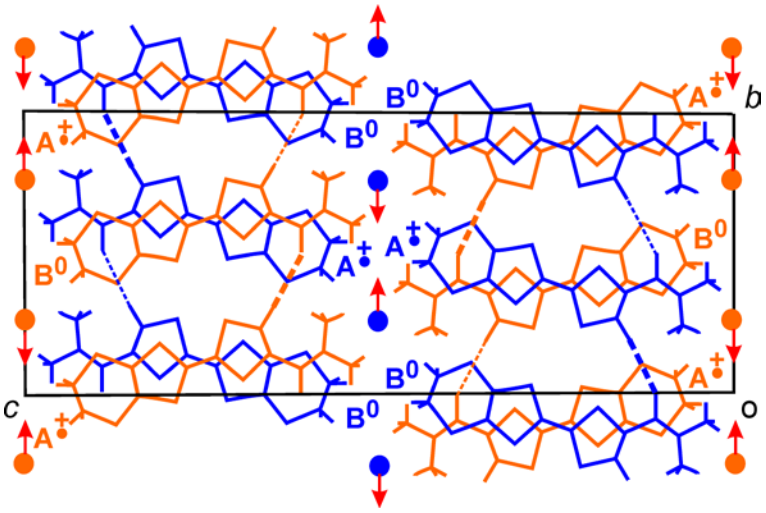

Figure 29. Schematic representation of the room temperature *P2nn* structure of the δ-(EDT-TTF-CONMe$_2$)$_2$Br salt showing the anti-phase anion displacement and its relationship with charge ordering. Blue and orange colors refer to molecules and anions in successive *bc* planes of the structure. The thick/thin dashed lines represent the stronger/weaker C_{sp2}-H···O hydrogen bonds. The *cationic* and *neutral* donors are labeled A^+ and B^0, respectively.[167] (Copyright 2009 from by The Royal Society of Chemistry)

In summary, the structural study clearly rationalizes that the development of a strong charge imbalance between two different donors of these salts is associated with *a concerted rearrangement of the hydrogen bonding network so as to dress the donor which will bear the larger hole density with the stronger set of hydrogen bonds*. As examined above for the Fabre salts and further developed in the next sections for several BEDT-TTF salts, this is a recurrent mechanism behind many charge ordering phenomena in molecular conductors which finds its origin in a subtle polarization mechanism of the donor molecules under the influence of the hydrogen bonded anions.

V. Role of the ethylene groups in structural and electronic instabilities of 2D (BEDT-TTF)$_2$X salts: case studies.

The preparation of the first BEDT-TTF salts [15-16,170-174] brought about an exciting new perspective to the field of molecular conductors. Up to this point molecular conductors were essentially uncovering a rich and novel 1D or pseudo-1D physics.[25-26] Because of the bulky outer ethylenedithio groups (see Fig. 30), the BEDT-TTF donors are usually not able to assemble in regular chain-like stacks, as for TMTSF or TMTTF salts, but in layers with substantial donor···donor interactions along several directions. As a result, their electronic structure is fundamentally different from those discussed in previous sections because the

bands around the Fermi level, i.e. those imposing the transport properties, exhibit substantial dispersion along several directions. The metallic BEDT-TTF salts thus usually exhibit closed Fermi surfaces and are not generally prone to the charge or spin density wave modulations discussed in previous sections. Thus, many of these salts keep their metallic behavior until very low temperatures and now and then they become superconducting. Actually, a large number of superconducting BEDT-TTF salts with different structural types have been prepared and characterized.[22]

A. Conformational flexibility of the outer ethylene groups in BEDT-TTF. A plethora of unexpected properties other than superconductivity have been reported for all structural families of BEDT-TTF salts with complex phase diagrams that have challenged chemists and physicists for a long time. In our opinion one of the more serious reasons behind the difficulty in rationalizing many of these observations has been the failure to recognize the essential role played by the supposedly *innocent* anions in guiding the structural and electronic properties of these salts. Anions are connected to the BEDT-TTF donors through a network of hydrogen bonds with the outer ethylenedithio groups (Fig. 6). The flexibility of the BEDT-TTF outer groups and the directionality of the hydrogen bonds with the anions lie behind numerous subtle structural variations at the donor-anion interface having a major influence on the structural and transport properties. In the following we will explore this question by considering some prototypical $(BEDT\text{-}TTF)_2X$ salts.

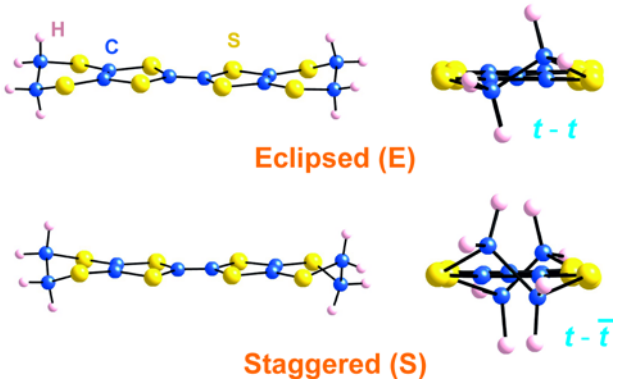

Figure 30. *Eclipsed* ($t - t$) and *staggered* ($t - \bar{t}$) conformations of the BEDT-TTF donor.

1- Ethylene groups and BEDT-TTF conformations. Because of the torsional strain associated with the outer six-membered rings of BEDT-TTF, conformations of such rings are quite puckered. The most stable one is the so-called *twist* form (*t*) in which the ethylene fragment is staggered. Viewing the six-membered ring along a direction perpendicular to the C=C double bond in the S-C=C-S plane, this conformation can be represented as in Fig. 31 (left). There are two different but equivalent *twist* conformations, t and $\bar{t}$, which can interconvert through a *boat* (*b*) conformation (Fig. 31 right) which is higher in energy with the ethylene group eclipsed. In between these two conformations there are two additional *half twist* (*ht*) and *tilted boat* (*tb*) conformations with intermediate energies. Whangbo and coworkers [175-176] found that the relative energies are roughly 0.0 (*t*), 0.6 (*ht*), 2.9 (*tb*) and

5.7 (*b*) kcal/mol. Thus, except for the *boat* form, the interconversion between different conformers requires only a modest energy.

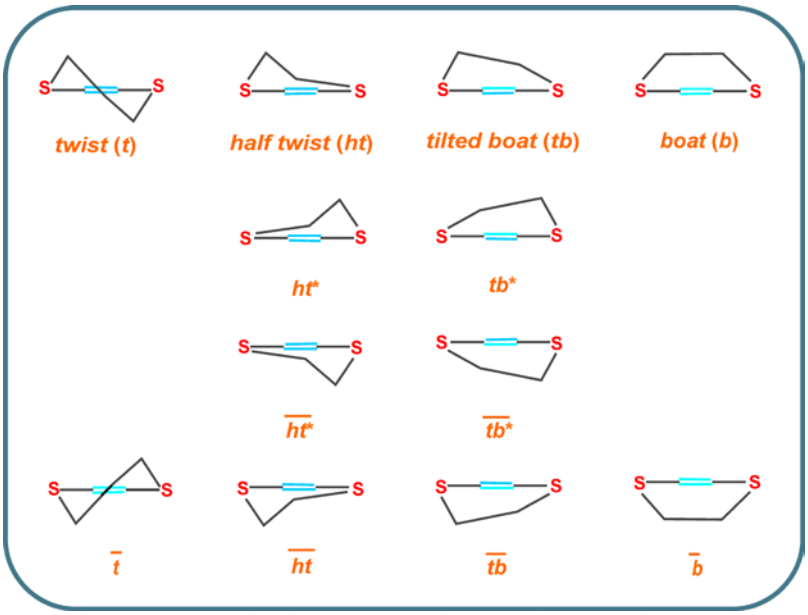

Figure 31. Labeling used to describe the different six-membered rings in BEDT-TTF salts.

When the six-membered ring is part of a larger organic molecule as in BEDT-TTF, it is convenient to distinguish different forms of the *twist*, *half twist*, *tilted boat* and *boat* ethylene group conformations according to the actual shape with respect to a reflection on two planes, one containing the S-C=C-S fragment and the other perpendicular to it. All these possibilities are noted in Fig. 31 with the same *t*, *ht*, *tb* and *b* labels and an additional sign, indicating the considered reflection plane (¯ for the plane containing the S-C=C-S fragment and * for the plane perpendicular to it). Since BEDT-TTF contains two six-membered rings we must consider different ways to combine the two conformations. For instance, assuming that both rings adopt the more stable *twist* conformation, there are two possible BEDT-TTF conformations: $t - t$ or *eclipsed* and $t - \bar{t}$ or *staggered* (Fig. 30). The energy difference between these two BEDT-TTF conformations is quite small, but the conversion from *t* to $\bar{t}$ requires an activation energy of approximately the energy difference between the *twist* and *boat* conformations. The similar stability of *eclipsed* and *staggered* conformations lies at the origin of the disorder exhibited by many BEDT-TTF salts.[44] Of course other combinations of conformations are also possible as it will be discussed in the following case studies.

To understand the conformations of the ethylenedithio groups in the actual crystal structures, one must take into account not only the intrinsic conformational preferences of individual six-membered rings, but also how these preferences may be modified by the presence of nearby anions and other donor molecules. BEDT-TTF usually interacts with neighboring anions through hydrogen bonds associated with hydrogen atoms on the ethylene groups. Neighboring donors can interact between them either through repulsive H···H or

attractive H···S interactions, again associated with the ethylene hydrogen atoms. [177] The global outcome of these interactions may easily cancel the intrinsic conformational preferences, conferring a remarkable adaptability of the ethylene end groups of BEDT-TTF to different environments. First-principles calculations of the interconversion between the eclipsed and staggered conformations of the BEDT-TTF donors in the κ-(BEDT-TTF)$_2$Cu[N(CN)$_2$]Br salt led to an activation energy of only 1.5 kcal/mol with very similar stabilities for the two conformations.[178] A few examples will illustrate the adaptability of BEDT-TTF donors to any type of environment. For instance, in the crystal structure of BEDT-TTF, one of the six-membered rings exhibits the most stable *twist* (*t*) conformation, but the other one looks like the less stable *boat* one (*b*). [179] Only the *eclipsed* $t - t$ (or $\bar{t} - \bar{t}$) form of BEDT-TTF occurs in β-(BEDT-TTF)$_2$IBr$_2$ [180], but one of the three independent molecules in α'-(BEDT-TTF)$_2$IBr$_2$ has the *staggered* ($t - \bar{t}$) conformation and two adopt the *eclipsed* one.[181] Interestingly, in β-(BEDT-TTF)$_2$I$_3$ at room temperature, one of the ethylene groups is disordered: BEDT-TTF occurs with almost equal probability with an *eclipsed* $t - t$ or *staggered* ($t - \bar{t}$) conformation. In contrast, under a pressure of 9.5 kbar disorder disappears and all molecules adopt a *staggered* conformation.[177]

2- Thermal crossover from ethylene disorder to commensurate order in κ-(BEDT-TTF)$_2$X phases. Let us now consider the κ-(BEDT-TTF)$_2$Cu[N(CN)$_2$]X (X = Cl, Br) phases to illustrate how the crystal structure of many BEDT-TTF based molecular conductors results from a delicate balance between several contributions. As mentioned above, the origin of the preferred eclipsed conformation for BEDT-TTF in this salt has been the subject of a first-principles DFT study.[178] However a more structurally based analysis is illuminating. The crystal structure of these phases has been the object of a large number of works [21,182-185]. At room temperature both salts exhibit conformational disorder in one of the terminal ethylene groups of BEDT-TTF. This aspect has been carefully studied in the more recent and comprehensive crystal structure studies adressing the evolution of disorder with temperature. According to the work of Hiramatsu et al [185] the evolution with temperature of the percentage of donors with an eclipsed ($t - t$) vs. staggered ($t - \bar{t}$) conformation is: 83% at 298 K, 84% at 250 K, 87% at 200 K and finally all donors exhibit the eclipsed conformation at 150 K in the κ-(BEDT-TTF)$_2$Cu[N(CN)$_2$]Cl salt. The κ-(BEDT-TTF)$_2$Cu[N(CN)$_2$]Br salt exhibits a similar trend but disorder is kept until very low temperatures (i.e. 97% at 9 K [184]). Both phases have the typical κ-type donor layers with BEDT-TTF dimers (see Fig. 7) where the two donors of each dimer are symmetry equivalent. In the following we consider the different anion···donor as well as donor···donor interactions occurring in κ-(BEDT-TTF)$_2$Cu[N(CN)$_2$]Cl whose competition mostly leads to the disorder and the stabilization of the eclipsed form at low temperatures, by using the crystal structures of ref [185].

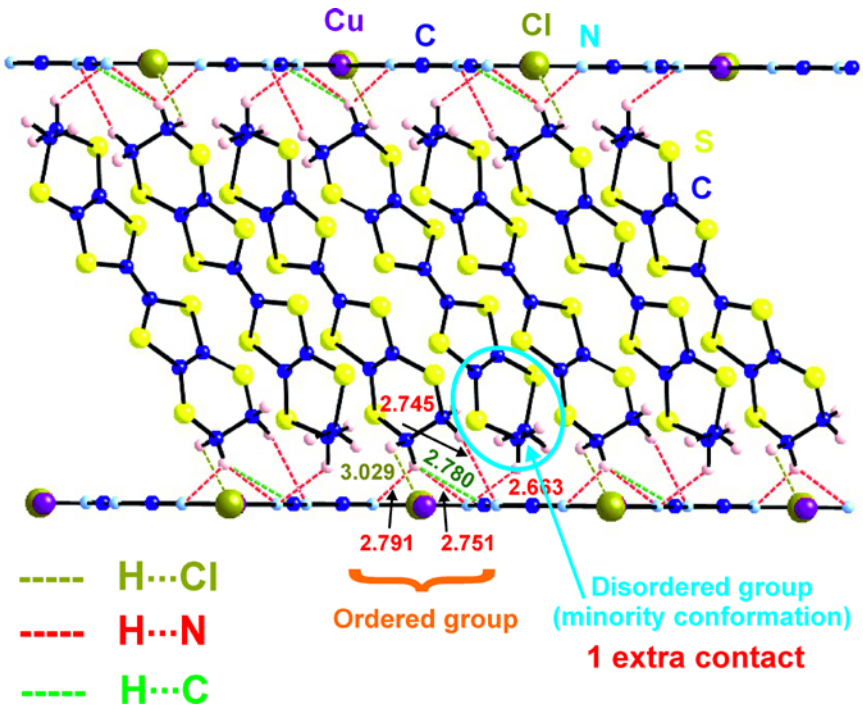

Figure 32. Projection of the crystal structure of κ-(BEDT-TTF)$_2$Cu[N(CN)$_2$]Cl at 250 K where the different short contacts between the BEDT-TTF donor and the anion layer have been highlighted. The BEDT-TTF donors are shown with the disordered ethylene group in the minority staggered conformation.

Shown in Fig. 32 is a projection of the structure at 250 K where the disordered C_2H_4 group is drawn in the minority staggered conformation, showing the H···N (red), H···C (green) and H···Cl (brown) short contacts between the hydrogen atoms of the terminal BEDT-TTF ethylene groups and the anion layers. All but one of the displayed hydrogen bonds are associated with the ordered C_2H_4 group. This is understandable since these interactions provide a strong stabilization of this ethylene group conformation which thus stays ordered. The shortest H···N contact (2.663 Å) is however associated with one hydrogen atom of the staggered minority conformation of the disordered ethylene group. Surprisingly, there is no short contact when the disordered group adopts the majority eclipsed conformation. This means that the donor···anion contacts indeed favor the minority staggered conformation. Consequently, there must be some structural feature within the donor layers that competes and ultimately dominates over this preference of the donor···anion interactions for the staggered conformation.

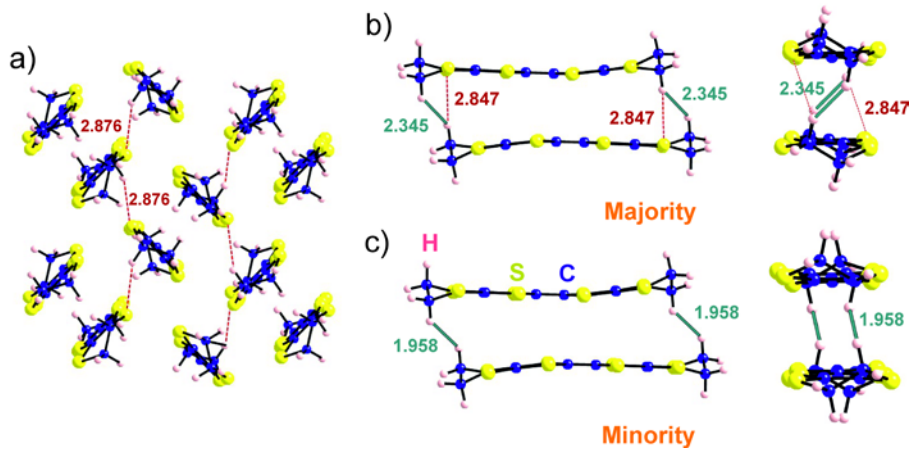

Figure 33. (a) Donor layers of κ-(BEDT-TTF)$_2$Cu[N(CN)$_2$]Cl at 250 K with donors shown with the disordered ethylene group in the minority staggered conformation. Inter-dimer H···S hydrogen bonds are shown. Short H···S and H···H intra-dimer contacts when the donors adopt the eclipsed majority (b) or staggered minority (c) conformations, respectively.

The detailed arrangement of the donor layers is shown in Fig. 33a with all BEDT-TTF donors shown in the minority staggered conformation. The H···S inter-dimer short contact shown is associated with the ordered ethylene side of the donors and there are no extra H···S short contacts when the disordered side of the donor is in the majority eclipsed conformation. Consequently, differences in the donor layers when the disordered ethylene group adopts one or the other conformation must originate from the intra-dimer interactions. As shown in Fig. 33b, when the two donors adopt the eclipsed conformation, there are two intra-dimer stabilizing H···S hydrogen bonds favoring this situation. More importantly, when the two dimers adopt the minority staggered conformation (Fig. 33c), there is a very short H···H contact. H···H contacts shorter than 2.4 Å are usually associated with repulsive interactions. 185] Thus every time that there is a shift from the staggered to the eclipsed conformation, the system is stabilized by loosing destabilizing H···H interaction and forming a stabilizing H···S hydrogen bond. Consequently, it is clear that whereas donor···anion interactions favor the staggered conformation, donor···donor interactions favor the eclipsed one and dominate over the former. When all the previously discussed contacts are followed as a function of temperature, the extra H···N hydrogen bond favoring the minority staggered conformation changes from 2.669 (295 K) to 2.643 Å (200 K), the intradimer H···S from 2.869 (298 K) to 2.839 Å (200 K) and the intradimer H···H contact from 1.920 (298 K) to 1.869 Å (200 K). Although the two last factors favor the majority eclipsed conformation, for H···H contacts as short as 1.869 Å, these interactions are strongly repulsive and must dominate the energy balance so that a further shortening would yield a too large destabilization and the minority conformation is not present anymore. The same analysis holds for κ-(BEDT-TTF)$_2$Cu[N(CN)$_2$]Br, but now the H···H contacts are consistently weaker; those occurring at

100 K are equivalent to those occurring between 250 and 200 K in κ-(BEDT-TTF)$_2$Cu[N(CN)$_2$]Cl salt so that although the proportion of the staggered minority conformation decreases continuously with temperature, a completely ordered situation is not reached at 9 K. In short, the stabilization of the eclipsed conformation in this salt results from the dominance of intra-dimer interactions over donor···anion and inter-dimer interactions.

Although the κ-(BEDT-TTF)$_2$Cu[N(CN)$_2$]X (X = Cl, Br) and κ-(BEDT-TTF)$_2$Cu(NCS)$_2$ phases may seem structurally very similar, the temperature evolution of the crystal structure is in fact different. Together they provide a good example of the adaptability of the BEDT-TTF salts to each type of anionic environment. The κ-(BEDT-TTF)$_2$Cu(NCS)$_2$ phase [19] is a bit more complex because there are two different BEDT-TTF donors, each one exhibiting disorder in one of the two ethylene ends.[20] However there is only one type of dimer in the donor layers. The kind of disorder is such that the staggered conformation of both donors is the majority component (around 60 % at 250 K) and between 200 and 150 K both donors become completely ordered exhibiting only the staggered conformation.[185] There are several remarkable differences between the crystal evolution of the κ-(BEDT-TTF)$_2$Cu[N(CN)$_2$]Cl and κ-(BEDT-TTF)$_2$Cu(NCS)$_2$ phases. First, they become ordered with the eclipsed conformation in the first case but with the staggered in the second one. Second, just before ordering occurs, there is a small proportion of minority component in the first salt (~13%) but still a large one in the second (~33%). Third, although in κ-(BEDT-TTF)$_2$Cu(NCS)$_2$ the volume decreases when lowering the temperature, the cell parameter associated with the interlayer direction, *a*, increases. In contrast, all cell parameters decrease with temperature in κ-(BEDT-TTF)$_2$Cu[N(CN)$_2$]Cl.

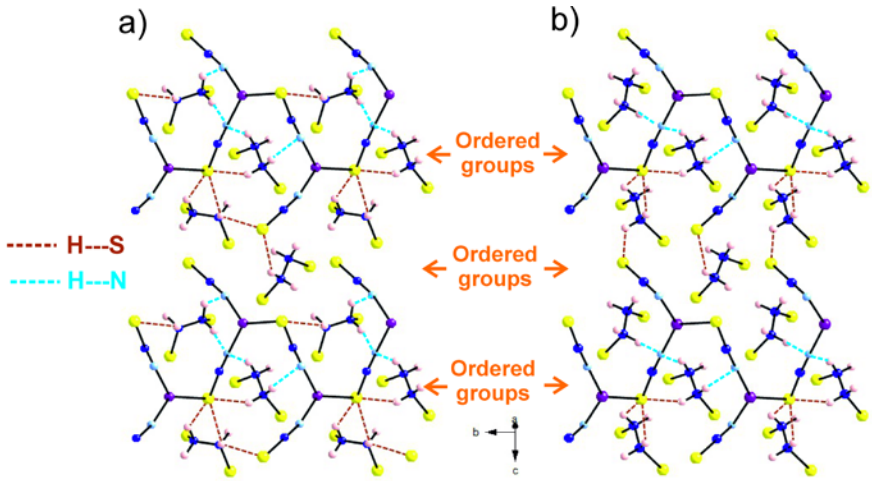

Figure 34. View perpendicular to the anion layer of the donor-anion interactions in κ-(BEDT-TTF)$_2$Cu(NCS)$_2$ at 200 K. The H···S (blue) and H···N (red) contacts shorter than 3.0 and 2.8 Å, respectively, have been plotted. For simplicity, BEDT-TTF has been represented

only by their ethylenedithio groups near the anion plane. In (a) and (b) the disordered ethylene ends have been represented in the staggered and eclipsed conformations, respectively.

In contrast with the case of κ-(BEDT-TTF)$_2$Cu[N(CN)$_2$]Cl, the stabilizing interdimer S···H interactions are now associated with the staggered conformation. For exactly the same reasons discussed for κ-(BEDT-TTF)$_2$Cu[N(CN)$_2$]Cl, when only the intra-dimer interactions are considered, the eclipsed conformation is preferred. However, a clear difference appears between the two types of phases when the evolution of the dimers with temperature is considered. From 298 K to 200 K, when disorder occurs, the intra-dimer stabilizing H···S interactions in the present case increase when temperature decreases (from 2.740 and 2.786 Å at 290 K to 2.623 and 2.635 Å at 200 K). However, the destabilizing H···H short contacts do not continuously shorten becoming more destabilizing when temperature goes down, as in κ-(BEDT-TTF)$_2$Cu[N(CN)$_2$]Cl, but become longer! These H···H contacts increase from 2.183 and 2.199 Å at 290 K to 2.218 and 2.233 Å at 200 K. This is obviously related with the anomalous lengthening of the *a* parameter. When temperature goes down and the system seeks to strengthen stabilizing H···S interactions, two possibilities arise. Either the donor layers adopt an eclipsed conformation to take advantage of intra-dimer S···H hydrogen bonds or indeed choose a staggered conformation to take advantage of inter-dimer S···H hydrogen bonds if they can reduce the destabilizing intra-dimer H···H interactions occurring in this conformation. The system finds a way against the increase of such destabilizing H···H interactions via a small shift of the two donors with the staggered conformation becoming preferred because donor-anion interactions are more stabilizing inthe staggered conformation. The important difference with κ-(BEDT-TTF)$_2$Cu[N(CN)$_2$]Cl is the presence of the additional S atoms in the anion. The disordered ends of the donors interact more strongly with the anionic layers, making H···S hydrogen bonds either stronger or more numerous (see for instance the upper of the initially disordered groups in Fig. 34, which is a view perpendicular to the anion layers at 200 K just before the ordering occurs). Consideration of the other types of hydrogen bonds do not modify the situation (for instance the eclipsed conformation makes a shorter H···N hydrogen bond with the anions but the staggered makes two such hydrogen bonds). The different shape and the occurrence of sulfur atoms on the anionic zigzag chains keeps the staggered conformation more tightly bound to the anions becoming ultimately the only conformation present in the crystal structure below 200-150 K. In this case, anion···donor interactions and inter-dimer S···H hydrogen bonds dominate over intra-dimer donor···donor interactions as temperature goes down, in contrast with the previous case.

The previous discussion highlights how the balance between anion···donors, inter- and intra-dimer interactions in κ-phases can subtly change among structurally similar compounds. The situation is more complex when disorder also occurs in the anion lattice, as for instance in κ-(BEDT-TTF)$_2$Cu$_2$(CN)$_3$.[185,187-189] adding an extra structural degree of freedom.

3- *Thermal crossover from ethylene disorder to incommensurate order in β-(BEDT-TTF)$_2$I$_3$*. Due to conformational flexibility, donor layers of BEDT-TTF and related salts can adopt even more complex structural alternatives such as structural modulations. Let us briefly consider the case of β-(BEDT-TTF)$_2$I$_3$. [22,44] The phase diagram of β-(BEDT-TTF)$_2$X (X = I$_3$, IBr$_2$, etc) salts has been studied in great detail and we only would like to highlight that the same competition between anion···donor and donor···donor interactions also occurs here despite the very different organization of the donor layers (see Fig. 7). In passing, let us note the landmark paper by Whangbo and coworkers [177] which provided one of the first in-depth discussions of the possible structural basis for superconductivity in this salt focusing on the donor···anion interactions. The donor layers are built from parallel stacks of BEDT-TTF donors along the (*a*+*b*)-direction (see Fig. 7).[171,173] At room temperature, one of the ethylene groups is disordered, i.e. BEDT-TTF occurs with almost equal probability with an *eclipsed* (*t* – *t*) or *staggered* (*t* – $\bar{t}$) conformation. In contrast, under a pressure of 9.5 kbar disorder disappears and all molecules exhibit the *staggered* conformation.[177,190] At ambient pressure and below 175 K a triply incommensurate modulation occurs [191-192] which vanishes under pressure.[193] Is there any simple reason behind the occurrence of disorder and the stabilization of the staggered conformation under pressure?

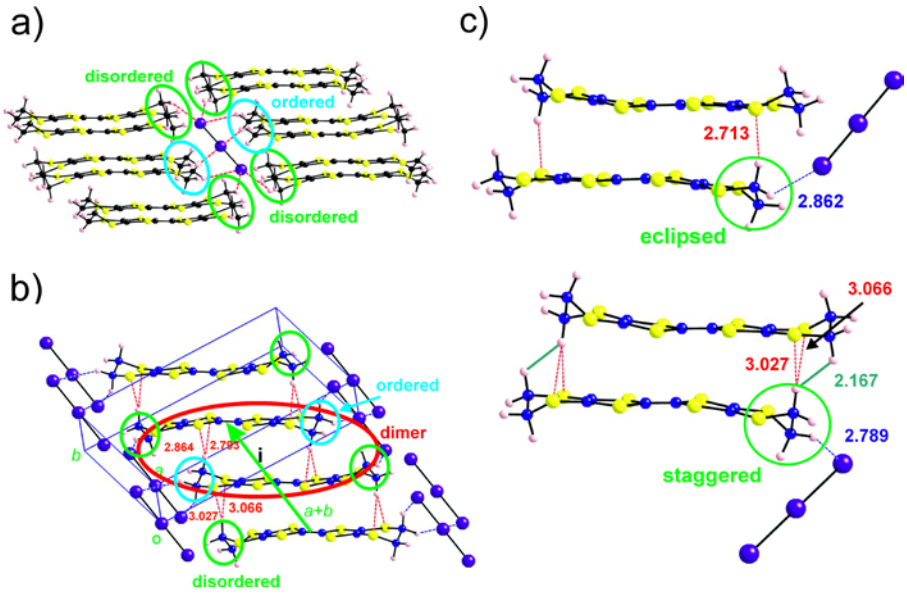

Figure 35. Crystal structure of β-(BEDT-TTF)$_2$I$_3$. (a) View showing the cavity of 12 donors where the anion is located. (b) View showing the stacks along the (*a*+*b*)-direction. The dimeric units as well as the ordered and disordered ethylene groups are highlighted. All donors are shown in the staggered conformation. Distances correspond to the average 125 K structure.[191] (c) Environment of the disordered ethylene groups in the eclipsed or staggered conformations (only H···I contacts shorter than 3.1 Å are shown).

The crystal structure of β-(BEDT-TTF)$_2$I$_3$ contains I_3^- anions within a cavity made by twelve BEDT-TTF donors (see Fig. 35a) [171,173] with only six of them making short H···I

contacts. Every terminal iodine of I_3^- is linked to two disordered and one ordered ethylenes (Fig. 35a) whereas the central iodine is linked to two ordered ones. Fig. 35b shows another view where the stacks along the (*a*+*b*)-direction are emphasized. Every pair of donors along the chain are related through an inversion center and when the different H···S hydrogen bonds between pairs of donors are considered, it is clear that the dimers are the basic units of the stacks (See Fig. 35b). Here we will only focus on the possible origin of the disorder in one of the ethylene ends. We show the shortest H···I, H···S and H···H contacts associated with the disordered group in the eclipsed or the staggered conformations in Fig. 35c. The H···I interactions favor the staggered conformation (2.789 vs 2.862 Å). When the disordered group adopts the staggered conformation there are two short H···S contacts (3.027 and 3.066 Å). In contrast, for the eclipsed conformation there is only one H···S contact, but it is shorter (2.713 Å). In addition, one relatively short H···H contact is generated in the case of the staggered conformation. Thus, the inter-donor interaction favors an eclipsed conformation whereas the donor···anion favors a staggered one so that there is no clear preference for one conformation and disorder occurs.

Although we will not discuss it in detail, the fact that only the staggered conformation occurs under pressure is not difficult to understand. Under pressure, the relative position of the I_3^- anions slightly rotates with respect to the donor layers.[177] As a result, one of the CH_2 groups of the ordered ethylene slightly turns and the destabilizing H···H interaction associated with the staggered conformation (Fig. 35c) disappears. Consequently, the staggered conformation is now favored becoming the only one present.

Fig. 35c nicely illustrates the subtlety of the competition between donor···anion, S···H stabilizing and H···H destabilizing donor···donor interactions in these solids. At ambient pressure, when the staggered conformation is adopted, the CH_2 group interacting with the anion is not involved in H···S hydrogen bonds with the adjacent donor, having more flexibility to look for stabilizing H···S interactions and finally generating two of them. When the eclipsed conformation is adopted, the same CH_2 group is involved in the H···I and H···S interactions and just a single S···H interaction occurs. However, in the first case, the generation of more S···H interactions has a price to pay: a destabilizing H···H interaction is created and the H···S interaction cannot be too strong. In the second case, the H···S interaction becomes stronger but then, the H···I interaction weaker. In other words, these three interactions are strongly interrelated.

The modulated structure occurring below 175 K has been solved assuming a sinusoidal occupancy wave among the eclipsed and staggered conformations of the disordered ethylene.[192] However, the modulation is not sinusoidal and up to the fifth Fourier component of the modulation has been detected.[194] Thus, sizeable spatial variations of the lattice deformation must occur. Under such circumstances it is appealing to speculate that the modulation may originate from a spatially dependent conformation of the ethylene groups

(i.e. a modulation wave of the ethylene group conformations optimizing the donor-anion interaction and weakly differing in energy as it is the case for the *t* and *ht* conformations).

B. Metal to insulator transition in α-(BEDT-TTF)$_2$I$_3$.

1- Unsolved aspects of the phase transition

α-(BEDT-TTF)$_2$I$_3$ is one of the first reported molecular metals based on BEDT-TTF [195-197] and yet very fundamental aspects of its physical behavior remained unclear for long time. The origin of the metal to insulator transition occurring at 135 K [195] has been a puzzle for almost thirty years. Initial studies of the crystal structure below the transition temperature failed to recognize an essential aspect of the transition, i.e. the change in the symmetry group.[198-199] Although an early study provided evidence for a decrease of the symmetry from P-1 to P1 at the transition (unfortunately the complete structure could not be solved),[200] the relevance of this finding was apparently unnoticed and the origin of the transition proved to be elusive.[201] Only more recently non-linear optical measurements revealed the ferroelectric nature of the insulating phase of α-(BEDT-TTF)$_2$I$_3$[202-203] and a low temperature synchrotron X-ray structural study [204] provided evidence for the disappearance of the inversion symmetry and detailed structural information below the transition temperature. α-(BEDT-TTF)$_2$I$_3$ has received renewed attention because of the occurrence under pressure of peculiar electronic properties interpreted as due to the presence of an anisotropic Dirac cone in the electronic structure. [205-206]

Based on theoretical work using an extended Hubbard approach in which the BEDT-TTF donors were treated as structure-less sites, a charge ordering phenomenon was proposed to be at the origin of the metal to insulator transition and a horizontal stripe charge pattern was predicted.[207-208] Such suggestion received support from NMR [209] and Raman studies.[210] The charge ordering mechanism was put on firmer ground by an estimation of the charge pattern based on the low temperature synchrotron X-ray structural study using an empirical relationship between the C-C and C-S bond lengths and the BEDT-TTF charge [207]: an horizontal stripe charge pattern as predicted by theory was found. Subsequent infrared, Raman and NMR studies [211-212] provided support for this pattern of charge distribution leading to a consensus that the origin of the metal to insulator transition, of the charge ordering type, had been finally understood.

Whereas the disappearance of the inversion symmetry and the subsequent charge disproportionation are undeniable experimental facts, this mechanism is, however, not free from criticism. In particular at the difference with Fabre (section III.D) and θ-(BEDT-TTF)$_2$X salts (part D of this section) the metal-insulator is not accompanied by a spin-charge decoupling expected for a CO transition. Furthermore spin susceptibility measurements in the insulating phase of α-(BEDT-TTF)$_2$I$_3$ evidence the opening of a 70 meV spin gap [213], of same magnitude as the charge gap obtained in conductivity measurements. In addition, recent transport measurements [214] show that before the 135 K transition, α-(BEDT-TTF)$_2$I$_3$ is a semimetal with the transport governed by the large mobility of electrons and holes, in contradiction with one of the basic assumptions of the extended Hubbard treatment namely,

that the system is a quarter-filled band system, i.e. containing only one type of carrier. From all these elements one has carefully to consider the metal to insulator transition in α-(BEDT-TTF)$_2$I$_3$ as a semi-metal to semiconductor transition. However, this does not preclude the participation of specific Coulomb interactions, such as those between electrons and holes of the semi-metallic state, at the mechanism of the transition.

Finally it is not easily conceivable that a mechanism relying only on Coulomb interactions *within the donor sublattice* may afford an appropriate description of the observed phenomena. The anions, completely ignored in this treatment, should then follow the changes in the donor layers. However this does not seem to be well suited for a salt with an anion with large atoms and highly concentrated charges. Thus based on crystallochemical ideas and first-principles DFT calculations in which the roles of donors and anions were taken into account on an equal foot, Alemany et al. [85] proposed a new and detailed microscopic mechanism of the metal-insulator transition in which anions play a major role, leading to the development of a simple model that clarifies the role of hydrogen bonds at the donor-anion interface in the stabilization of charge ordered states which, as discussed in the present work, provided important clues to analyze also other charge and anion ordering phenomena.[30,84,215]

2- Crystal structure.

The crystal structure of α-(BEDT-TTF)$_2$I$_3$ contains layers of BEDT-TTF donors alternating along the *c*-direction with layers of I_3^- zigzag chains. The donor and I_3^- layers are linked through a series of I···H-C hydrogen bonds shown in Fig. 36a. As it will be shown later, these hydrogen bonds play a key role in the metal to insulator transition. The donor layers contain two different types of BEDT-TTF stacks along the *a*-direction. One of them (labeled *stack 2* in Fig. 36b) is made from two different centrosymmetric donor molecules, B and C. Both donors are in a staggered conformation (B: $\bar{t}$ - $\bar{t}$, C: *t* - *t*). Note, however, that the inclination of the two donors is different. The second type of stack (*stack 1* in Fig. 36b) contains only one type of donor molecules at room temperature, since the two molecules noted A and A´ with an *ht* – *ht** (or equivalently $\overline{ht}$ – $\overline{ht}^*$) conformation are related by an inversion center that is lost when the metal to insulator transition occurs with donors A and A´ becoming non-equivalent. These two types of stacks pack alternately into a layer of the so-called α type [216] containing many S···S contacts shorter than 3.7 Å (dashed red lines in Fig. 36a) that ensure the electronic delocalization within the layer.

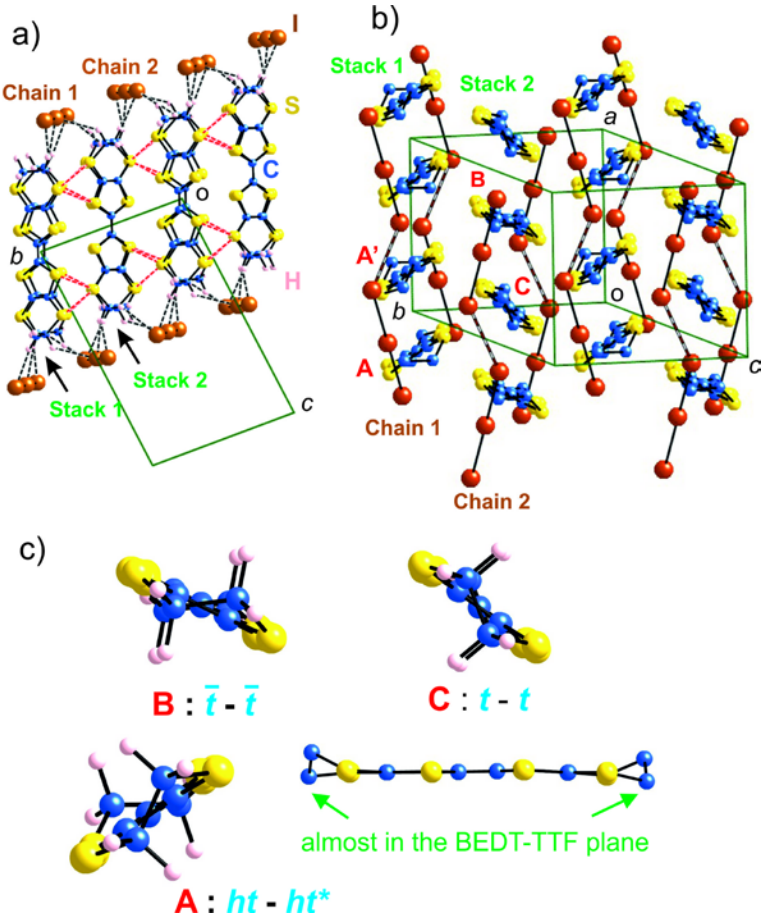

Figure 36. (a) Crystal structure of α-(BEDT-TTF)$_2$I$_3$ showing the alternation of BEDT-TTF and anion layers along *c*. (b) View with different donors, stacks and chains important for analyzing the charge ordering transition are labeled (hydrogen atoms are not shown for clarity). [85] (c) Different types of BEDT-TTF donor molecules present in the structure with their ethylene group conformation indicated. In the ht or ht* conformations one C atom of the ethylene group is almost in the molecular plane. ((a) and (b) from ref [85] (Copyright 2012 by the American Physical Society.)

3- Electronic structure.

The calculated band structure near the Fermi level above the phase transition is shown in Fig. 37a.[85] The bands are built almost exclusively from the HOMOs of the four BEDT-TTF donors. Since iodine is present as I_3^-, these bands must contain two holes. The two upper bands slightly overlap and therefore above the phase transition α-(BEDT-TTF)$_2$I$_3$ is predicted to behave as a semimetal with very small hole and electron pockets as found in transport measurements [214]. Even very subtle structural modifications may open a gap at the Fermi level in this band structure. The partition of holes in the HOMO bands among the three donors is calculated to be: +0.521 (A), +0.546 (B) and +0.382 (C).

The calculated band structure below the transition temperature is shown in Fig. 37b. It is clear that a band gap separates now the two upper bands. The new partition of the two holes

is: +0.638 (A), +0.438 (A´), +0.577 (B) and +0.359 (C). Thus, the rearrangement of holes associated with the transition leaves those of B and C practically unaltered, leading to a redistribution confined to the A-A dimeric units. The trend in the variation agrees with those derived empirically from X-ray or Raman studies.[203,212] The important observation when the band structures above and below the transition temperature are compared is that the gap opening is associated with a quasi-rigid shift of the two overlapping upper bands and an important task is to understand their nature.

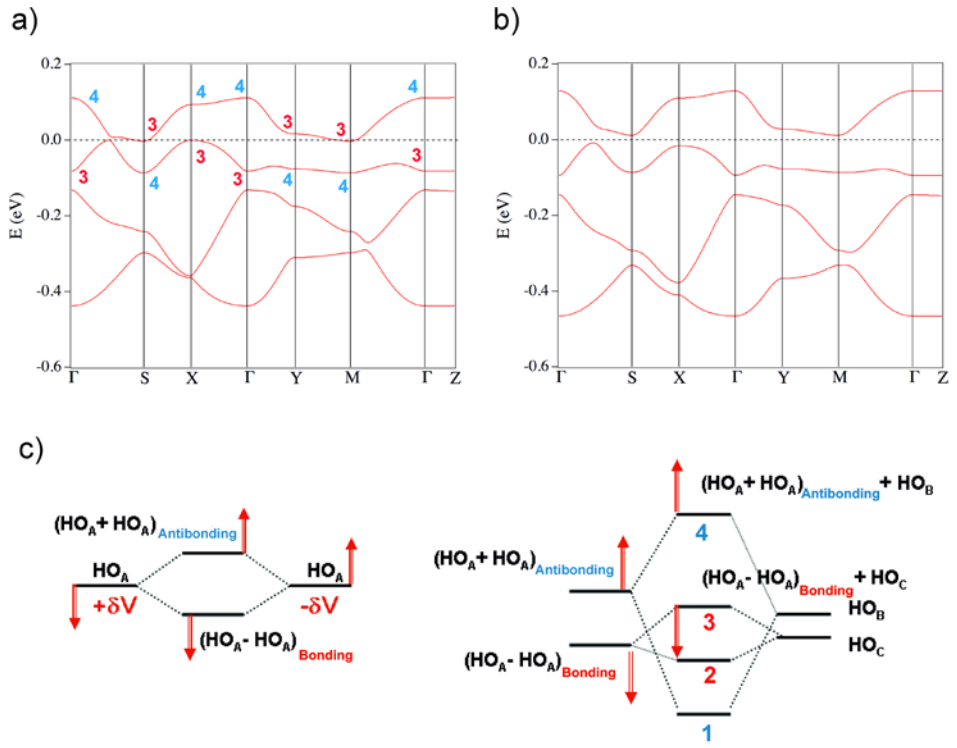

Figure 37. Calculated band structure for α-(BEDT-TTF)$_2$I$_3$ above (a) and below (b) the phase transition where Γ = (0,0,0), X = (1/2,0,0), Y = (0,1/2,0), Z = (0,0,1/2), M = (1/2,1/2,0), and S = (-1/2,1/2,0) in units of the reciprocal lattice vectors. (c) Schematic diagram showing the nature of the bands. The extra splitting of the energy levels caused by a modulation of the site potential on molecules A is represented by red arrows. Labels **3** and **4** in (a) refer to the main character of the bands as indicated in (c).[85] (Copyright 2012 by the American Physical Society)

Analysis of the crystal orbitals shows that a convenient way to describe the nature of the two upper overlapping bands in Fig 37 is to considering the donor layers as being built from a series of A-A dimers coupled by B and C donors.[85] The A-A dimers are those facing the donor C (see Fig. 36b). As schematically shown in Fig. 37c, the two HOMOs of the A-A dimer interact giving a bonding (out of phase) and an anti-bonding (in phase) combination. In the solid these dimer orbitals repeat with the appropriate phases and couple through the HOMOs of B and C. The stronger interactions in the solid occur between the upper, anti-bonding level of the A-A dimers and the HOMO of B leading to the upper and lower HOMO

levels (see Fig. 37c right). The HOMO of C mostly interacts with the bonding orbital of the A-A dimer leading to two new levels lying in between the previous ones (see Fig.37c right). Levels noted **4** and **3** are those giving the two overlapping bands as indicated in Fig. 37a. In the actual band structure there are, however, many hybridizations (avoided crossings) that obscure a bit this simple description. Most of the details of the band structure and density of states may be understood on the basis of this simple scheme.[85] Note that except for very small fillings, the upper HOMO band has a 1D behavior along the *b*-direction, somewhat which is easily understandable on the basis of this approach.[217] The essential results of this analysis are: (i) in the region of the semi-metallic overlap the two bands originate from the type **3** and type **4** orbitals of Fig. 37c, and (ii) the dimer orbital component of **4** and **3** comes from the anti-bonding and bonding combinations, respectively, of the HOMOs of the A molecules forming the dimer.

4- Hole distribution before the charge ordering transition.

In the room temperature crystal structure [198] it is striking to see that the two I_3^- zigzag chains, despite being non-equivalent by symmetry, are essentially identical. For instance, chain 1 (Fig. 36b) exhibits I-I bond lengths of 2.929 Å, I···I inter-unit contacts of 3.882 Å (shorter than the sum of the van der Waals radii) and a zigzag angle of 140.2º. In chain 2 these parameters are 2.927 Å, 3.885 Å and 140.2º, respectively. This means that at room temperature I_3^- chains adopt a structure that optimizes the I_3^- ··· I_3^- interactions, independently of the neighboring donor layers. In other words, the structure is made of charged donor and acceptor subsystems in which the anion lattice keeps its optimized structure while the donors adapt to it. The stronger directing force in assembling the final structure is provided by hydrogen bonding. This is especially so in this case because the negative charge of the anion is concentrated on the two terminal iodine atoms of the I_3^- units and, as it is well known, hydrogen bonds involving anions are especially strong. [218]

Looking at the donor-anion interface it is clear that there is a series of very short I···H-C hydrogen bonds (i.e., < 3.0 Å) involving the charged terminal iodine atoms (Fig. 38a). Donors A participate in two such hydrogen bonds with I···H distances of 2.851 Å and 2.929 Å, donor B in two inversion related hydrogen bonds with 2.905 Å I···H distances while donor C does not participate in hydrogen bonds shorter than 3.0 Å. What is then the role of donor C in the crystal structure if it does not contribute to the strong donor-anion interactions? The answer is that it is engaged in the strongest S···S contacts within the donor layer. and thus it does not contribute effectively to the stability of the phase throughout donor-anion interactions, although it plays an important role in ensuring electronic delocalization within the donor layers.

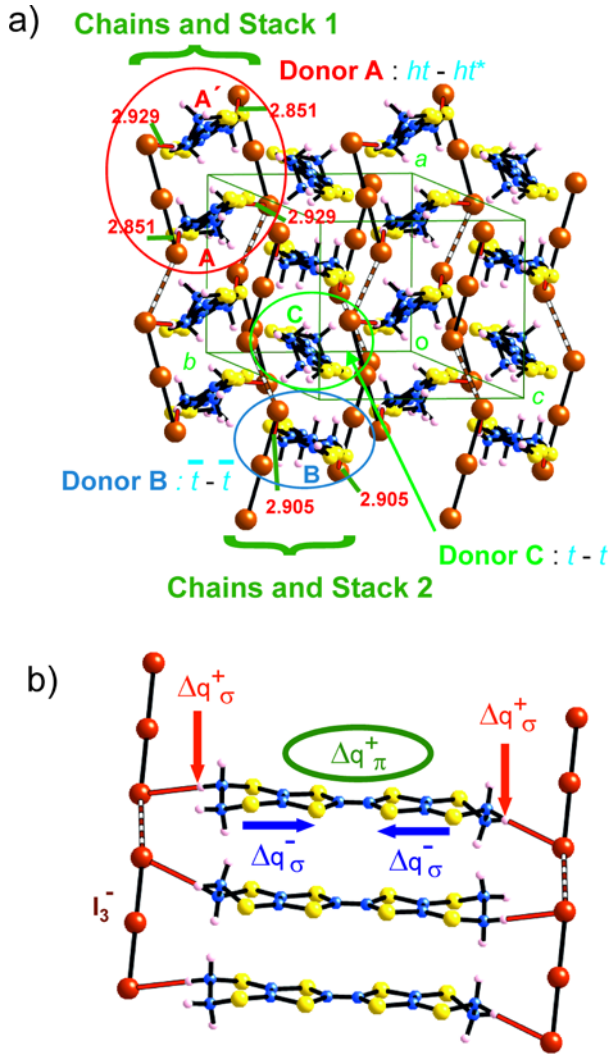

Figure 38. (a) $I^{-1/2}\cdots$H-C hydrogen bonds shorter than 3 Å in the room temperature crystal structure of α-$(BEDT\text{-}TTF)_2I_3$. (b) Schematic diagram showing how the development of a positive σ charge in the H atom making a hydrogen bond with the anion and a positive π charge in the central core of BEDT-TTF are correlated through a negative σ charge shift.[85] (Copyright 2012 by the American Physical Society)

As mentioned above, donors and anions are linked through hydrogen bonding interactions and the strength of these hydrogen bonds and the concentration of holes in the π-type HOMO of a given donor are connected through a subtle mechanism discussed in section III, which in the present case can be schematized as in Fig. 38b. Simply speaking, an increase of the positive charge of a hydrogen atom making a hydrogen bond with the anion is coupled with an increase of the positive charge in the inner π system via the polarization induced in the σ electron density. Thus, an anion shift towards the donor will increase the strength of the hydrogen bonding and make the terminal hydrogen atoms more positively charged inducing in this process a negative charge shift towards the inner part of the donor and, consequently, stabilizing a more positive charge in the inner π system. If the donor molecule would be

completely isolated from other donor molecules in the neighborhood, the π system would simply polarize, but if there is some electronic connection (i.e. a non-nil transfer integral) with the nearest neighbor donor molecules, the shift results in a transfer of holes from one donor to the other (see bottom part of Fig. 14b). The charge distribution in the donor layers is thus easy to understand. Both donors A and B are associated with two short hydrogen bonds with the anions (2.851 and 2.929 Å for A and 2.905 and 2.905 Å for B). Since the both have the same number of hydrogen bonds with very similar average distances, calculated charges are also very similar (+0.521 for A and +0.546 for B). In contrast, donor C is not associated with any short hydrogen bond and its calculated charge is considerably smaller (+0.382).

5-Hole distribution after the charge ordering transition.

Thermal contraction should bring a differentiation of the two I_3^- zigzag chains because of their quite different ways to interact with BEDT-TTF stacks. Chain 1 makes short hydrogen bonds with *all* donors of the BEDT-TTF stack 1 (see Fig. 38a) which are of the *ht – ht** type, i.e. not in the most stable *twist* conformation, but in the *half twist* one. Thus, both stack 1 and chain 1 are in a quite constrained situation. In contrast, chain 2 makes hydrogen bonds with only one of the two donors of the stack (i.e. donor B, see Fig. 38a) so that stack 2 and chain 2 are much less constrained. Since the two terminal iodine atoms are negatively charged, thermal contraction should mostly bring a decrease of the zigzag I-I··I angle allowing to keep the inter-unit I···I contacts almost constant. Looking at Fig. 38a it is clear that zigzag chains 2, with less hydrogen bonds with BEDT-TTF donors, are more easily deformable than zigzag chains 1 which is indeed what is reflected in the low temperature structure. Chain 2 exhibits I···I inter-unit contacts of 3.856 Å and a zigzag angle of 135.8 degrees. Thus, the inter-units contacts are barely changed while the zigzag angle has clearly decreased (note that the I_3^- unit is very long and thus small changes in the angle have a strong effect on the iodine contacts). We conclude that chains 2 exhibit a "normal" behavior. In contrast, chains 1 exhibit I···I inter-unit contacts of 3.807 Å and a zigzag angle of 137.0 degrees, i.e., a smaller angular change and, more importantly, a clear reduction in the inter-unit contacts. This "abnormal" behavior should be associated to some additional stabilizing structural change which should more than counteract the inherent destabilization associated with the shortening of the contacts between negatively charged iodine atoms.

Hydrogen bonded molecules sitting on symmetrical sites almost invariably move at low temperatures so that the symmetry is lost. The reason is that when the thermal energy of the molecule is reduced it is energetically advantageous to strengthen one of the hydrogen bonding interactions at the expense of the other one. This is what occurs in the present case for molecules A forming centro-symmetric dimers in the room temperature structure. The shorter of the two hydrogen bonds at low temperature becomes 2.807 Å for donor A and 2.823 Å for donor A´. The other hydrogen bond becomes 2.895 Å for donor A and 2.908 Å for donor A´ while these hydrogen bonds were 2.851 and 2.929 Å, respectively, at room temperature. In addition, the two hydrogen bond distances for donor B molecules that were identical at room temperature (2.905 Å) are now 2.842 and 2.869 Å. Thus, each of the three types of short hydrogen bonds in the room temperature structure becomes a pair of bonds

differing by 0.01-0.02 Å at low temperature. These changes, associated with the thermal contraction *and* loss of the inversion symmetry, modify in a different way the strength of the hydrogen bonding for the different donor molecules and, consequently, lead to a modification of their charges. Note that donor A is associated with the shorter hydrogen bonds of each type (2.807 vs. 2.823 Å and 2.895 vs. 2.908 Å) whereas the opposite is true for donor A´. According to the mechanism outlined before (Fig. 38b) hydrogen bonding associated with donor A will increase in a very sizable way so that the positive charge associated with the π system of the molecule will increase. This is indeed what is found both theoretically [85] and experimentally.[203,212] In donor B molecules the consequences of the loss of the inversion symmetry are much weaker since by initially having two identical hydrogen bonds, the changes in the hydrogen bonding partly cancel. Consequently, a considerably smaller charge increase is expected and clearly reflected in both theoretical [85] and experimental studies.[203,212]

6- Structural instability and the metal-insulator transition.

The crystal structure of α-(BEDT-TTF)$_2$I$_3$ can be seen as containing two different blocks: the anion chains and donor stacks of type 1, and those of type 2 (see Figs. 36b and 38a). The first one is quite constrained as clearly shown by the unusual *half twist* conformation of the ethylene groups of BEDT-TTF and the occurrence of two short hydrogen bonds per donor. The second, with only two hydrogen bonds for every two donors and all ethylene groups in the more stable *twist* conformation, is much less constrained. Thermal contraction boosts the tensions associated with the first block and, at a certain point, the system must relieve these tensions by modulating the strength of the I···H-C hydrogen bonds. The easiest way to achieve this is by breaking the inversion symmetry of the A-A dimers allowing the relaxation of constraints around one of the donors. Consequently, the dimer becomes of the A-A´ type, with two different donor molecules. One of them (A´) has two weakened hydrogen bonds and thus, through the polarization mechanism outlined in Fig. 38b, becomes hole-poor (i.e. less positively charged). Just the opposite change occurs for the other donor (A), which exhibits stronger hydrogen bonds and thus becomes hole-rich (i.e. more positively charged). This results in a charge ordering within the donor layers with a horizontal stripe pattern.

Differentiation of the two initially identical donor molecules A has an important implication for the transport properties.[85] As can be easily understood by looking at the diagram in Fig. 36c, the development of different charges in the two A donors will increase the splitting between the bonding and anti-bonding HOMO based levels of the A-A´ dimers. As shown in Fig. 36c this also enhances the separation between the energy level **3**, resulting from the combination of the bonding dimer level with the HOMO of donor C, and the energy level **4**, resulting from the combination of the anti-bonding dimer level with the HOMO of donor B. As the valence and conduction bands originate from these two levels, the modulation of the hydrogen bonding network and thus, of the site potential (by ±δV in Fig. 37c), along the stacks 1 together with the increased band hybridization because of the symmetry lowering leads to the small band gap opening in the band structure at the transition.

7- Conclusion

The DFT-based crystallochemical analysis provides a structural basis to understand the origin of charge ordering effects as well as most of the experimental observations concerning the metal (i.e. semi-metal) to insulator (i.e. semiconductor) transition of α-(BEDT-TTF)$_2$I$_3$. This analysis highlights the essential role played by the anions which, by modulating the strength of the donor-anion hydrogen bonding interactions, modify the charges on the donors HOMOs through a subtle polarization mechanism of their σ and π electron densities, leading to the opening of a small band gap of less than 0.1eV. Since the driving force for the charge redistribution and gap opening originates in the I_3^- zigzag chains which couple successive donor layers, the process is transmitted through the whole 3D structure. Interestingly, recent transport measurements [214] have evidenced the presence of disorder affecting the transport and dielectric properties. These effects can be explained on the basis of disorder in the anion zigzag chains which is transmitted to the organic donor layers through the anion-donor hydrogen bonds.[219] Although not explicitly considered here, electron-electron inter-site repulsions between the π electrons of the donors (or more likely the electron-hole Coulomb repulsion in the semi-metallic state which in general generates excitonic effects) must also play a role in the phase transition mechanism favoring the charge disproportion between donors. They are, however, not the driving force for the previous mechanism. In the next section we will see that hydrogen bonding at the donor-anion interface also plays an essential role in the structural modulation of α-(BEDT-TTF)$_2$KHg(SCN)$_4$ even if it proceeds through a completely different mechanism.[84,220]

Finally let us remark that if the semi-metal to semiconducting transition corresponds to a positive rigid band shift between the two upper overlapping HOMOs bands (see section 3) a negative rigid band shift allows to obtain the band structure of pressurized α-(BEDT-TTF)$_2$I$_3$.[85] In particular, the collapse of the small band gap in the ΓS direction should give rise to a Dirac cone dispersion with massless carriers. Also hole (electron) pockets located at X (S and M) points could be stabilized, giving rise to massive carriers. In addition to Dirac carriers, massive hole carriers have been detected by magneto-transport measurements performed in pressurized α-(BEDT-TTF)$_2$I$_3$.[221-222] This finding also agrees with recent optical conductivity measurements showing the coexistence of trivial (massive) and massless Dirac carriers in pressurized metallic α-(BEDT-TTF)$_2$I$_3$.[223]

C. Charge Density wave instability in α-(BEDT-TTF)$_2$KHg(SCN)$_4$.

1- *Nature of the instability*

Despite being iso-structural and exhibiting almost identical band structures and Fermi surfaces, salts of the α-(BEDT-TTF)$_2$MHg(XCN)$_4$ (M = K, Rb, NH$_4$, Tl; X = S, Se) family [224-227] show a quite different low-temperature behavior. For instance, whereas the K(S), Rb(S) and Tl(S) phases exhibit a resistivity anomaly at 8 K, 12 K, and 10 K, respectively,[228-230] the NH$_4$(S) and Tl(Se) salts do not. Among these two, the first becomes superconducting at 1 K and ambient pressure [231] whereas the second one stays metallic until very low temperatures without becoming superconducting.[232]

The origin of the low temperature resistivity anomaly of the K(S), Rb(S), and Tl(S) salts has been a subject of discussion for many years. The presence of both planar sheets and closed cylinders in the Fermi surface [217,224,233] led to the suggestion that such anomaly was related to the development of some kind of density wave, either charge (CDW) or spin (SDW), modulation. However it has been difficult to clearly determine its CDW, SDW or some kind of mixed CDW/SDW character. Angular magneto-resistance oscillations (AMRO) studies were extremely useful in establishing the wave vector associated with this modulation.[234] Analysis of the magnetic phase diagram of the low temperature phase was more suggestive of some kind of CDW rather than SDW, but it was not until some years later [235] that direct X-ray diffuse scattering evidence for a CDW state in the α-(BEDT-TTF)$_2$MHg(SCN)$_4$ (M = K, Rb) salts was provided. However, it was only after a combined X-ray diffuse scattering and first-principles DFT study [220] that the nature of the low temperature anomaly could be explained in detail. Combination of the calculated Lindhard response function and the observed modulation vectors gave strong support to the CDW scenario for α-(BEDT-TTF)$_2$KHg(SCN)$_4$. The CDW instability was found to be considerably more involved than those following a standard Peierls mechanism, but a detailed microscopic description of the modulation involving the anion layers could be proposed, rationalizing an important number of physical data in the literature.

.

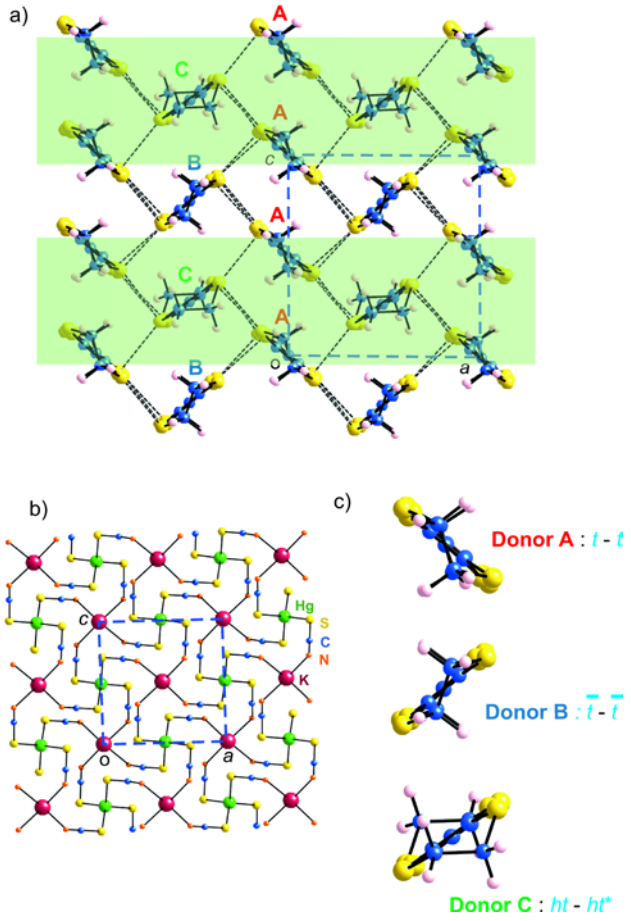

Figure 39. Crystal structure of α-(BEDT-TTF)$_2$KHg(SCN)$_4$. (a) BEDT-TTF donor layers, (b) anion layers, and (c) different types of BEDT-TTF molecules in the structure. The ethylene group conformation of the three types of donors is indicated. Shadowed regions in (a) refer to the 1D chains of interacting HOMOs (see text).

2- Crystal structure.

The crystal structure of α-(BEDT-TTF)$_2$KHg(SCN)$_4$ is built from BEDT-TTF layers alternating with anion layers along the *b*-direction (Fig. 6). Donor and anion layers are shown in detail in Figs. 39a and b, respectively. As for α-(BEDT-TTF)$_2$I$_3$, donor layers are of the α type [216] containing two different stacks: (i) inclined stacks containing only one type of donor molecules, A, and (ii) stacks containing two different types of donors, B and C, with different inclinations. These layers exhibit numerous intermolecular S···S contacts shorter than the sum of the van der Waals radii (dashed black lines in Fig. 39a) ensuring electronic delocalization. Note that the B and C donor labels are interchanged in the structural description of the α-(BEDT-TTF)$_2$KHg(SCN)$_4$ and α-(BEDT-TTF)$_2$I$_3$ salts in the literature: i.e. the less inclined molecule in stack 2 is B for α-(BEDT-TTF)$_2$I$_3$ but C for α-(BEDT-TTF)$_2$KHg(SCN)$_4$. In order to facilitate the comparison with other publications we have kept here this labeling. There is a subtle difference between the donor layers of the two salts: although the general architecture is the same (α type with three different types of donors) the conformation of the donor molecules is different. As shown in Fig. 39c, in the present case donors A and B are in a staggered conformation (A: *t* – *t* and B: $\bar{t}$ - $\bar{t}$) whereas C ones are in a *ht* – *ht** conformation. This feature clearly shows that *the different nature of the anion layers* in α-(BEDT-TTF)$_2$KHg(SCN)$_4$ and α-(BEDT-TTF)$_2$I$_3$ *induces subtle changes in the donor layers, displacing the more constrained regions.*

The anion layers in α-(BEDT-TTF)$_2$KHg(SCN)$_4$ (see Fig. 39b) are made of a sheet of K^+ and Hg^{2+} cations sandwiched between two sheets of SCN^- thiocyanate anions. The Hg^{2+} cations are tetrahedrally coordinated by the S atoms of four SCN^- anions with Hg-S distances just slightly longer than the sum of covalent radii, suggesting that these tetrahedral units are very robust. The K^+ cations are coordinated to four nitrogen atoms of the SCN^- anions leading to a square pyramid with K^+ in the top position. The K···N distances are typical for ionic bonds of this type. There are four additional longer, but non negligible K···S contacts with the four nearest S atoms included in Fig. 39b (these bonds are not drawn in the figure because they are relatively long), which try to complete a square antiprismatic coordination for potassium, a rather usual coordination environment for K^+ ions. Note that every SCN^- anion is coordinated to one K^+ and one Hg^{2+} cation in an infinite polymeric anionic network that can be described as a series of $[Hg(SCN)_4]^{2-}$ tetrahedral units kept together by the K^+ cations in the cavities of the lattice. It has, however, has quite strict cation size requirements as shown by the fact that it only exists for monovalent cations with radii in the range 1.3-1.5 Å (i.e., K^+,

Tl^+, Rb^+, NH_4^+) whereas Cs^+, with an ionic radius of 1.65 Å, leads to a different polymeric network.

A continuous network of hydrogen bonding interactions occurs both within the BEDT-TTF donor layers (H···S inter- and intra-stack hydrogen bonds) and between donor and anion layers (H···S, H···N and H···C hydrogen bonds between the thiocyanate SCN^- groups and the hydrogen atoms of the terminal ethylene groups of BEDT-TTF (Fig. 6 in section I), providing a strong structural cohesion. In view of the analysis developed in section B, it is important to notice the presence of two different sources of instability in this structure: (i) the region around type C donors, with the relatively unstable *half twist* conformation of the BEDT-TTF ethylene groups, and (ii) the region around the K^+ cation, with an irregular square antiprismatic coordination.

3- Insight from X-ray diffuse scattering studies.

The X-ray diffuse scattering study of α-$(BEDT\text{-}TTF)_2KHg(SCN)_4$ provided a series of crucial observations in order to grasp the nature of the instability behind the 8 K transition of this material. [221] First, the structural modulation exhibits up to three harmonics (q_1, q_2 , q_3) and the fundamental component of the modulation wave vector is q_1= [0.13(5). 0.15(5), 0.42(5)], in good agreement within experimental error with the wave vector of the superstructure deduced from AMRO measurements: q_{AMRO} = [1/8, 3/16, 3/8].[234] Second, the satellite reflections/diffuse spots are detected until 250-300 K. Third, the local modulation is strongly non-harmonic (i.e. the q_1, q_2 and q_3 Fourier components of the modulation have similar amplitudes) whatever the coherence of the modulation. Fourth, the correlation length of the modulation is very sensitive to sample quality. These observations reveal that the process leading to the 8 K transition is initiated well above this temperature (i.e. around room temperature) and that it is strongly linked to the anionic sublattice.

4- Electronic structure.

The band structure calculated using the 104 K crystal structure of α-$(BEDT\text{-}TTF)_2KHg(SCN)_4$ is shown in Fig. 40a. With the usual oxidation states of K^+, Hg^{2+} and SCN^-, the four HOMO bands (the unit cell contains four donor molecules) should contain two holes exactly, as for α-$(BEDT\text{-}TTF)_2I_3$. However, the band dispersions are now larger and the two upper bands overlap strongly, leading to a metallic situation. This is an important difference with α-$(BEDT\text{-}TTF)_2I_3$ imposed by the different nature of the anionic network. The calculated Fermi surface is shown in Fig. 40b. It contains tubes with an elliptical cross section along *b** and a pair of slightly warped planes perpendicular to *a**. The tubes are associated with the lowest upper band and correspond thus to holes, whereas the warped planes are associated with the highest upper band and correspond to electrons. The distribution of holes among the three types of donors is: +0.520 for each of the two A type donors, +0.424 for B type ones and +0.527 for C type donors. Since the BEDT-TTF stacks occur along the *c* direction (see Fig. 39) it is not obvious why the planar sheets of the Fermi surface should be perpendicular to *a**. However, Rousseau *et al*. [220] noticed that even if there are no S···S contacts shorter than the sum of the van der Waals radii within the stacks, one of the two

different transfer integrals associated with type 1 stacks is relatively large whereas the other one is very small. This means that stack 1 can be described as a chain of A-A dimers, as far as the HOMO-HOMO interactions are concerned. These dimers face C type BEDT-TTF molecules of the next stack with which they interact strongly, leading to chains of BEDT-TTF HOMOs interacting along the *a* direction. These chains (shown as shaded green stripes in Fig. 39a) are those associated with the bottom part of the upper HOMO band, and thus with the 1D portion of the Fermi surface.

Fig. 40c shows the (*a**, *c**) section of the Lindhard response function calculated at 104 K, the temperature at which the crystal structure was solved. Three different features are labeled as A, B and C in this figure. The maximum of response appears in the region A as a broadened contribution along *c**, ~ 0.17 *a** + (0.38-0.24) *c**. Two much less intense additional features appear in the regions B and C. A detailed analysis allows the identification of the portions of the Fermi surface associated with these features, as schematically shown in Fig. 40b. The strong maximum A corresponds to the nesting of the planar sheets (i.e., the 1D components of the FS). The very weak features of regions B and C are associated with the considerably weaker 1D-2D and 2D-2D nestings, respectively. The maximum of response in A is in good agreement with the wave vector of the superstructure deduced from both the X-ray diffuse scattering [220] and AMRO [234] studies mentioned above.

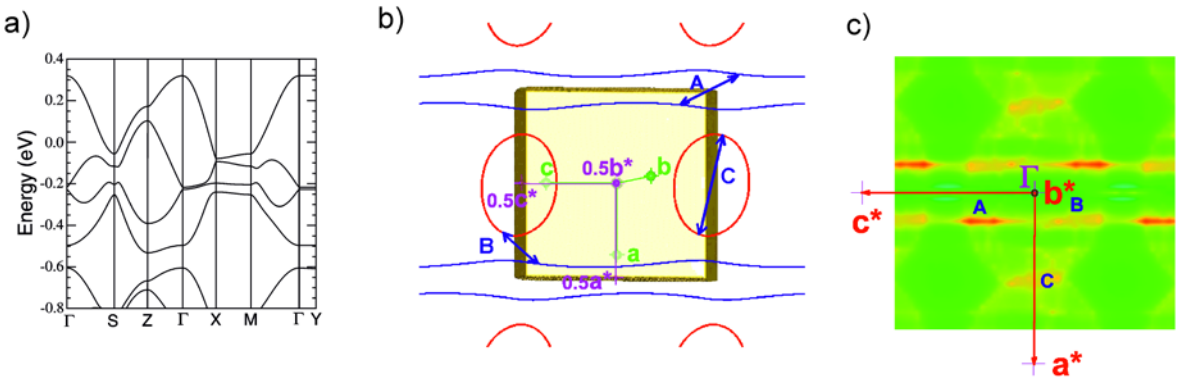

Figure 40. Calculated (a) band structure, (b) Fermi surface and Brillouin zone viewed along a direction perpendicular to the (*a**, c*) plane, and (c) (*a**, *c**) section of the Lindhard response function for α-(BEDT-TTF)$_2$KHg(SCN)$_4$ at 104 K. The energy zero in (a) corresponds to the Fermi level and Γ = (0,0,0), X = (1/2,0,0), Y = (0,1/2,0), Z = (0,0,1/2), M = (1/2,1/2,0), and S = (-1/2,1/2,0) in units of the triclinic reciprocal lattice vectors. The vectors noted A, B and C in the Fermi surface (b) illustrate the type of nesting vectors associated with the A, B, and C maxima in the Lindhard function (c).[220] (Copyright 2010 by the American Physical Society)

5- Nature of the density wave instability.

The *a** and *c** (i.e. intralayer) components of the Lindhard response function are in good agreement with those of the observed q_1 modulation wave vector, thus proving that α-(BEDT-

TTF)$_2$KHg(SCN)$_4$ *undergoes a* $2k_F$ *CDW instability*. It is worth pointing out that since maximum A of the Lindhard function is associated with the best nesting of the 1D component of the Fermi surface, the intrachain a^* component of the modulation should be close to the average $2k_F$ wave vector of the 1D warped component of the Fermi surface (Fig. 40b). Since the stoichiometry dictates that there must be two holes in the four HOMO bands of α-(BEDT-TTF)$_2$KHg(SCN)$_4$, the number of electrons associated with the 1D band must be equal to the number of holes in the 2D band. This means that the area associated with the closed 2D Fermi surface should be ($2k_F \times 100$) % of the cross-section of the Brillouin zone. The values derived from the X-ray diffuse scattering or DFT studies are thus ~13% and ~17%, respectively, in fair match with the value obtained from the AMRO measurements, ~15.7%.

The results of the X-ray diffuse scattering study mentioned above, however, strongly suggest that such instability is not of a standard Peierls type. To begin with, the pretransitional fluctuations do not exhibit any significant broadening along the reciprocal directions perpendicular to the chain direction, as it is usual above the Peierls transition in 1D systems. Second, the q_1 satellite reflections are about one order of magnitude stronger than typical $2k_F$ reflections observed below a Peierls transition. Third, three different harmonics of the modulation with similar intensity are observed. Fourth, the modulation is clearly sensitive to the thermal treatment.

As discussed in detail elsewhere, [84,220] a consistent explanation taking into account all these observations is the following: α-(BEDT-TTF)$_2$KHg(SCN)$_4$ undergoes a high temperature $2k_F$ CDW instability and then, at around 8 K, a second order CDW transition. This instability seems to be triggered by the anion polymeric sublattice (most likely around the K cations because of the unfavorable SCN^- environment) whose anharmonic modulation gives rise to diffuse spots or satellite reflections, depending on the crystallographic quality of the samples, detected above 250 K. As schematically illustrated in Fig. 41a, a local deformation (**u**) of the anionic layer perturbs the hydrogen bonding between the donor and anion layers, a perturbation that is transferred to the central core of the BEDT-TTF donors via a polarization mechanism similar to that given in Fig. 38b. The electronic perturbation at the BEDT-TTF cores can be modeled by a local potential δV, to which the π electron gas reacts via the Lindhard function. The maximum of this response function at q_1 sets an electronic CDW, $\rho(q_1)$, with two consequences. First, through a polarization type mechanism such as that in Fig. 38b it induces a q_1 dependent hydrogen bond polarization wave which leads to a collective deformation wave of the anion layer, $u(q_1)$. Second, the CDW $\rho(q_1)$ induces a structural modulation $w(q_1)$ of the BEDT-TTF layer via the electron-phonon coupling (g_{ep}). The deformation wave of the anion layer, $u(q_1)$, is mostly probed by X-ray measurements and it occurs for all temperatures below 250K-300K. The BEDT-TTF $w(q_1)$ modulation is progressively set down below 200K when additional infrared modes due to the breaking of the inversion symmetry of the BEDT-TTF donors is detected [236] and a pseudo-gap develops in the charge degrees of freedom. [237] The BEDT-TTF $w(q_1)$ short range order (SRO) progressively grows until ~8 K, where a long range order (LRO) is set according to the observation of thermodynamic anomalies and significant changes in the BEDT-TTF NMR spectra. The full process is summarized in Fig. 41b.

This mechanism is qualitatively sustained by ^{13}C NMR measurements in the M = Rb salt [238] which in addition allow to label the type of the BEDT-TTF molecule involved in the different steps of the CDW instability since the development of the CDW modulation on BEDT-TTF of a given type is accompanied by decrease of its local density of states at the Fermi level (due to the formation of a pseudo-gap). The NMR study shows that the density of states of type C donors strongly decreases from room temperature, while the one of type A and B ones drops only below about 120K.

It is worth noting that although the three types of donors participate in hydrogen bonding interactions with the anion lattice, there are those of type C (i.e. those associated with the more constrained regions of the donor layers, as well as with the electronic 1D chains) that are the strongest ones. [220] Thus, the two constrained regions of the donor and anion layers are tightly connected though hydrogen bonds and the instability in the anion layers is easily connected to the $2k_F$ instability of the 1D chains of the BEDT-TTF lattice. The mechanism being that a modulation of type C BEDT-TTF position will strongly modulate the transfer integral between C and A-A molecules forming the chains giving rise to a sizeable electron-phonon coupling necessary to have a CDW-Peierls instability. Thus in agreement with NMR the donor layer modulation, $u(q_1)$ starts locally on type C BEDT-TTF strongly coupled to the anion layer, then via the setting of an effective electron-phonon coupling the CDW instability is collectively transmitted to types A and B donors, inducing the CDW modulation $w(q_1)$.

Also the strong coupling of the donor and anion sublattices through hydrogen bonds can also naturally explain the interlayer component (b^*) of the modulation. The coupling between the anion layer modulation $u(q_1)$ and the BEDT-TTF π electron density $\rho(q_1)$, will be maximized if at the two sides of each BEDT-TTF molecule the local anion deformations occur in opposite directions, $+u$ and $-u$ (see Fig. 41a). As the two local anion deformations are separated by $b+(a+c)/2$, the optimal modulation wave vector q_1 achieving the π phase shift should be given by $q_1 \cdot [b+(a+c)/2] = \pi$. This leads to the relationship $q_a+2q_b+q_c = 1$ which is indeed followed by the wave vector components of the measured q_1 (0.85±0.20) and $3q_1$ (1±0.1) reflections. [220] Since q_a and q_c are also associated with the maximum of the Lindhard function, the above relationship fully accounts for the experimentally observed interlayer q_b component providing a strong argument for the validity of the proposed $2k_F$ CDW mechanism.

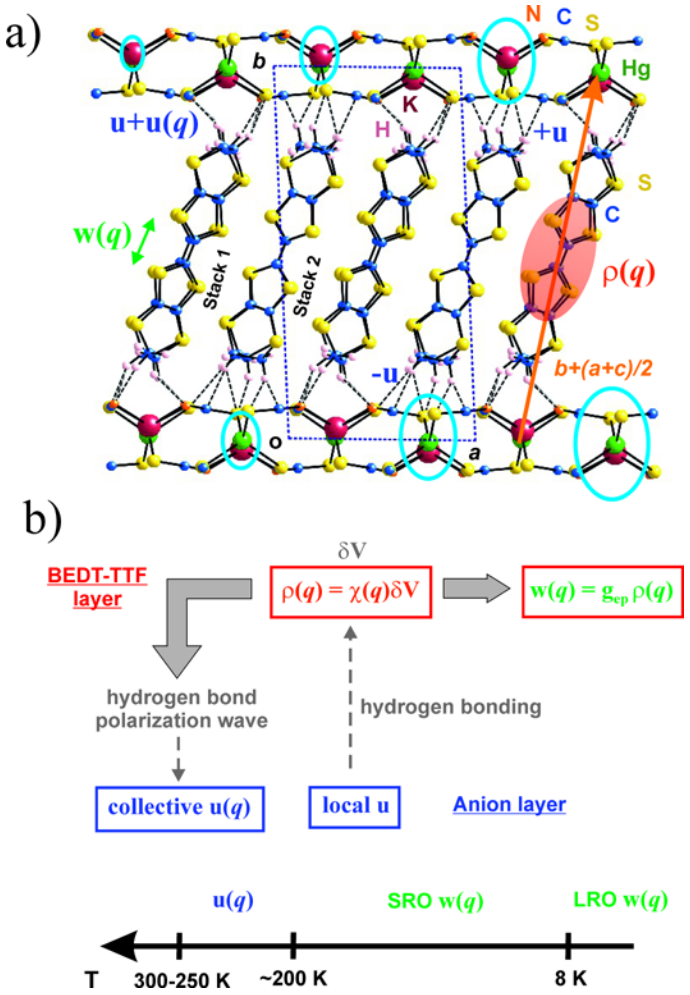

Figure 41. (a) Structure of α-(BEDT-TTF)$_2$KHg(SCN)$_4$ showing the alternation of anion and BEDT-TTF layers along *b* and the hydrogen bonding network coupling them. Empty blue ellipses schematize the modulation wave for the anion layer. The BEDT-TTF central core π-cloud is schematized by a red shaded ellipse. The π phasing between modulations separated by *b*+(*a*+*c*)/2 is schematized by the ±*u* displacement vector at the two sides of a BEDT-TTF molecule. (b) Schematic representation of the proposed mechanism. The thermal dependence of the different structural degrees of freedom considered in the text is indicated in the lower part of the figure. The notations are defined in the text and in part (a).[84] (Copyright 2012 by John Wiley and Sons.)

Finally although the donor layers of α-(BEDT-TTF)$_2$KHg(SCN)$_4$ are of the same structural type as those considered before in α-(BEDT-TTF)$_2$I$_3$, a more in-depth analysis indicates that the structural and electronic constraints induced by the different anions through hydrogen bonds are quite different. As a consequence, *the hydrogen bonding modulations* induced in the salt at low temperature in order to partially relieve such constraints are also quite different. This is at the origin of the vastly different low temperature behavior of the two salts.

D. Metal to insulator transition in the θ-(BEDT-TTF)$_2$RbM'(SCN)$_4$ (M' = Co, Zn) salts.

1- General aspects

θ-(BEDT-TTF)$_2$X salts (where X = I_3, $CsCo(SCN)_4$, $CsZn(SCN)_4$, $RbZn(SCN)_4$, $TlCo(SCN)_4$, ...) are molecular conductors with donor layers of the θ-type [216] where the donor molecules hold an average charge of +1/2, i.e. they are quarter-filled hole band systems. The ambient pressure phase diagram is extremely dependent on the nature of the X anion.[239] For instance, for M = Rb and M' = Zn or Co (except otherwise stated we will refer to the different salts of this family as θ-(M, M'), i.e. θ-(Rb, Zn or Co) in the present case) the salts exhibit a first-order metal to insulator transition at 190-200 K [240-242] and the insulating phase shows a charge disproportionation. [243] In contrast, the θ-(Cs, Zn or Co) salts are bad metals. The resistivity increases gradually below about 50 K with a steeper increase below ~20 K, but no phase transition occurs. [240] For X = I_3 the salt undergoes a metal to superconductor transition at 3.6 K. [244-245] The cooling rate dependence of the nature of the electronic state in θ-(BEDT-TTF)$_2$X salts has also been considered in detail.[246]

The first order transition of the θ-(Rb, Zn or Co) salts has been suggested to be of the CO type as a result of the Coulomb interaction between holes. [208] The metal to insulator transition is associated with a doubling of the periodicity (3D order with q_2 = (0, 0, 1/2)) such that the new unit cell contains two different BEDT-TTF molecules, one charge rich and the other one charge poor, with different tilt angles. [243] Structural work below the transition suggests that the initial +0.5 charge of the donors evolves towards two clearly different values, +0.8 and +0.2. [247-249] The situation in the θ-(Cs, Zn or Co) salts is more complex, with different competing local orders. [47,250] The nature of the phase transition in the θ-(Rb, Zn or Co) salts has been previously analyzed on the basis of different extended Hubbard type approaches where the BEDT-TTF molecules are considered as structureless sites. [208,251-256] Although these treatments provided valuable information, they do not consider the structural degrees of freedom and how they couple with the relevant electronic interactions. Recently using a first-principles DFT treatment a new detailed microscopic mechanism for the metal to insulator transition was suggested. [215] The way in which the conformational degrees of freeedom of the BEDT-TTF six-membered rings respond to the nature of the anion layers plays a key role in this mechanism.

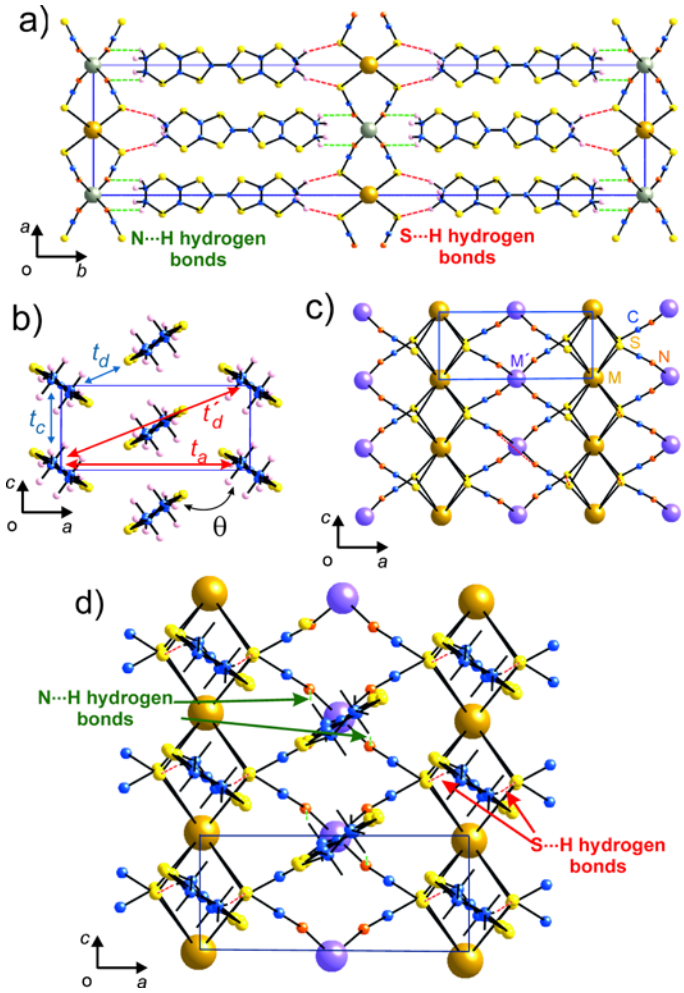

Figure 42. Crystal structure of the θ-(BEDT-TTF)$_2$MM'(SCN)$_4$ salts: (a) and (d) are two views of the interaction between donor and anion layers through N···H (green) and S···H (red) hydrogen bonds. In (a) and (d) the disordered ethylene groups are represented in the majority *t* - $\bar{t}$ staggered conformation; (b) BEDT-TTF donor layer viewed along the long molecular axis. The first (blue) and second (red) nearest-neighbor transfer integrals used in the discussion are defined; (c) anion layer showing the different coordination of M (square prismatic) and M' (tetrahedral).[215] (Copyright 2015 by IOP Publishing)

2-Room Temperature crystal structure of θ-(BEDT-TTF)$_2$MM'(SCN)$_4$ salts.

In these salts donor layers alternate with polyanion layers along the *b*-direction (Fig. 42a). The unit cell contains two sets of symmetry equivalent layers. The donor layers (Fig. 42b) are of the θ-type, built from two symmetry equivalent, uniform chains of inclined donors along *c* related through a 2_1 screw axis. At room temperature there is only one symmetry non-equivalent donor molecule per unit cell. Anion layers (Fig. 42c) are made of M^+ cations coordinated by eight S atoms of the SCN^- ligands in an approximately square-prismatic way and M'^{2+} cations coordinated by four N atoms of the SCN^- ligands forming a distorted tetrahedron. As for α-(BEDT-TTF)$_2$KHg(SCN)$_4$, the donor and anion layers are

interconnected through S···H and N···H hydrogen bonds between the H atoms of the BEDT-TTF molecules and the SCN^- groups in the anion layer. An in-depth analysis of these interactions is not possible because of the conformational disorder of the ethylenedithio groups of the donors in some of these salts (see next paragraph). In Fig. 42 we have plotted the BEDT-TTF donors with the apparently majority *t* - $\bar{t}$ staggered conformation for the terminal ethylenedithio groups. As shown in Fig. 42a each BEDT-TTF molecule makes four hydrogen bonds, two with the S atoms coordinating the M^+ cation and two with the N atoms coordinating the M'^{2+} cation. Consequently, the tetrahedral coordination polyhedron around M'^{2+} interacts with the C_2H_4 groups of two BEDT-TTF molecules (one per donor layer), whereas the square prismatic coordination polyhedron around M^+ interacts with the C_2H_4 groups of four BEDT-TTF (two per donor layer).

A crucial feature of these layers is the occurrence of conformational disorder in the donor ethylenedithio groups revealed by the too short CC bond length and the abnormally high Debye-Waller factors of the C atoms obtained in structural refinements. The extent of disorder changes from salt to salt. For instance, the two ethylenedithio groups are disordered in θ-(Rb, Zn or Co) but only one of them in θ-(Cs, Zn or Co) (i.e. the group facing the Zn or Co coordination polyhedra) and none for X = I_3 (of *t* – *t* type). The extent of disorder occurring in the different structures is controlled by two different interactions: (1) the donor···donor interaction through H···H contacts between two adjacent donors along *c* and, (2) the strength of the hydrogen bonding interactions with the SCN^- ligands of the anion layer. The first interaction should be mostly controlled by the *c* parameter and the tilting angle of the BEDT-TTF molecules with respect to the *c* direction.

3- Crystal structure of the θ-(Rb, Zn or Co) salts after the metal to insulator transition.

When the metal to insulator transition occurs, the periodicity of the crystal structure of θ-(Rb, Zn) doubles along the *c* direction. [243] The most remarkable features associated with this change are the following. First, both the C-C bond length and the Debye-Waller factors of the ethylenedithio carbon atoms become normal. Thus, the C_2H_4 groups order and the BEDT-TTF molecules adopt the *t* – *t* staggered conformation. Second, as shown in Fig. 43a, there is a tilt in opposite directions of adjacent donors along *c*. Third, a structural analysis of the inner parameters of the BEDT-TTF molecules indicates clearly that there is a charge disproportionation, i.e. one of the two donors becomes hole rich (+0.8, molecule B) and the other one hole poor (+0.2, molecule A) as shown in Fig. 43a. [243] Fourth, the donor-anion hydrogen bonding interactions become clearly different for the two types of donors (Fig. 43b).

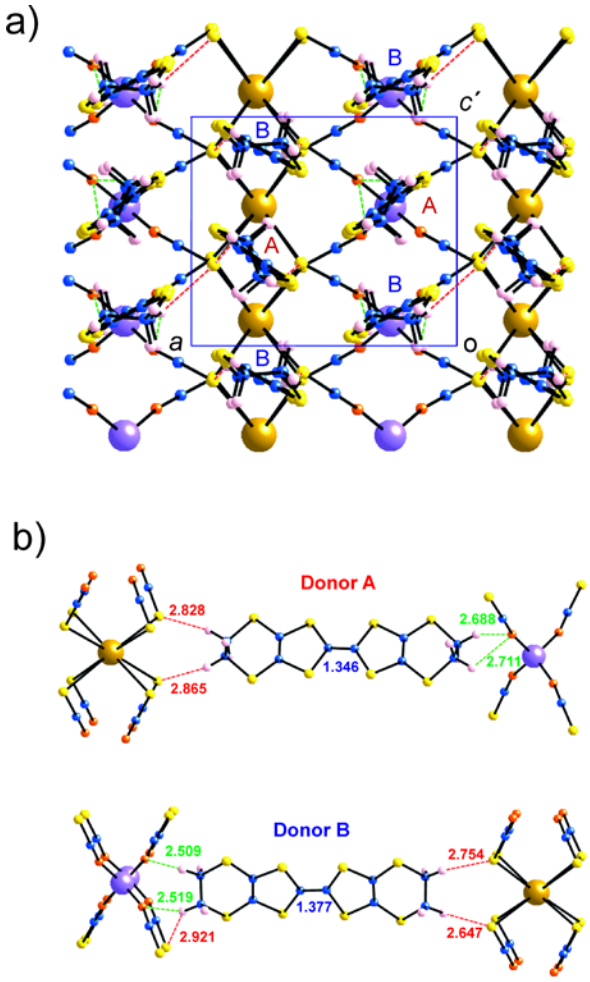

Figure 43. Crystal structure of θ-(BEDT-TTF)$_2$RbZn(SCN)$_4$ at 90 K (below the transition): (a) BEDT-TTF layer viewed along the long molecular axis of the donors showing the two different donor molecules (A and B). (b) Hydrogen bonding donor-anion interactions, N···H (green) and S···H (red), associated with the two different BEDT donors. All highlighted distances are given in Å. [215] (Copyright 2015 by IOP Publishing)

4- Electronic structure of the θ-(Rb, Zn or Co) salts before the metal to insulator transition.

The calculated band structure of the θ-(Rb, Zn) salt using the crystal structure above the metal to insulator transition is shown in Fig. 44a and the associated Fermi surface in Fig. 44b (i.e. the b^*= 0.0 section). Because of the stoichiometry, the two bands (built from the HOMO of BEDT-TTF) contain one hole and the upper band is half-filled. However, since the donor chains have just one donor as the repeat unit, these salts should be considered as quarter-filled band systems. Since the dispersion along the a^* and c^* directions is comparable the system is predicted to behave as a typical 2D metal. Because of the symmetry equivalence of the two layers, the bands appearing in Fig. 44a are actually two superposed bands. The dispersion along the interlayer direction is very small (less than 1 meV) so that the 3D Fermi surface

practically does not exhibit warping along this direction. Previous Extended Hückel tight-binding calculations [240,243] led essentially to similar results, even if the Fermi surface is less elongated and more rounded in the first-principles calculation. The Fermi surface of Fig. 44b does not exhibit any nesting feature that could justify a doubling of the periodicity along the *c*-direction, so that a classical Peierls-type mechanism cannot be at the origin of the metal to insulator transition.

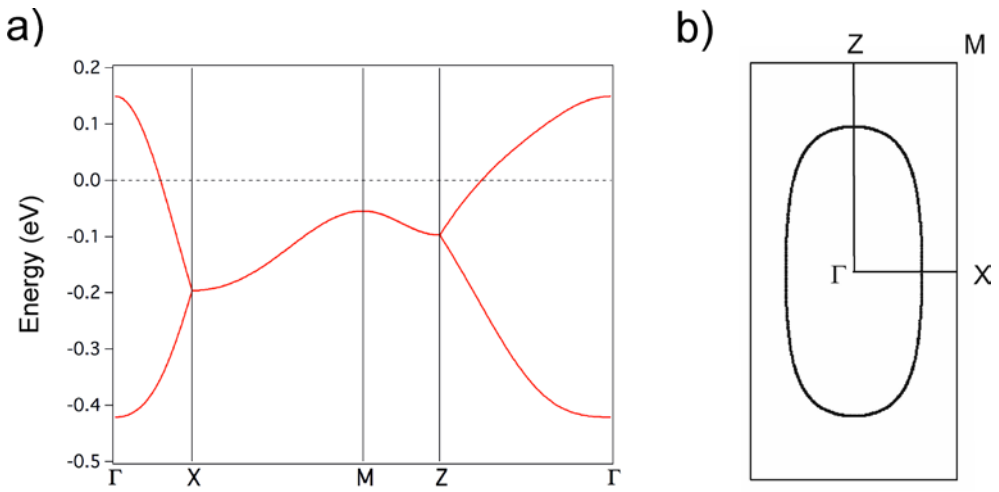

Figure 44. Calculated (a) band structure (b) Fermi surface (*b** = 0.0 section) for θ-(BEDT-TTF)$_2$RbZn(SCN)$_4$ above the metal to insulator transition (220 K). The energy zero in (a) corresponds to the Fermi level and Γ = (0,0,0), X = (1/2,0,0), Z = (0,0,1/2) and M = (1/2,0,1/2) in units of the orthorhombic reciprocal lattice vectors. [215] (Copyright 2015 by IOP Publishing)

5- 1D character of the electronic structure of the θ-(Rb, Zn or Co) salts after the metal to insulator transition.

The band structure for the 90 K structure (i.e. below the metal to insulator phase transition) of θ-(Rb,Zn) is shown in Fig. 45a. The 220 K band structure (Fig. 44a) calculated using an $a \times b \times 2c$ unit cell is reported in Fig. 45b. A comparison of the two band structures reveals that the changes brought about by the transition are very substantial, and especially those around the Fermi level. Most noticeably, there is a strong degeneracy loss at the M' and Z' (upper band) points of the Brillouin zone associated with the loss of the 2_1 screw axis along *c*, leading to a complete reconstruction of the band structure very close to the Fermi level. The Fermi surface (Fig. 45c) can be described as series of closed hole and electron pockets around the X and M' points, respectively. It is worth pointing to the double degeneracy and very small dispersion along the X-M' line, clearly indicating that this system should be described as a weakly warped pseudo-1D system, as sketched in Fig. 45d. The effective transfer integral

in the transverse direction, $t_{\perp}$, is 8 meV, which is considerably smaller than the transition temperature, T_{MI} = 200 K (17 meV). Consequently, the warping of the Fermi surface is not relevant in discussing the mechanism of the transition.

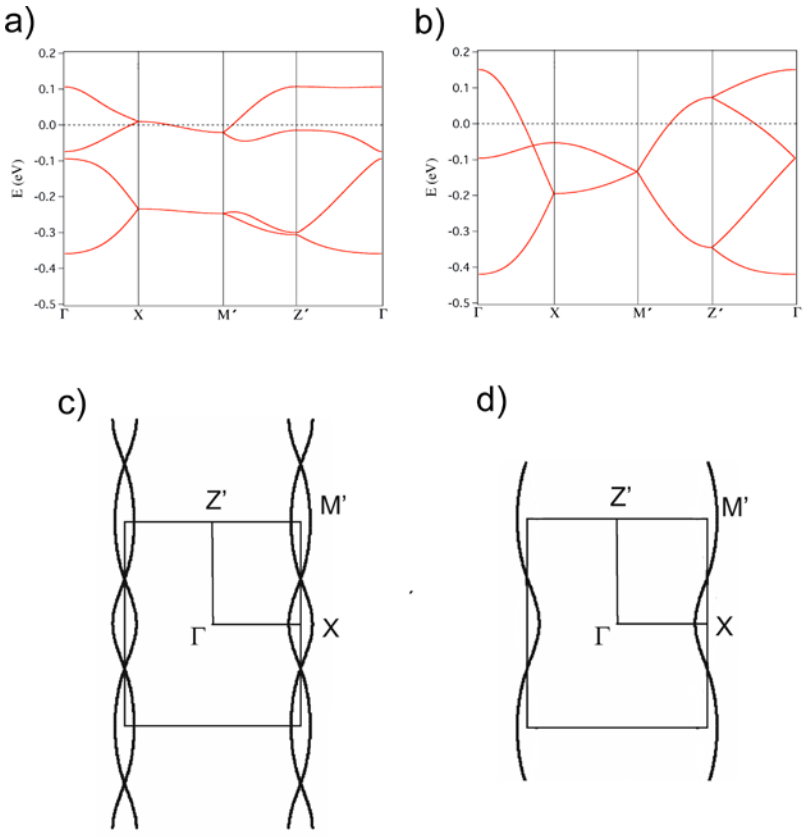

Figure 45. Calculated band structure for θ-(BEDT-TTF)$_2$RbZn(SCN)$_4$ below the metal to insulator transition (90 K crystal structure) (a), and using the crystal structure above the transition (220 K) and a double $a \times b \times 2c$ cell (b). The energy zero corresponds to the Fermi level and Γ = (0,0,0), X = (1/2,0,0), Z' = (0,0,1/2) and M' = (1/2,0,1/2) in units of the $a \times b \times 2c$ orthorhombic reciprocal lattice vectors. Shown in (c) and (d) are two different representations of the 90 K Fermi surface (b^* = 0.0 section). [215] (Copyright 2015 by IOP Publishing)

Although it is a crucial observation in understanding the nature of the metal to insulator transition, it may be surprising that the 1D character of the electronic structure around the Fermi level (see Fig. 45d) is not along the chains (*c*-direction), but along the inter-chains (*a*-direction). The different HOMO-HOMO interactions in the low-temperature structure of θ-(Rb,Zn) are noted in Fig. 46a. Evaluation of the different transfer integrals [243] using the 90 K crystal structure show that (i) c-type transfer integrals are only of secondary importance after the transition, (ii) p-type transfer integrals exhibit a strong modulation such that $|p_4| > |p_2|$ and $|p_1 (\approx p_4)| > |p_3|$. This means that the chains relevant to understand the insulating property

below the transition temperature are the zigzag chains of AB donor dimers along the *a*-direction shown in Fig. 46b. Such chains can be characterized by using two transfer integrals, p1 and p4, and the energy difference between the HOMOs of the A and B donors.[215]

We thus conclude that the transition tends to stabilize a purely 1D electronic system where the holes have a coherent wave function only along the direction of the chains (i.e, the *a*-direction). Analysis of the density of states led to the conclusion that the hole concentration on donors A and B (see Fig. 43) after the transition is +0.37 and +0.63, respectively (i.e. a charge disproportion of 0.26 electrons, in agreement with the reported values for the central C=C bond lengths in the low temperature crystal structure (Fig. 43).

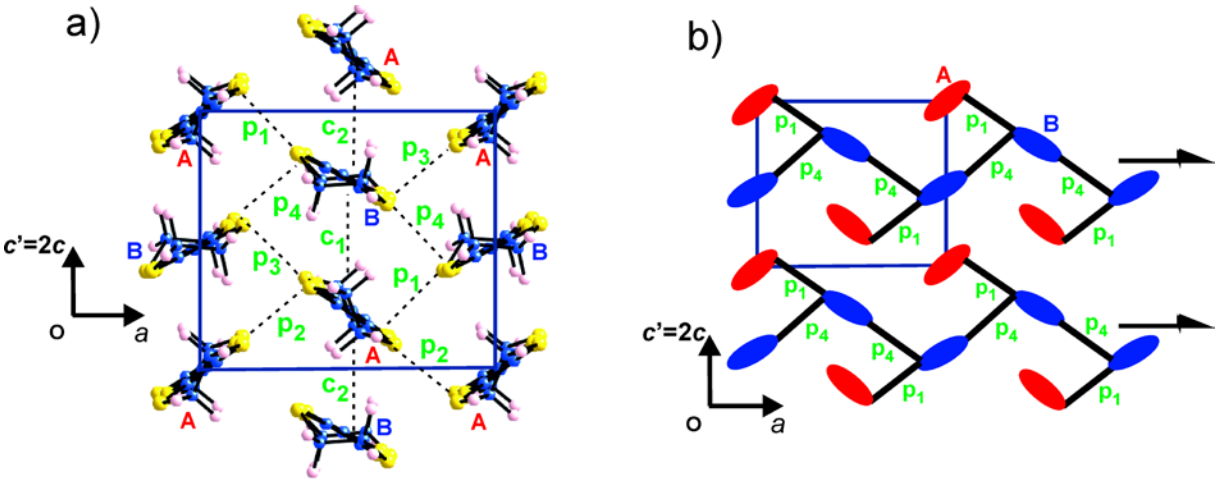

Figure 46. Donor layer of θ-(BEDT-TTF)$_2$RbZn(SCN)$_4$ below the metal to insulator transition where the different transfer integrals are labeled. (b) Schematic representation of (a) emphasizing the 1D character along the *a*-direction. [215] (Copyright 2015 by IOP Publishing)

6- Mechanism of the metal to insulator transition.

It is very important to remember that the metal insulator transition of θ-(Rb, Zn or Co) is a first order phase transition.[240]. This means that a strong coupling between electronic and structural degrees of freedom should be involved in the mechanism of the transition. More explicitly, the DFT study clearly establishes that the structural changes occurring when the system goes through the transition modify the dimensionality of the electron gas from 2D (high temperature) to pseudo-1D along *a* (low temperature). Such reduction of dimensionality makes possible other scenarios than those arousing from extended Hubbard approaches for a 2D electron gas.[208] For instance, since the electron gas becomes pseudo-1D a $4k_F$ instability becomes a real possibility. Let us consider step-by-step all potential mechanisms consistent with a 1D electron gas and examine if they would be consistent with the experimental information. Taken at his right face the Fermi surface of Fig. 45b would predict a metal to metal transition, in disagreement with the metal to insulator experimental result. There are essentially two different mechanisms that can open a gap at the Fermi level and thus

correctly explain the experimental observation. First, the insulating behavior can originate from a Peierls-type mechanism with $2k_F = a^*$. Such a dimerization process of the zigzag chains would lead to the opening of a gap at X and to the disappearance of the 2_1 screw axis along *a*. This would be at odds with the experimental results since the screw axis is kept in the crystal structure below the transition. Second, if the Coulomb repulsions are strong enough, a Mott-Hubbard localization of one hole per AB repeat unit (i.e. every *a*/2 repeat fragment) can occur. In this framework the opening of a gap of charge simply results from a $4k_F = 2a^*$ instability of the 1D electronic system whose treatment is usually beyond the DFT approach. [73,86] In addition, the predominant 1D coupling, p_4 (or t_{BB}), between the localized holes leads to a 1D antiferromagnetic coupling ($J = 2p_4^2/U$) between the ½ spins. Thus, this process would not only explain the insulating property of the low-temperature structure, but also the observed thermal dependence of the spin susceptibility that corresponds to that of a spin ½ antiferromagnetic chain.

However, even if the $4k_F$ Mott-Hubbard localization provides a simple explanation for the insulating and magnetic properties of the low temperature structure, this mechanism can only be relevant if at the same time the main structural feature of the transition, i.e. the doubling along the *c*-direction, as well as the charge disproportionation within the AB dimer can naturally be accounted for. We now show that this is indeed the case. The metal to insulator transition is a first-order one so that several order parameters (structural, electronic) must cooperate in stabilizing the insulating ground state. As mentioned above, the metal to insulator transition is a first-order one so that several order parameters (structural, electronic) must cooperate in stabilizing the insulating ground state. Above the transition the donors the donors of the θ-(Rb, Zn or Co) salts exhibit conformational disorder of the two ethylenedithio groups. Below the transition, both of these groups are in exactly the same staggered conformation so that two of the C-H bonds point out directly towards the anion layer. This feature together with the rotation of the molecular plane of the donor with respect to the *c*-direction allows the simultaneous establishment of two hydrogen bonds involving these H atoms at both sides of the donor (see for instance Figs. 42a and 43b). The two other H atoms point up and down, in a direction not far from perpendicular to the molecular plane, so that destabilizing short H···H inter-donor contacts would be generated if the 2_1 screw axis along *c* was maintained. The simplest way to reduce the destabilizing H···H interactions is a series of opposite rotations around the *b* axis of successive donors along the stacks in the *c*-direction (Figs. 43a and 47). In that way the 2_1 screw axis is destroyed and the repeat unit along *c* doubles. Looking at the H···H contacts within the donor layer it is found that, even after such rotations, relatively short H···H contacts of 2.28 Å (Fig. 47) still remain. H···H intermolecular contacts shorter than 2.4 Å (i.e. shorter than twice the van der Waals radius of H) [256-257] are usually repulsive. Consequently, when the temperature decreases and the ethylenedithio groups tend to order (see a detailed discussion of the process in the next section) it would become increasingly difficult for them to overcome the inter-donor H···H repulsive interactions. Thus, they avoid them by coupling the conformational change associated with the ordering process with the simplest possible motion: a set of alternate opposite rotations

that minimize the repulsive H···H interactions between donor molecules along the stacks while keeping the hydrogen bonding interaction with the anion layers as strong as possible.

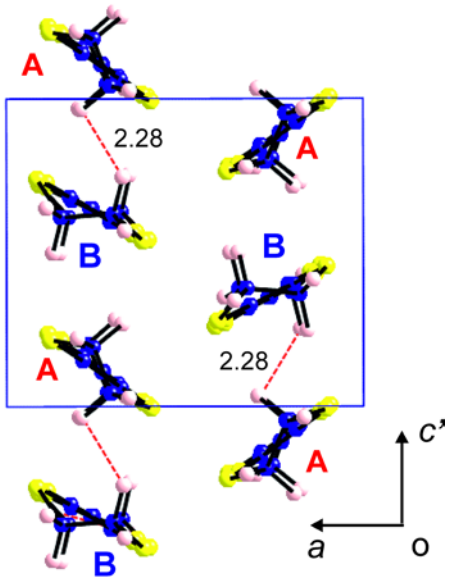

Figure 47. Donor layer of θ-(BEDT-TTF)$_2$RbZn(SCN)$_4$ below the metal to insulator transition. [215] (Copyright 2015 by IOP Publishing)

After the transition, the two donors A and B are no more equivalent and the question of how the hole is distributed among them emerges. As shown in Fig. 43b, donor B makes shorter S···H and N···H hydrogen bonds with the anion layers. As discussed in previous sections and elsewhere [30,84,85,215] there is a subtle electronic mechanism relating the strength of the hydrogen bonding interactions of a donor with the density of holes in the HOMO (see for instance Fig. 38b) such that the donor involved in the stronger hydrogen bonds with the anions develops a larger positive charge in the HOMO and vice versa. Consequently, donor B in θ-(Rb, Zn) below the transition should carry a larger hole density. This is in agreement with the first-principles calculations mentioned at the end of the previous section, as well as with the evaluation using an empirical relationship between the donor charge and structural parameters of the low temperature crystal structure. [247-249]

In conclusion, *the metal to insulator transition of θ-(Rb, Zn or Co) is triggered by an order-disorder structural transition doubling the periodicity along c. By doing this, the donor layers are driven into a pseudo-1D electronic system subject to a $4k_F$ charge localization of the holes*. The structural rearrangement is such that a larger density of holes is associated with the inner zigzag chain of B donors (Fig. 46b) due to the stronger hydrogen bonds established by these with the anion layers. The net result is a spin-charge decoupling with the opening of a gap in the charge but not in the spin degree of freedom Note that in agreement with the possible instabilities of 1D AF spin localized systems (see Figs 10 and 12), a spin gap develops below 25K in the 1D spin susceptibility [239], suggesting the occurrence of a spin-Peierls transition such as the one observed in the 1D Fabre salts (see section III). Here in θ-(Rb, Zn or Co) the SP transition should break the screw axis symmetry along *a* (see Fig. 46b).

The CO mechanism described here is entirely different from those based on extended Hubbard models in which neither the anions nor the change in dimensionality of the electron gas from 2D to pseudo-1D explicitely play a role. [208,251-255].

E. Competition between local orders in θ-(BEDT-TTF)$_2$CsM'(SCN)$_4$ (M' = Co, Zn).

The instability of the metallic state in the θ-(Cs, Zn or Co) salts is considerably more complex. As mentioned, these salts are bad metals and their resistivity increases gradually below ~50 K, with a steeper increase below ~20 K. However, no phase transition occurs. [240] Two different competing 2D local orders, q_1' = (2/3, *k*, 1/3) and q_2' = (0, *k*, 1/2), develop below 120 K in these salts. [47,250] For instance, the origin of the bad metallic behavior lies in a charge localization induced by the q_1'/q_2' structural disorder. Below 50 K the increase of resistivity correlates with the development of a local 3D q_2 order (0, 0, 1/2) [47] like that at the origin of the insulating phase of the θ-(Rb, Zn or Co) salts. In fact, even for the θ-(Rb, Zn or Co) salts the phase diagram may depend on external parameters such as the cooling rate or the application of electric fields. Also situations other than the simple stabilization of the q_2 superstructure are reported in the whole series of θ-(M, M') salts: for instance, occurrence of a different local order q_3' = (2/3, *k*, 1/4) in θ-(Rb, Zn or Co) salts or competition with the different q_1' local order in θ-(Cs, Zn or Co). In this section we will examine how order-disorder processes involving the ethylene groups are most likely at the origin of this situation.

1- Intra-stack ordering of ethylene groups.

Let us consider the uniform stack of BEDT-TTF donors shown in Fig. 48. The repeat unit is just one $t - t$ donor molecule with the molecular plane making an angle ϕ with the stack direction. This chains, referred to as $\cdots(t - t)\cdots$, are very stable because (i) the two six-membered rings of the donor molecules are in the most stable *twist* conformation, and (ii) they contain two pairs of H···S hydrogen bonds linking each pair of donors. This type of inclined chain is the essential building block of the donor layers in the θ salts.[215] In particular, the $\cdots(t - t)\cdots$ chain occurs in θ-(I_3). The two angles ϕ (Fig. 48) and θ (Fig. 42b) are related by ϕ = θ/2. When ϕ increases, repulsive interactions between two pairs of hydrogen atoms develop (see blue arrows in Fig. 48) because the H···H distance becomes too short. Under such conditions a $\cdots(t - t)\ (\bar{t} - \bar{t})\ \cdots$ chain in which one out of each two donors is found in the $\bar{t} - \bar{t}$ form becomes more stable. This is the kind of chain present in the low temperature q_2 superstructure of the θ-(Rb, Zn or Co) salts [243,258] (see Fig. 47). Still another possibility is the uniform $\cdots(t - \bar{t})\cdots$ chain found in the room temperature structure of the θ-(Rb, Zn or Co) [243,258-259] and θ-(Cs, Zn or Co) salts [259] (see Fig. 42).

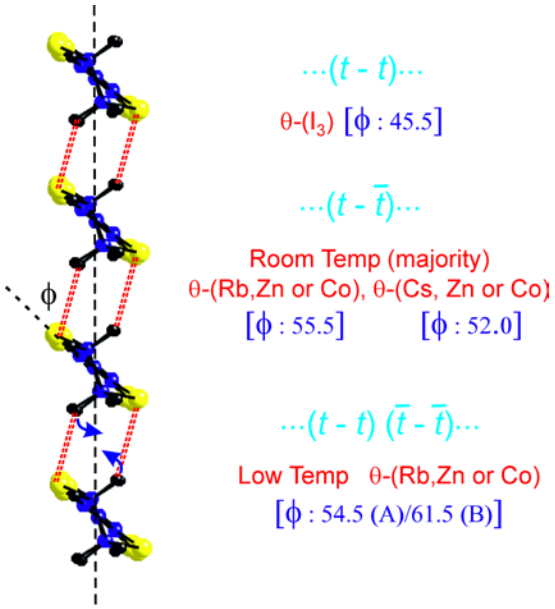

Figure 48. Uniform stack of *t* – *t* BEDT-TTF donors inclined with an angle ϕ with respect to the chain axis. Intermolecular H···S hydrogen bonds are shown as dashed red lines. [215] (Copyright 2015 by IOP Publishing)

The three kinds of chains are all built from BEDT-TTF molecules with both six-membered rings of the most stable *twist* type. Consequently, their stability mostly depends on the ϕ (= θ/2) angle that controls the extent of destabilizing H···H interactions and the number of inter-donor H···S hydrogen bonds. The uniform chain in Fig. 48 is increasingly destabilized as θ increases then a $\cdots(t - \bar{t})\cdots$ chain, and later, a dimerized $\cdots(t - t)\ (\bar{t} - \bar{t})\ \cdots$ chain become increasingly stabilized. In practice this means that as θ increases, there will be a region of the phase diagram for which the stability of the $\cdots(t - t)\cdots$ and $\cdots(t - \bar{t})\cdots$ stacks will be comparable at a local level and consequently, disorder will be observed in one side of the molecule. As θ further increases, disorder will be induced in both six-membered rings. This is exactly what has been observed in the series of θ salts studied at room temperature: as θ increases, disorder is induced first in one end of the donor chains of θ-(Cs, Zn or Co) [259] and then in the two ends of the θ-(Rb, Zn or Co) salts. [243,258-259]

2- Interaction with the anion layers.

The two six-membered rings interact with different regions of the anion layer: the N ends of the SCN^- ligands around M'^{2+} or the S ends of the SCN^- ligands around M^+ (see Fig. 42a). Which of the two six-membered rings will be more prone to exhibit such disorder? Disorder will be more important for weaker hydrogen bonds with the anionic layer. Since the N ends of the ligand face a dication, whereas the S ends face a monocation, it is expected that the later will have their electrons more free to interact with the C-H bonds of the donors. This simple idea agrees with the fact that the actual hydrogen bond distances in these salts (see for instance Fig. 43b) exhibit a larger percentual decrease with respect to the sum of the $r_H + r_X$

van der Waals radii [260] for the S···H interactions than for the N···H ones. Thus, disorder should affect both six-membered rings for larger θ values, but only those facing the M'^{2+} cations for smaller θ values. This is in agreement with the fact that, according to the too short C-C bond length and the abnormally high Debye-Waller factors of the C atoms in the structural refinements, the two ethylidenedithio groups are disordered in θ-(Rb, Zn or Co) [243,258-259] but only the group facing the Zn^{2+} or Co^{2+} coordination polyhedra in θ-(Cs, Zn or Co) [259], and none of them for X = I_3. [244,261]

There is however an important restriction that one must keep in mind. The transition from the uniform $\cdots(t - \bar{t})\cdots$ to the dimerized $\cdots(t - t)\ (\bar{t} - \bar{t})\ \cdots$ chain found in the low temperature structure of the θ-(Rb, Zn or Co) phases, implies formally the change of conformation in one end of a given donor molecule, but in the opposite end of the adjacent ones. Consequently, only when both sides of the donors exhibit disorder in the chain at high temperature there is a possibility of structural transition towards the dimerized stack. This means that the metal to insulator transition associated with q_2 can only occur for salts with large enough θ values, as it is the case of the θ-(Rb, Zn or Co) [243,258-259] and θ-(Tl, Zn or Co) salts. [242] Even if the inter-conversion between *t* and $\bar{t}$ proceeds through a *boat* conformation and must overcome an energy barrier, the previously mentioned calculations by Whangbo and coworkers [22,175-176] have shown that the energy difference is not too high. In addition, for the intermediate conformations of the six-membered ring as well as for the highest point of the barrier (*boat* conformation) the four H atoms of the ethylenedithio group face the anion layer instead of simply two in the *twist* conformation, and can provide a sizable additional stabilization so that the barrier should be relatively low. For instance, both *twist* and *boat* conformations are found in the crystal structure of neutral BEDT-TTF. [176,179]

In the θ-(Cs, Zn or Co) salts, with intermediate θ values,[259] the tendency to undergo conformational changes still occurs, but it is smaller. The first consequence is that disorder will only occur in one of the two six-membered rings (on the M'^{2+} side) thus preventing the metal to insulator transition towards the q_2 superstructure. The second consequence is that the tendency to develop ordered superstructures is decreased and only local orders should be possible. Thus, these phases are expected to keep the metallic character, although when such local orderings develop they will become worse metals. It follows that the $q_2' = (0, k, 1/2)$ local order developed in these phases, even if it implies that the doubling along *c* is not of same nature as the one occurring for salts with larger θ values. Several possibilities arise in which successive donors facing the M'^{2+} cation exhibit either different combinations of *twist* forms, or some of the slightly higher energy conformations between the *twist* and *boat* ones. This possibility is probably the easiest to be realized because the system can partially relieve the H···H interactions without having to overcome a conformational energy barrier. Interestingly, this option opens the possibility of stabilization of longer periodicities along *c* as for the q_1' phase of θ-(Cs, Zn or Co) [250,262] by modulating the conformation of the six-membered ring facing M'^{2+}.

3- Interchain coupling and local orders.

Some of the local orderings occurring in these salts, for instance q_1' and q_3', contain a component along the inter-chain direction, *a*. X-ray diffuse scattering measurements have revealed the occurrence of diffuse lines along the $2a^* + c^*$ and $2a^* - c^*$ directions in θ-(Cs, Zn or Co) [250] and along the $4a^* + 3c^*$ and $4a^* - 3c^*$ directions in θ-(Rb, Zn or Co). [258,263] This means that the disorder of the ethylenedithio groups is not randomly distributed since already at room temperature they are locally correlated with a superlattice periodicity along the $a - 2c$ and $a + 2c$ directions in the former salts and along the $3a - 4c$ and $3a + 4c$ directions in the latter. These anisotropic structural correlations are very surprising because they cannot be adequately explained as a lattice response to a charge localization simply achieved by 2D quite isotropic Coulomb coupling models [208,251-255] and there are no short H···H contacts between the donors of different chains which could provide a correlation between them. In addition, the direction of the 1D correlations depends upon the nature of the M cation or, more likely, if the ethylenedithio groups in contact with M are ordered or disordered.

An important question relied to these observations is to realize that the BEDT-TTF molecules are inclined with respect to the *c* (intrastack) direction and that they establish hydrogen bonds with two SCN^- ligands of the tetrahedrally coordinated M'^{2+} cations (see Fig. 42d). These two ligands point approximately along one of the two 'diagonal' directions, depending on the donor layer we are considering. Thus, the small structural distortions associated with hydrogen bonding occurring around a BEDT-TTF molecule facing the M'^{2+} chain *are necessarily transmitted to a BEDT-TTF donor in the next chain*, located in between M^+ cations. By this process, two BEDT-TTF molecules facing chains of M^+ cations (i.e. two BEDT-TTF molecules related by $a + c$) are correlated. Consequently, *even if the ordering is described as occurring along the c direction, the ordering in different chains may be correlated.*

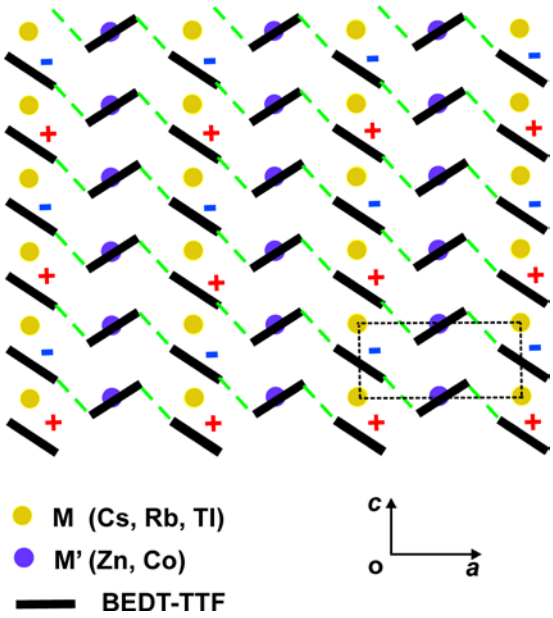

Figure 49. Schematic representation of the lattice in Fig. 42d where links between different chains are drawn as dashed green lines. Plus and minus signs are used to indicate a dimerization along the chain direction, *c*.[215] (Copyright 2015 by IOP Publishing)

A simple example will clarify this point. Let us consider the case of correlations along the $a + 2c$ and $a - 2c$ directions in θ-(Cs, Zn or Co). Disorder only affects the ethylenedithio groups facing M'^{2+} cations because hydrogen bonding with the S atoms around the M^{+} cations is stronger than with the N atoms around the M'^{2+} cations. If the H···H interactions along the chains tend to favor some kind of dimerization along this direction, the fluctuations in equivalent chains along *a* may be in- or out-of-phase. If the link in the 'diagonal' direction of two such equivalent chains is such that they are out-of-phase, a lattice with periodicity along the $a - 2c$ and *c* directions in one layer (but $a + 2c$ and *c* directions in the next layer) will be generated (see Fig. 49). In such case, 1D structural correlations along the $a - 2c$ (and $a + 2c$) directions will be observed. To summarize, the $a + 2c$ periodicity is due to the addition of the correlation of orientation of ethylenedithio groups of two BEDT-TTF molecules facing a M' cation along *c*, and their correlation with the BEDT-TTF molecules of the two neighboring chains along $(a + c)/2$. The latter correlation is fixed by the inclination of the central BEDT-TTF molecule. For the opposite inclination the correlation is along a - 2c. Note that these two intertwined correlations limit the 1D short-range order at about one periodicity along $a \pm 2c$. The observation of diffuse lines along the $2a^* \pm c^*$ reciprocal directions at room temperature in θ-(Cs, Zn or Co) shows that correlations along the $a \pm 2c$ directions are robust.[250] Only the q_1' = (2/3, *k*, 1/3) and q_2' = (0, *k* , 1/2) transverse correlations grow below 120 K by developing a weaker coupling along *c*. According to the present analysis, *the interconversion of the different 2D local orders can be simply achieved by local conformational changes of the ethylenedithio groups.* Such different 2D orders are due to the development along the direction of the stacks of a local periodicity of 3*c* and 2*c* for the q_1' and q_2' modulations, respectively. This local order extends about 6*c*. [264] Since the conformational changes do not require large energies, the inter-conversion of the different local orders with the quenching rate or under the action of an electric field, for instance, must be relatively easy. We thus conclude that with simple structural consideration the smaller value of θ in θ-(Cs, Zn or Co) is at the origin of the very different physical behavior for the two series of θ-(Rb, Zn or Co) and θ-(Cs, Zn or Co) salts.

VI. Concluding remarks.

Along this review we have considered the structural and electronic properties of three-quarter filled electron (or one-quarter filled hole) 1D/2D organic D_2X conductors, emphasizing the role of the interaction of the donor stack/layer with the anion sublattice. Special attention has been devoted to order-disorder phenomena both on the anion sublattice and on the methyl groups or ethylene terminal fragments of the TMTSF, TMTTF and BEDT-TTF donors. We have also shown that Coulomb coupling with the anions often plays a

decisive role when the conduction electron gas confined on stacks or layers of the donors suffers sizeable Coulomb repulsions. Another important observation is that very subtle effects arise from the formation of polarizable H bonds between the anions and mobile terminal groups on the donors.

Fig. 50 gives a schematic illustration of the interactions between donors and anions in the Bechgaard and Fabre salts. Because of the presence of an underlying 1D electron gas, the electronic subsystem of these phases is subject to intrinsic $2k_F$ and $4k_F$ CDW and BOW instabilities (as well as $2k_F$ SDW or AF instabilities). The anion potential also couples directly or indirectly (via hydrogen bond formation) to the charge instabilities. We have shown that anions contribute to the $4k_F$ BOW charge localization phenomenon of the Fabre salts and, through their displacement inside the methyl group cavities, help in stabilizing the $4k_F$ CDW or CO/ferroelectric ground state of these salts. The analysis of the CO structure of δ-(EDT-TTF-CONMe$_2$)$_2$Br has shown that in addition to the shift of the Br anion towards the hole-rich donors, there is a significant modulation of hydrogen bond distances between Br anions and hole-rich (hole-poor) donors, in such a way that stronger hydrogen bonds occur with donors having a larger hole density.

Since non-symmetric anions are disordered in their soft methyl group cavities in the Bechgaard and Fabre salts at RT, an important class of structural instabilities concerns the anion ordering (AO) process upon cooling because of entropic effects. However, such transitions substantially modify the donor electronic structure because of the Coulomb coupling of orientationally ordered anions with the π holes as well as the elastic deformations induced by the AO mechanism. For instance, AO induces a metal-insulator $2k_F$ Peierls-type transition in the X = ReO_4 Bechgaard salts, an inter-stack incommensurate charge transfer in the X = ClO_4 Bechgaard salts, and a metal-$4k_F$ CO/anti-ferroelectric insulator transition in the X = SCN Fabre salt.

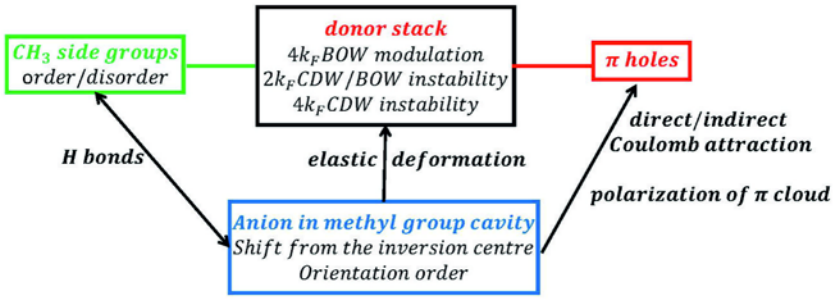

Figure 50. Interactions between donors and anions in the quasi-1D Bechgaard and Fabre salts.

Fig. 51 gives a schematic illustration of the interactions between donor and anion layers in 2D (BEDT-TTF)$_2$X salts. The terminal ethylene groups of the donor play a crucial role in the transport and structural properties of these salts. One must bear in mind several features in trying to rationalize the behavior of these compounds. First, the ethylene groups can adopt several conformations; among them the *t* and *ht* ones being very close in energy. Second, as

there are two ethylene groups per BEDT-TTF donor, several conformations can be realized, the eclipsed (*t* - *t*) and staggered (*t* - $\bar{t}$) ones being the more frequent ones. Third, ^{1}H NMR studies show that conformations of the ethylene groups tend to freeze below about 200 K. Fourth, ethylene groups form hydrogen bonds with the anion layer whose geometry depends upon their structure. Finally, ordered ethylene groups present H···H inter-donor interactions which are repulsive if their relative distance is below the sum of van der Waals radii (2.4 Å).

An important aspect of BEDT-TTF salts is the existence of different ethylene conformations which are very close in energy. This is particularly the case of the *t* and *ht* ones. BEDT-TTF molecules with an ethylene group adopting the terminal *ht* conformation are observed for type A and type C BEDT-TTF molecules in α-(BEDT-TTF)$_2$I$_3$ and α-(BEDT-TTF)$_2$KHg(SCN)$_4$, respectively. Such a conformation which most likely results from the constraints exerted by their close environment seems to be the source of structural instabilities. Indeed, the CO and CDW instabilities occurring in α-(BEDT-TTF)$_2$I$_3$ and α-(BEDT-TTF)$_2$KHg(SCN)$_4$, respectively, would achieve a reduction of such constraints. Additionally, periodic order between ethylene low energy conformations, such as *t* and *ht*, can lead to the formation of long period modulations. Possible candidates for exhibiting such modulations are the ambient pressure incommensurately modulated phase of β-(BEDT-TTF)$_2$I$_3$ and the long period superstructures of pressurized θ-(Cs, Zn or Co). Disorder between conformations of close energy is also very difficult to resorb upon cooling. A remnant local disorder between such conformations can lead to a glassy behavior such as that observed around 70-80 K in κ-(BEDT-TTF)$_2$X with X = Cu[N(CN)$_2$]Br or Cl and X = Cu(NCS)$_2$. [32]

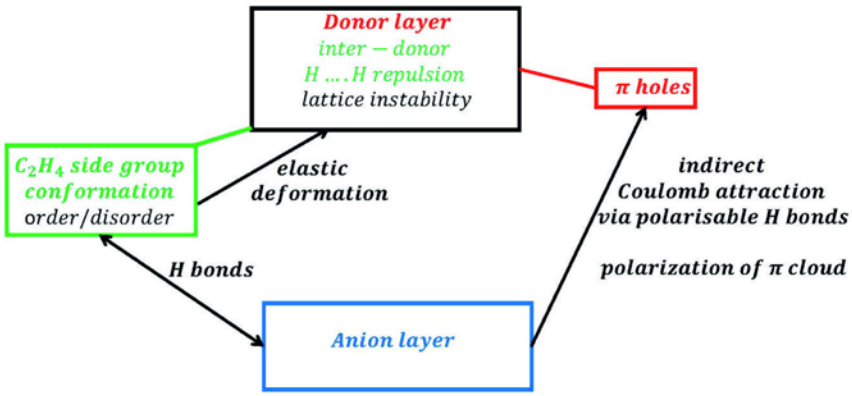

Figure 51. Interactions between anions and donors in the 2D (BEDT-TTF)$_2$X salts.

The onset of H···H repulsions associated with the ordering of ethylene groups may also be at the origin of a structural instability. For example, the ordering of the ethylene groups in θ-(Rb, Zn or Co) induces H···H intermolecular repulsions which induce a staggered tilt of neighboring BEDT-TTF donors leading to a 2*c* superstructure. Such inter-donor H···H repulsions could also be reduced by setting the ambient pressure incommensurate modulation of β-(BEDT-TTF)$_2$I$_3$. It is also important to remind that the donor packing strongly depends

on the conformation of terminal ethylene groups via their hydrogen bonds with the anions. Thus, any variation in the geometry of the hydrogen bond network should modify the packing of BEDT-TTF donor molecules and thus, the donor's electronic structure. In θ-(Rb, Zn or Co) the setting of the 2*c* superstructure changes the dimensionality of the donor electron gas from 2D to 1D. The influence of the eclipsed or staggered molecular conformation over the 2D electronic structure has been carefully studied for several κ-(BEDT-TTF)$_2$X salts [265]. Ethylene groups ensure the coupling between the π-hole inner part of BEDT-TTF molecules and the anion layer via a modulation of the hydrogen bond network. The formation of linked ethylene/anion entities help stabilizing a 3D long range CO pattern, as observed in α-(BEDT-TTF)$_2$I$_3$ and θ-(Rb, Zn or Co). In this respect, notice that a disordered hydrogen bond network could induce a disordered π-charge pattern and a relaxor-type of ferroelectricity (see below).

When charges become localized due to important electron-electron repulsions, a decoupling between charge and spin degrees of freedom is observed with each hole bearing a spin 1/2 which remains available for AF exchange coupling and thus, for low temperature magnetic transitions. In nearly metallic D$_2$X salts, where the gap of charge Δ_ρ is only of a few 10 meV (see Fig. 3), the charge (one hole) is weakly localized on several donor sites. In this case, when charge localization is stabilized by an anion shift, its displacement, u_A, can displace the spin ½ localized hole [86]. This should modify the exchange interaction *J* between neighboring spins. Fig. 52 schematically illustrates how a deformation of the ionic sublattice changing the coupling with donor molecules can modulate inter-donor electronic interactions inducing a strong magneto-elastic coupling, which, as shown in Fig. 52, could be at work in the SP pairing mechanism of (TMTTF)$_2$PF$_6$. [67]

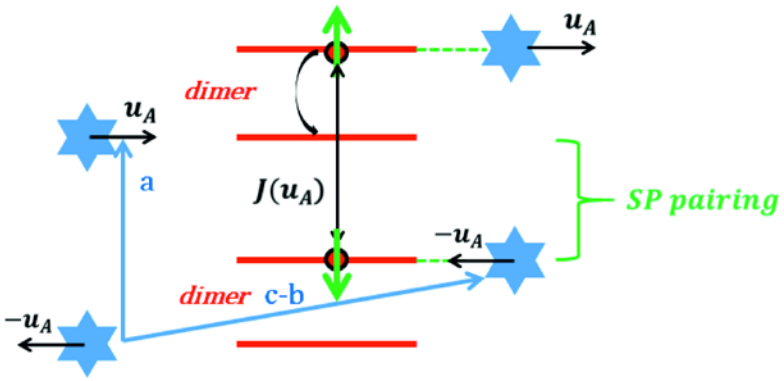

Figure 52. Schematic representation of a dimerized TMTTF stack with its anion environment (blue stars). One hole is localized on each dimer in close contact (dotted green lines) with anions located on the right side of the stack. The staggered acoustic displacement of anions, ± u_A, achieves a hole transfer in the upper dimer with the consequence of modifying the exchange integral *J* between two neigbouring spins which thus can be paired in a spin singlet S = 0 state.

An important phenomenon recently evidenced in the D$_2$X families considered in this review concerns the electronic ferroelectricity associated with CO [51,266-267] having an ionic contribution several orders of magnitude smaller [147] that arises from the anion

sublattice whose deformation stabilizes the CO pattern. In many cases the dielectric constant of D_2X salts does not really exhibit a true divergence at the ferroelectric transition, but a broad frequency-dependent maximum suggestive of a relaxor dielectric response, typical of the formation of local ferroelectric domains. Such a polarisation disorder can be easily rationalized if the anion lattice, whose role is to stabilize the CO, presents some disorder. This occurs in the Fabre salts for kinetic reasons if the ferroelectric transition is at a temperature too low to achieve a spatially coherent displacement of the anions [146]. In α-(BEDT-TTF)$_2$I$_3$ the relaxor type of dielectric response [214] could be related to the presence of disordered hydrogen bonds linked to disordered I_3 entities.[220] In the CO phase several D_2X salts exhibit also an AF ground state. It has thus been suggested that organic materials undergoing a CO instability can be good candidates for multiferroicity.[268] A correlation driven multiferroicity due to dimer formation has been predicted in the Fabre salts.[269-270] However, until now, experimental evidence of multiferroicity has only been reported in κ-(BEDT-TTF)$_2$Cu[N(CN)$_2$]Cl.[36] The observation of a relaxor ferroelectricity in this salt due to a local CO pattern and of a noticeable interlayer lattice anomaly accompanying the AF magnetic transition, suggest, however, that the anion polymeric chain should participate in the multiferroicity phenomenon.

In general, hydrogen bonding tunes the charge transfer/electronic polarization between donor and anion sub-lattices. Fig. 53 shows schematically that a donor stack linked by hydrogen bonds to counter-ions can be modeled by a two level electronic system made of a π hole conduction band and an inner σ electron molecular level linked to anions via hydrogen bonds. If the core of a given donor bears an excess of π hole, intra-molecular Coulomb effects should induce a displacement of σ electrons, $\delta\sigma_e$ (i.e. a polarization of the σ bonds) towards the center of the molecule. This σ charge displacement should be accompanied by a shrinking of the hydrogen bond between the anion and the donor molecule. Then a second hole moving in the stack direction feels the polarization effect induced by the first hole. It results an effective attraction between the two holes. Such a polarization mediated attractive coupling resembles the pairing mechanism proposed more than 50 years ago by Little for excitonic superconductivity as an alternative for the electron-phonon coupling pairing mechanism. [271-272] Such pairing mechanism was illustrated using a hypothetic 1D structure where electrons moving on a C spine linked to polarizable side groups pair up through the polarization of the side groups. As discussed in our work D_2X organic systems exhibit electronic structures which can handle such a mechanism. However it is not yet known if the superconductivity observed in some of these materials could involve the exciton pairing mechanism proposed by Little (for a recent review on organic superconductivity see [56]).

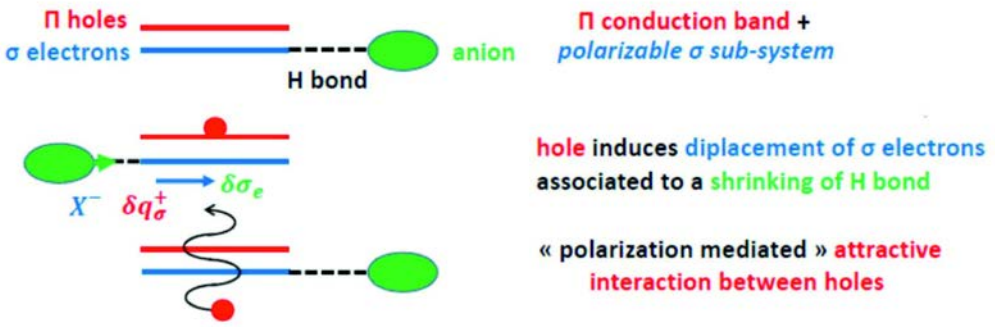

Figure 53. Schematic representation of the π hole (red segment) and inner σ type (blue segment) electronic levels of a donor stack. Hydrogen bonds (dashed black line) couple anions (green ellipse) to σ inner electrons. In the middle of the stack, the occupancy (red circle) of the π hole level polarizes the inner σ bond system (blue arrow) and its hydrogen bond linkage to the anion (green arrow). The wavy vertical black arrow schematizes the attraction of a second hole represented by a red circle.

CONFLICTS OF INTEREST

There are no conficts to declare.

ACKNOWLEDGMENTS

Work in Spain was supported by MINECO (Spain) through Grants FIS2015-64886-C5-4-P and CTQ2015-64579-C3-3-P, and Generalitat de Catalunya (2017SGR1506, 2017SGR1289 and XRQTC). E.C. acknowledges support of the Spanish MINECO through the Severo Ochoa Centers of Excellence Program under Grant SEV-2015-0496. This review is based on recent collaborative works and pertinent discussions with N. Avarvari, P. Batail, C. Bourbonnais, C. Coulon, M. de Souza, M. Dressel, M. Fourmigué, P. Foury-Leylekian, V. Ilakovac, D. Jérome, M. Lang, E. Molins, Y. Nogami, C. Pasquier, H. Sawa and S. Tomić.

REFERENCES

[1] H. Akamatu, H. Inokuchi and M. Matsunaga, Nature **173**, 168 (1954).

[2] C. K. Chiang, C. R. Fincher, Jr, Y. W. Park, A. J. Heeger, H. Shirakawa, E. J. Louis, S. C. Gau and A. G. MacDiarmid, Phys. Rev. Lett. **39**, 1098 (1977).

[3] D.S. Acker, R.J. Harder, W.R. Hertler, W. Mahler, L.R. Melby, R.E. Benson and W.E. Mochel, J. Am. Chem. Soc. **82**, 6408 (1960).

[4] F. Wudl, G.M. Smith and E.J. Hufnagel, Chem. Commun. 1453 (1970).

[5] R. G. Kepler, P. E. Bierstedt and R. E. Merrifield, Phys. Rev. Lett. **5**, 503 (1960).

[6] Such a partial charge transfer has been recently calculated by *ab-initio* methods; see P. Alemany, E. Canadell and J.-P. Pouget, Europhys. Lett. **113** 27006 (2016).

[7] L. R. Melby, Can. J. Chem. **43**, 1448 (1965).

[8] A. J. Heeger and A. F. Garito, AIP Conf. Proc. **10**, 1476 (1972).

[9] J. H. Pearlstein, J. P. Ferraris, V. V. Walatka and D. O. Cowan, AIP Conf. Proc. **10**, 1494 (1972).

[10] D. Jérome and H. J. Schulz, Adv. Phys. **31**, 299 (1982).

[11] D. Jérome, A. Mazaud, M. Ribault, and K. Bechgaard, J. Phys. Lett. (Paris) **41**, L95 (1980).

[12] G. Brun, B. Liautard, S. Peytavin, M. Maurin, E. Toreilles, J. M. Fabre, L. Giral and J. L. Galigné, J. Physique Colloques **38** , C7-266 (1977).

[13] K. Bechgaard, C. S. Jacobsen, K. Mortensen, H. J. Pedersen and N. Thorup, Solid State Commun. **33**, 1119 (1980).

[14] K. Bechgaard, K. Carneiro, M. Olsen and F. B. Rasmussen, Phys. Rev. Lett. **46**, 852 (1981).

[15] G. Saito, T. Enoki, T. Toriumi and H. Inokuchi, Solid State Commun. **42**, 557 (1982).

[16] S. S. P. Parkin, E. M. Engler, R. R. Schumaker, R. Lagier, V. Y. Lee, J. C. Scott and R. L. Greene, Phys. Rev. Lett. **50**, 270 (1983).

[17] V.N. Laukhin, E.E. Kostyuchenko, Yu. Y. Sushko, I.F. Schegolev and E.B. Yagubskii, JETP Lett. **41**,81 (1985).

[18] K. Murata, M. Tokumoyo, H. Anzai, H. Bando, G. Saito, K. Kajimura and T. Ishiguro, J. Phys. Soc. Jpn **54**, 1246 (1985).

[19] H. Urayama, H. Yamochi, G. Saito, K. Nozawa, T. Sugano, M. Kinoshita, S. Sato, K. Oshima, A. Kawamoto and J. Tanaka, Chem. Lett. 55 (1988).

[20] H. Urayama, H. Yamochi, G. Saito, S. Sato, A. Kawamoto, J. Tanaka, T. Mori, Y. Maruyama and H. Inokuchi, Chem. Lett. 463 (1988).

[21] A. M. Kini, U, Geiser, H. H. Wang, K. D. Carlson, J. M. Williams, W. K. Kwok, K. G. Vandervoort, J. E. Thompson, D. Stupka, D. Jung and M.-H. Whangbo, Inorg. Chem. **29**, 2555 (1990).

[22] J. M. Williams, J. R. Ferraro, R. J. Thorn, K. D. Carlson, U. Geiser, H. H. Wang, A. M. Kini and M.-H. Whangbo, *Organic Superconductors (Including Fullerenes): Synthesis, Structure, Properties and Theory*; Inorganic and Organometallic Chemistry Series (Prentice Hall 1992).

[23] K. Miyagawa, K. Kanoda and A. Kawamoto, Chem. Rev. **104**, 563 (2004).

[24] N. Toyota, M. Lang M, and J. Müller, *Low-Dimensional Molecular Metals* (Springer, Berlin 2007).

[25] T. Ishiguro, K. Yamaji and G. Saito *Organic superconductors*, Springer Series in Solid State Sciences Vol. 88 (2nd edition, Springer-Verlag 1998).

[26] C. Bourbonnais and D. Jérome, Science, **281**, 1155 (1988).

[27] R. Laversanne, C. Coulon, B. Gallois, J. P. Pouget, and R. Moret, J. Phys. (Paris), Lett. **45**, L393 (1984).

[28] J.P. Pouget, P. Foury-Leylekian, D. Le Bolloc'h, B. Hennion, S. Ravy, V. Cardoso and A. Moradpour, J. Low Temp. Physics **142**, 147 (2006).

[29] K. Kanoda, Physica C **282 -287**, 299 (1997)

[30] P. Alemany, J.-P. Pouget and E. Canadell, Phys. Rev. B **89,** 155124 (2014).

[31] E. Gati, M. Garst, R. S. Manna, U. Tutsch, B. Wolf, L. Bartosch, H. Schubert, T. Sasaki, J. A. Schlueter and M. Lang, Sci. Adv. **2**, e1601646 (2016).

[32] J. Müller, M. Lang, F. Steglich, J.A. Schlueter, A.M. Kini and T. Sasaki, Phys. Rev. B **65**, 144541 (2002).

[33] J. Müller, B. Hartmann and T. Sasaki, Phil. Mag. **97**, 3477 (2017).

[34] Y. Nogami, J.P. Pouget, H. Ito, T. Ishiguro and G. Saito, Solid State Comm. **89**, 113 (1994).

[35] A. Deluzet, H. Mayaffre, P. Wzietek, P. Sotta, E.Dumont and D. Jérome, Adv. Mater. **10**, 797 (1998) and earlier references there in.

[36] P. Lunkenheimer, J. Müller, S. Krohns, F. Schrettle, A. Loidl, B. Hartmann, R. Rommel, M. de Souza, C. Hotta, J. A. Schlueter and M. Lang, Nature Materials **11**, 755 (2012).

[37] M. Pinterić, D. Rivas Góngora, Z.Rapljenović, T. Ivek, M. Culo, B. Korin-Hamzić, O. Milat, B. Gumhalter , P. Lazić, M. Sanz Alonso , W.Li, A.Pustogow, G. G. Lesseux, M. Dressel and S.Tomić, Crystals, **8**, 190 (2018).

[38] S. Ravy, R. Moret, J.P. Pouget, R. Comès and S.S.P. Parkin, Phys. Rev. B Rapid Comm. **33**, 2049 (1986).

[39] M.-H. Whangbo, J. Ren, W. Liang, E. Canadell, J.P. Pouget, S. Ravy, J. M.Williams and M. A. Beno, Inorg. Chem. **31**, 4169 (1992).

[40] The volume compressibility, κ_V, at ambient conditions of organic conductors $(TMTSF)_2PF_6$ ($\kappa_V \approx 10^{-10}$ Pa^{-1},[41]) $(TMTTF)_2PF_6$ ($\kappa_V \approx 0.9\ 10^{-10}$ Pa^{-1}, [42]) α-(BEDT-$TTF)_2I_3$ ($\kappa_V \approx 1{\cdot}1\ 10^{-10}$ Pa^{-1}, [43]) β-(BEDT-$TTF)_2I_3$ ($\kappa_V \approx 0.8\ 10^{-10}$ Pa^{-1}, [44]), *κ*-(BEDT-$TTF)_2Cu(SCN)_2$ ($\kappa_V \approx 0.8 10^{-10}$ Pa^{-1} [45]), *κ*-(BEDT-$TTF)_2Cu[N(CN)_2]Cl$ ($\kappa_V \approx 0.710^{-10}$ Pa^{-1}

[46]) and of θ-(BEDT-TTF)$_2$CsCo(SCN)$_4$ ($\kappa_V \sim 1 \cdot 110^{-10}$ Pa^{-1} [47]) is one order of magnitude larger than κ_V of typical metals. In the 1D organic salt (TMTSF)$_2$PF$_6$ the largest uniaxial component of the compressibility tensor, $0 \cdot 6\ 10^{-10}$ Pa^{-1}, is slightly tilted with respect to the stack direction. In the 2D metal θ-(BEDT-TTF)$_2$CsCo(SCN)$_4$ the largest uniaxial compressibility, $\sim 10^{-10}$ Pa^{-1}, is along the stacking direction (*c*) of donor molecules (see Fig. 42). Note that thermal volume contraction of (TMTSF)$_2$PF$_6$ from RT to low T is equivalent to the application of a pressure of 7 kbar at RT [41] and that deuteration of (TMTSF)$_2$PF$_6$ is equivalent to the application of a negative pressure of 5 kbar in the hydrogenated compound. [48]

[41] B. Gallois, J. Gaultier, C. Hauw, T. Lamcharfi, and A. Filhol, Acta Crystallogr. Sect. B **42**, 564 (1986).

[42] E. Rose, C. Loose, J. Kortus, A. Pashkin, C. A. Kuntscher, S. G. Ebbinghaus, M. Hanfland, F. Lissner, Th. Schleid and M. Dressel, J. Phys.: Condens. Matter **25**, 014006 (2013).

[43] I. Tamura, H. Kobayashi and A. Kobayashi, J. Phys. Chem. Solids **63**, 1255 (2002).

[44] R. P. Shibaeva and E. B. Yagubskii, Chem. Reviews **104**, 5347 (2004).

[45] D. Chasseau, J. Gaultier, M. Rahal, L. Ducasse, M. Kurmoo and P. Day, Synth. Metals **41-43**, 2029 (1991).

[46] A.J. Schultz, U. Geiser, H.H. Wang, J.M. Williams, L.W. Finger and R.M. Hazen, Physica C **208**, 277 (1993).

[47] Watanabe M, Nogami Y, Oshima K, Mori H and Tanaka S, *J. Phys. Soc. Japan* **68**, 2654 (1999)

[48] P. Foury-Leylekian, S. Petit, I. Mirebeau, G. André, M. de Souza, M. Lang, E. Ressouche, A. Moradpour and J.-P. Pouget, Phys. Rev. B **88**, 024105 (2013).

[49] W. Kang, G. Creuzet, D. Jerome, and C. Lenoir, J. Physique (Paris) **48**, 1035 (1987).

[50] S. Ravy, R. Moret and J.P. Pouget, Phys. Rev. B **38**, 4469 (1988).

[51] S. Tomic and M. Dressel, Rep. Prog. Phys.78, 096501 (2015).

[52] J.P. Pouget, Mol. Cryst. Liq. Cryst. **230**, 101 (1993).

[53] Physics of Organic Conductors and Superconductors, edited by A. G. Lebed, Springer Series in Materials Sciences (Springer-Verlag, Berlin, 2008), Vol. 110.

[54] P. Monceau, Adv. Physics **61**, 325 (2012).

[55] R.T. Clay and S. Mazumdar, arXiv:1802.01551v1 [cond-mat.supr-con] 5 Feb 2018.

[56] A. Ardavan, S. Brown, S. Kagoshima, K. Kanoda, M. Kuroki, H. Mori, M. Ogata, S. Uji, and J. Wosnitza, J. Phys. Soc. Jpn. **81**, 011004 (2012).

[57] J. L. Galigne, B. Liautard, S. Peytavin, G. Brun, J. M. Fabre, E. Toreilles and L. Giral, C. R. Acad Sc. Paris Serie C **285,** 435 (1977).

[58] N. Thorup, G. Rindorf, H. Soling, and K. Bechgaard, Acta Crystallogr. Sect. B **37**, 1236 (1981).

[59] V. J. Emery, J. Phys. (Paris) **44**, C3-977 (1983).

[60] A. Pashkin, M. Dressel, M. Hanfland and C. A. Kuntscher, Phys. Rev. B **81**, 125109 (2010).

[61] J. Hubbard, Phys. Rev. B **17**, 494 (1978).

[62] F. Castet, A. Fritsch and L. Ducasse, J. Phys. I **6**, 583 (1996).

[63] L. Ducasse, A. Fritsch and F. Castet, Synth. Metals **85**, 1627 (1997).

[64] L. Cano-Cortés et al, Eur. Phys. J. B 56, 173 (2007))

[65] K. Nakamura, Y. Yoshimoto, T. Kosugi, R. Arita and M. Imada, J. Phys. Soc. Japan **78**, 083710 (2009).

[66] F. Mila, Phys. Rev. B **52**, 4788 (1995).

[67] J.-P. Pouget, P. Foury-Leylekian, S. Petit, B. Hennion, C. Coulon, and C. Bourbonnais, Phys. Rev. B **96**, 035127 (2017).

[68] J.-P. Pouget, Eur. Phys. J B **20**, 321 (2001).

[69] V. Ilakovac, S. Carniato, P. Foury-Leylekian, S. Tomić, J.-P. Pouget, P. Lazić, Y. Joly, K. Miyagawa, K. Kanoda, and A. Nicolaou, Phys. Rev. B, 96, 184 303 (2017)

[70] J.-P. Pouget, C. R. Phys. **17**, 332 (2016).

[71] C. S. Jacobsen, K. Mortensen, J. R. Andersen and K. Bechgaard, Phys. Rev. B **18**, 905 (1978).

[72] L. Ducasse, M. Abderraba and B. Gallois, J. Phys. C.: Solid State Phys. **18**, L947 (1985).

[73] J.-P. Pouget, Physica B **407**, 1762 (2012).

[74] H. Seo, J. Phys. Soc. Japan **69**, 805 (2000).

[75] H. Seo, J. Merino, H. Yoshioka and M. Ogata, J. Phys. Soc. Japan **75**, 051009 (2006).

[76] C. Bourbonnais and D. Jérome, in Ref. [53], p. 357.

[77] H. Yoshioka, Y. Otsuka and H. Seo, Crystals **2**, 996 (2012).

[78] S. Barisic and S. Brazovskii, in *Recent Developments in Condensed Matter Physics*, edited by J. T. Devreese, Vol.1 (Plenum, New York, 1981), p.327.

[79] V. J. Emery, R. Bruinsma and S. Barisic, Phys. Rev. Lett. **48**, 1039 (1982).

[80] S. Brazovslii and V. Yakovenko, J. Phys. Lett. (Paris) **46,** L111 (1985).

[81] J. Riera and D. Poilblanc, Phys. Rev. B **63**, 241102(R) (2001).

[82] J.-P. Pouget in *Low Dimensional Conductors and Superconductors***,** edited by D. Jérome and L.G. Caron, NATO ASI, B **155** (Plenum Publishing Corporation 1987) p.17.

[83] J.-P. Pouget in *Physics and Chemistry of Low-Dimensional Inorganic Cobductors*, Edited by P. Delhaes and M. Drillon, NATO ASI B**168** (Plenum Publishing Corporation, 1988) p.185.

[84] J.-P. Pouget, P. Foury-Leylekian, P. Alemany and E. Canadell, Phys. Status Solidi B **249**, 937 (2012).

[85] P. Alemany, J.-P. Pouget, and E. Canadell, Phys. Rev. B **85**, 195118 (2012).

[86] J.-P. Pouget, Physica B **460**, 45 (2015).

[87] J.-P. Pouget and S. Ravy, J. Phys. I (France) **6**, 1501 (1996).

[88] J.-P. Pouget, Crystals **2**, 466 (2012).

[89] M. Lang, J. Müller, F. Steglich, A. Brühl, B. Wolf, and M. Dressel, J. Phys. IV (France) **114**, 111 (2004).

[90] M. de Souza, P. Foury-Leylekian, A. Moradpour, J.-P. Pouget, and M. Lang, Phys. Rev. Lett. **101**, 216403 (2008).

[91] M. de Souza and J.-P. Pouget, J. Phys.: Condens. Matter **25** 343201 (2013).

[92] M. de Souza, D. Hofmann, P. Foury-Leylekian, A. Moradpour, J.-P. Pouget, and M. Lang, Physica B **405**, S92 (2010).

[93] V. J. McBrierty, D. C. Douglass, and F.Wudl, Solid State Commun. **43**, 679 (1982).

[94] W. Yu, F. Zhang, F. Zamborszky, B. Alavi, A. Baur, C. A. Merlic, and S. E. Brown, Phys. Rev. B **70**, 121101(R) (2004).

[95] K. Furukawa, T. Hara, and T. Nakamura, J. Phys. Soc. Jpn. **74**, 3288 (2005).

[96] J. C. Scott, H. J. Pedersen, and K. Bechgaard, Phys. Rev. B **24**, 475 (1981).

[97] V. J. McBrierty, D. C. Douglass, F. Wudl, and E. Aharon-Shalom, Phys. Rev. B **26**, 4805 (1982).

[98] J. C. Scott, E. M. Engler,W. G. Clark, C. Murayama, K. Bechgaard and H. J. Pedersen, Mol. Cryst. Liq. Cryst. **79**, 61 (1982).

[99] P. C. Stein, A. Moradpour, and D. Jérome, J. Phys. Lett. (Paris) **46**, L241 (1985).

[100] P. M. Chaikin, T. Tiedje, and A. N. Bloch, Solid State Commun. **41**, 739 (1982).

[101] M. Poirier, A. Langlois, C. Bourbonnais, P. Foury-Leylekian, A. Moradpour, and J.-P. Pouget, Phys. Rev. B **86**, 085111 (2012).

[102] J. M. Delrieu, M. Roger, Z. Toffano, A. Moradpour, and K. Bechgaard, J. Phys. (Paris) **47**, 839 (1986).

[103] In TMTSF-DMTCNQ there is one donor or acceptor per stack periodicity, a. For a quarter-filled band there is on average half a hole per donor which leads, as shown in Fig. 8, to $2k_F = a^*/4$, where $G = a^* = 2\pi/a$ is the stack reciprocal wave vector. This relation is used throughout section II to define the wave length of the modulated states. Fabre and Bechgaard salts are built from a dimer of donors so that the stack periodicity becomes $\tilde{a} \approx 2a$. The 1D band structure associated to the stack of dimers can be viewed as the band structure of Fig. 8 folded at $\pm\tilde{a}^*/2$ reciprocal positions. One thus has $2k_F = \tilde{a}^*/2$ where $\tilde{a}^* = 2\pi/\tilde{a} \approx \pi/a$ is the dimer stack reciprocal periodicity. This definition of $2k_F$ is used throughout section III for the discussion of the Bechgaard and Fabre salts.

[104] S. Megtert, J.-P. Pouget and R. Comés, Ann. New York Academy of Sciences **313**, 234 (1978).

[105] J-.P. Pouget, P. Foury-Leylekian, and M. Almeida, Magnetochemistry **3**, 13 (2017).

[106] J.-P. Pouget and S. Ravy, Synth. Metals **85**, 1523 (1997).

[107] S. Nagata, M. Misawa, Y. Ihara and A. Kawamoto, Phys. Rev. Lett. **110**, 167001 (2013)

[108] S. Kagoshima, Y. Saso, M. Maesato, R. Kondo, and T. Hasegawa, Solid State Commun. 110, 479 (1999);

[109] S. Kagoshima, Y. Saso, M. Maesato, R. Kondo, T.Yamaguchi, V.A. Bondarenko, and T. Hasegawa, Synth.Met. 117, 39 (2001).

[110] H. Bakrim and C. Bourbonnais, Phys. Rev. B **90**, 125119 (2014).

[111] J.-P. Pouget, R. Moret, R. Comès and K. Bechgaard, J. Physique Lett. **42**, L543 (1981).

[112] S. Kumeta, T. Kawamoto, T. Shirahata, Y. Misaki and T. Mori, J. Phys. Soc. Japan **85**, 094701 (2016).

[113] O. Jeannin, E. W. Reinheimer, P. Foury-Leylekian, J.-P. Pouget, P.Auban-Senzier, E. Trzop, E. Collet, and M.Fourmigué, IUCrJ **5**, 361 (2018).

[114] F. Zwick, M. Grioni, G. Margaritondo, V. Vescoli, L. Degiorgi, B. Alavic and G. Grűner, Commun. **113** 179 (2000).

[115] J.-P. Pouget, R. Moret, R. Comès, K. Bechgaard, J.M. Fabre and L. Giral, Mol. Cryst. Liq. Cryst. **79**, 129 (1982).

[116] C. S**.** Jacobsen, H. J. Pedersen, K. Mortensen, G. Rindorf, N. Thorup, J. B. Torrance and K. Bechgaard, J. Phys. C: Solid State Phys. **15**, 2651 (1982).

[117] B. Korin-Hamzić, E. Tafra, M. Basletić, A. Hamzić, G. Untereiner and M. Dressel, Phys. Rev. B **67**, 014513 (2003).

[118] From the C=C central bond length of 1.344 Å for molecule A and 1.324 Å for molecule B one can estimate, using the relationship between C=C bond lengths and *ab-initio* calculation of the charge transfer for $(TMTSF)_2ClO_4$ and NO_3 [23], that the charge transfer from A to B should be of $2\delta\rho \sim 0.04$ electrons, which is nearly one order of magnitude smaller than the value of $2\delta\rho \approx 0.3$ electrons obtained from X-ray diffraction [119] and infra-red [120] data at the AO transition of $(TMTTF)_2ReO_4$. [111]

[119] Y. Nogami and T. Nakamura, J. Phys. IV (France) **12**, Pr9-145 (2002).

[120] A. Pustogow, T. Peterseim, S. Kolatschek, L. Engel, and M. Dressel, Phys. Rev. B

[121] G. Rindorf, H. Soling and N. Thorup, Acta Cryst. C**40** 1137 (1984).

[122] R. Moret, J.-P. Pouget, R. Comès and K. Bechgaard, Phys. Rev. Lett. **49**, 1008 (1982).

[123] L. Ducasse, M. Abderrabba, B. Gallois and D. Chasseau, Synth. Metals **19**, 327 (1987).

[124] Assuming that the site energy on molecules A and B is the same because of the charge compensation, the AO band gap is simply given by the difference of the interdimer transfer integrals. One thus obtains $2\Delta = 2|t_{AA}-t_{BB}| \approx 0.16$ meV, which is close to the experimental gap $2\Delta_{AO} \approx 0.17$-$0.20$ meV. This interpretation contradicts the earlier proposition of refs. [116] and [125] suggesting that the AO gap is intrinsically due to the anion potential.

[125] R. Bruinsma and V. J. Emery J. Phys. (Paris) **44**, C3-1115 (1983).

[126] R. Moret, S. Ravy, J.-P. Pouget, R. Comès and K. Bechgaard, Phys. Rev. Lett. **57**, 1915 (1986).

[127] S. S. P. Parkin, D. Jérome and K. Bechgaard, Mol. Cryst. Liq. Cryst. **79**, 213 (1981).

[128] S. Tomić, D. Jérome and K. Bechgaard, J. Phys. C: Solid State Phys. **17**, L11 (1984).

[129] J.-P. Pouget, R. Moret, R. Comès, G. Shirane, K. Bechgaard, and J. M. Fabre, J. Phys. (Paris) **44**, C3-969 (1983).

[130] J.-P. Pouget, G. Shirane, K. Bechgaard and J. M. Fabre, Phys. Rev. B **27**, 5303 (1983).

[131] D. Le Pévelen, J. Gaultier, Y. Barrans, D. Chasseau, F. Castet, and L. Ducasse, Eur. Phys. J. B **19**, 363 (2001).

[132] S. Yonezawa, Y. Maeno, K. Bechgaard and D. Jérome, Phys. Rev. B **85**, 140502 (R) (2012).

[133] J.-P. Pouget, S. Kagoshima, T. Tamegai, Y. Nogami, K. Kubo, T. Nakajima and K. Bechgaard, J. Phys. Soc. Japan **59**, 2036 (1990).

[134] S. Yonezawa, C.A Marrache-Kikuchi, K. Bechgaard, and D. Jérome, Phys. Rev. B **97**, 014521 (2018).

[135] C. Coulon, P. Delhaès, S. Flandrois, R. Lagnier, E. Bonjour, J. M. Fabre, J. Phys. (France) **43**, 1059 (1982).

[136] Note that if Fig. 9d gives the picture of strongly localized charges on the bonds, the holes are in fact weakly localized in the Fabre salts. The localization length can be estimated, from the charge gap $2\Delta_\rho^{BOW} \sim 60meV$ measured below T_ρ (Fig. 3), as:

$\xi_{loc} = \frac{\hbar v_F}{2\Delta_\rho^{BOW}} = \frac{at}{\sqrt{2}\Delta_\rho^{BOW}}$, which, with the intrastack transfer integral $t \sim 0.2$eV, amounts to 5 stack periods a, $\xi_{loc} \approx 35$ Å.

[137] R. Bozio, M. Meneghetti and C. Pecile, J. Phys. Chem. **76**, 5785 (1982).

[138] D. S. Chow, F. Zamborszky, B. Alavi, D. J. Tantillo, A. Baur, C. A. Merlic and S. E. Brown, Phys. Rev. Lett. **85**, 1698 (2000).

[139] M. Dumm, M. Abaker and M. Dressel, J. Physique IV, **131**, 55 (2005).

[140] M. Dressel, M. Dumm, T. Knoblauch and M. Masino, Crystals **2**, 528 (2012).

[141] S. Kitou, T. Fujii, T. Kawamoto, N. Katayama, S. Maki, E. Nishibori, K. Sugimoto, M. Takata, T. Nakamura and H. Sawa, Phys. Rev. Lett. **119**, 065701 (2017).

[142] C. Coulon, A. Maaroufi, J. Amiell, E. Dupart, S. Flandrois, P. Delhaes, R. Moret, J.-P. Pouget, J.P. Morand, Phys. Rev. B **26**, 6322 (1982).

[143] P. Monceau, F. Y. Nad and S. Brazovskii, Phys. Rev. Lett. **86**, 4080 (2001).

[144] F. Nad and P. Monceau, J. Phys. Soc. Japan **75**, 051005 (2006).

[145] H.H.S. Javadi, R. Laversanne and A. J. Epstein, Phys. Rev.B **37** 4280 (1988).

[146] D. Starešinić, K. Biljaković, P. Lunkenheimer and A. Loidl, Solid State Commun. **137**, 241 (2006).

[147] M. de Souza, L. Squillante, C. Sônego, P. Menegasso, P. Foury-Leylekian, and J.-P. Pouget, Phys. Rev. B **97**, 045122 (2018).

[148] K. Medjanik, A. Chernenkaya, S. A. Nepijko, G. Öhrwall, P. Foury-Leylekian, P. Alemany, E. Canadell, G. Schönhense and J.-P. Pouget, Phys. Chem. Chem. Phys., **17**, 19202 (2015).

[149] K. Medjanik, A. Chernenkaya, X. Kozina, S. A. Nepijko, G. Öhrwall, P. Foury-Leylekian, P. Alemany, G. Schönhense, E. Canadell, and J.-P. Pouget, J. Phys. Chem. A **120**, 8574 (2016).

[150] There is a similar rate of decrease of the $Se/S_{donor}\cdots F_{anion}$ short contact distance between RT and 4 K in $(TMTSF)_2PF_6$ (3.23 Å *vs.* 3.06 Å) and $(TMTTF)_2PF_6$ (3.30 Å *vs.* 3.14

Å). Note that $(TMTSF)_2PF_6$ has even a stronger anion-donor coupling than $(TMTTF)_2AsF_6$ because the $Se_{donor}\cdots F_{anion}$ contact of 3.23Å, significantly shorter than the sum of van der Waals radii (3.37 Å), is larger than the $S_{donor}\cdots F_{anion}$ contact of 3.27Å, which coincides with the sum of van der Waals radii (3.27 Å). Also note that the F1s spectra is observed at higher photon energy for the PF_6 anion in $(TMTSF)_2PF_6$ than for the AsF_6 anion in $(TMTTF)_2AsF_6$ (see Fig. 21).

[151] P. Foury-Leylekian, S. Petit, G. André, A. Moradpour and J.-P. Pouget, Physica B **405**, S95 (2010).

[152] M. de Souza, A. Brűhl, J. Műller, P. Foury-Leylekian, A. Moradpour, J.-P. Pouget and M. Lang, Physica B **404**, 494 (2009).

[153] K. Medjanik, M. de Souza, D. Kutnyakhov, A. Gloskovskii, J. Műller, M. Lang, J.-P. Pouget, P. Foury-Leylekian, A. Moradpour, H.-J. Elmers and G. Schönhense, Eur. Phys. J. B **87**, 256 (2014).

[154] C. Coulon, G. Lalet, J.-P. Pouget, P. Foury-Leylekian, A. Moradpour and J. M. Fabre, Phys. Rev. B **76**, 085126 (2007).

[155] C. Coulon, P. Foury-Leylekian, J. M. Fabre and J.-P. Pouget, Eur. Phys. J. B **88**, 85 (2015).

[156] T. J. Kistenmacher, Solid State Commun. **50**, 729 (1984).

[157] B. Köhler, E. Rose, M. Dumm, G. Untereiner, and M. Dressel, Phys. Rev. B **84**, 035124 (2011).

[158] R. Rösslhuber, E. Rose , T. Ivek , A. Pustogow, T. Breier, M. Geiger, K. Schrem, G. Untereiner and M. Dressel, Crystals, **8**, 121 (2018).

[159] H. Bakrim and C. Bourbonnais, Phys. Rev. B **76**, 195115 (2007).

[160] B. Liautard, S. Peytavin, G. Brun and M. Maurin, J. Physique **43**, 1453 (1982).

[161] F. Zamborszky, W. Yu, W. Raas, S. E. Brown, B. Alavi, C. A. Merlic, and A. Baur, Phys. Rev. B **66**, 081103(R) (2002).

[162] M. Nagasawa, F. Nad, P. Monceau and J.-M. Fabre, Solid State Commun. 136, 262 (2005).

[163] J. E. Hirsch and E. Fradkin, Phys. Rev. B **27**, 4302 (1983).

[164] P. Foury-Leylekian, D. Le Bolloc'h, B. Hennion, S. Ravy, A. Moradpour, and J.-P. Pouget, Phys. Rev. B **70**, 180405(R) (2004).

[165] A. Langlois, M. Poirier, C. Bourbonnais, P. Foury-Leylekian, A. Moradpour and J.-P. Pouget, Phys. Rev. B **81**, 125101 (2010).

[166] D. S. Chow, P. Wzietek, D. Folliatti, B. Alavi, D. J. Tantillo, C. A. Merlic, and S. E. Brown, Phys. Rev. Lett. **81**, 3984 (1998).

[167] L. Zorina, S. Simonov, C. Mezière, E. Canadell, S. Suh, S. F. Brown, P. Foury-Leylekian, P. Fertey, J.-P. Pouget and P. Batail, J. Mater. Chem. **19**, 6980 (2009).

[168] K. Heuzé, M. Fourmigué, P. Batail, C. Coulon, R. Clérac, E. Canadell, P. Auban-Senzier, S. Ravy and D. Jérome, Adv. Mater. **15**, 1251 (2003).

[169] P. Auban-Senzier, C. Pasquier, D. Jérome, S. Suh, S. E. Brown, C. Mezière and P. Batail, Phys. Rev. Lett. **102**, 257001 (2009).

[170] K. Bender, K. Dietz, H. Endres, H. W. Helberg, I. Hennig, H. J. Keller, H. W. Schäfer and D. Schweitzer, Mol. Cryst. Liq. Cryst. **107**, 45 (1984).

[171] E. B. Yagubskii, I. F. Schegolev, V. N. Laukhin, P. A. Kononovich, M. V. Kartsovnik, A. V. Zvarykina and L. A. Buravov, JETP Lett. **39**, 12 (1984; R. P. Shibaeva, V. F. Kaminskii and V. K. Bel'skii, Sov. Phys. Crystallogr. **29**, 638 (1984).

[172] T. Mori, A. Kobayashi, T. Sasaki, H. Kobayashi, G. Saito and H. Inokuchi, Chem. Lett. 957 (1984).

[173] J. M. Williams, T. J. Emge, H. H. Wang, M. A. Beno, P. T. Copps, L. N. Hall, K. D. Carlson and G. W. Crabtree, Inorg. Chem. **23**, 2558 (1984).

[174] S. S. P. Parkin, E. M. Engler, V. N. Lee and R. R. Schumaker, Mol. Cryst. Liq. Cryst. **119**, 375 (1985).

[175] J. J. Novoa, M.-H. Whangbo and J. M. Williams, Mol. Cryst. Liq. Cryst. **181**, 25 (1990).

[176] M.-H. Whangbo, D. Jung, J. Ren, M. Evain, J. J. Novoa, F. Mota, S. Alvarez, J. M. Williams, M. A. Beno, A. M. Kini, H. H. Wang and J. R. Ferraro in *The Physics and Chemistry of Organic Superconductors*, G. Saito and S. Kagoshima Eds., Springer-Verlag Berlin, Heidelberg, 1990, pp. 262-266.

[177] M.-H. Whangbo, J. M. Williams, A. M. Schultz, T. E. Emge and M. A. Beno, J. Am. Chem. Soc.**109**, 90 (1987).

[178] A. Aburto and E. Orgaz, Phys. Rev. B **78**, 113104 (2008).

[179] H. Kobayashi, A. Kobayashi, Y. Sasaki, G. Saito and H. Inokuchi, Bull. Chem. Soc. Jpn. **59**, 301 (1986).

[180] J. M. Williams, H. H. Wang, M. A. Beno, T. J. Emge, L. M. Sowa, P. T. Copps, F. Behroozi, K. D. Carlson and G. W. Crabtree, Inorg. Chem. **23**, 3839 (1984).

[181] R. P. Shibaeva, R. M. Lobkovskaya, M. A. Simonov, E. B. Yagubskii and A. A. Ignat'ev, Sov. Phys. Crystallogr. **31**, 654 (1986).

[182] J. M. Williams, A. M. Kini, H. H. Wang, K. D. Carlson, U. Geiser, L. K. Montgomery, G. J. Pyrka, D. M. Watkins, J. M. Kommers, S. J. Boryschuk, A. V. Strieby Crouch, W. K. Kwok, J. E. Schirber, D. L. Overmyer, D. Jung and M.-H. Whangbo, Inorg. Chem. 29, 3272 (1990).

[183] U. Geiser, A. J. Schultz, H. H. Wang, D. M. Watkins, D. L. Stupka, J. M. Williams, J. E. Schirber, D. L. Overmyer, D. Jung, J. J. Novoa and M.-H. Whangbo, Physica C **174**, 475 (1991).

[184] A. U. B. Wolter, R. Feyerherm, E. Dudzik, S. Süllow, Ch. Strack, M. Lang and D. Schweitzer, Phys. Rev. B **75**, 104512 (2007).

[185] T. Hiramatsu, Y. Yoshida, G. Saito, A. Otsuka, H. Yamochi, M. Maesato, Y. Shimizu, H. Ito and H. Kishida, J. Mater. Chem. C **3**, 1378 (2015).

[186] C. Lemouchi, K. Iliopoulos, L. Zorina, S. Simonov, P. Wzietek, T. Cauchy, A. Rodríguez-Fortea, E. Canadell, J. Michl, D. Gindre, M. Chrysos and P. Batail, J. Am. Chem. Soc. **135**, 9366 (2012).

[187] U. Geiser, H.H Wang, K.D. Carlson, J.M. Williams, H.A. Charlier, J.E. Heindl, G.A. Yaconi, B.J. Love, M.W. Lathrop, J.E. Schirber, D.L. Overmeyer, J. Ren, M.H. Whangbo, Inorg. Chem. **30**, 2587 (1991).

[188] H. O. Jeschke, M. de Souza, R. Valenti, R. Sekhar Manna, M. Lang, J. A. Schlueter, Phys. Rev. B, **85**, 035125 (2012).

[189] P. Foury-Leylekian, V. Ilakovac, V. Balédent, P. Fertey, A. Arakcheeva, O. Milat, D. Peterman, G. Guillier, K. Miyagawa, K. Kanoda, P. Alemany, E. Canadell, S. Tomic and J. P. Pouget, Crystals **8**, 158 (2018).

[190] V. N. Molchanov, R. P. Shibaeva, V. F. Kaminski, E. B. Yagubskii, V. I. Simonov, B. K. Vainshtein, Dokl. AN SSSR **286**, 637 (1986).

[191] P. C. W. Leung, T. J. Emge, M. A. Beno, H. H. Wang, J. M. Williams,V. Petricek and P. Coppens, J. Am. Chem. Soc. **106**, 7644 (1984).

[192] P. C. W. Leung, T. J. Emge, M. A. Beno, H. H. Wang, J. M. Williams,V. Petricek and P. Coppens, J. Am. Chem. Soc. **107**, 6184 (1985).

[193] A. J. Schultz, H. H. Wang, J. M. Williams and A. Filhol, J. Am. Chem. Soc. **108**, 7853 (1986).

[194] S. Ravy, J. P. Pouget, R. Moret and C. Lenoir, Phys. Rev. B **37**, 5113 (1988).

[195] K. Bender, I. Henning, D. Schweitzer, K. Dietz, H. Endres and H. J. Keller, Mol. Cryst. Liq. Cryst. **108**, 359 (1984).

[196] R. P. Shibaeva, V. P. Kaminskii and E. B. Yagubskii, Mol. Cryst. Liq. Cryst. **119**, 361 (1985).

[197] H. Kobayashi, R. Kato, A. Kobayashi, Y. Nishio, K. Kajita, and W. Sasaki, Chem. Lett. **15**, 833 (1986)

[198] T. J. Emge, P. C. W. Leung, M. A. Beno, J. M. Williams, M.-H, Whangbo and M. Evain, Mol. Cryst. Liq. Cryst. **138**, 393 (1986).

[199] H. Endres, H. J. Keller, R. Swietlink. D. Schweitzer, K. Angermund and C. Krüger, Z. Naturforsch. A **41**, 1319 (1986).

[200] Y. Nogami, S. Kagoshima, T. Sugano and G. Saito, Synth. Met. **16**, 367 (1986)

[201] H. Kino and H. Fukuyama, Synth. Met. **65**, 921 (1995).

[202] K. Yamamoto, S. Iwai, S. Bokyo, A. Kashiwazaki, F. Hiramatsu, C. Okabe, N. Nishi and K. Yakushi, J. Phys. Soc. Jpn. **77**, 074709 (2008).

[203] K. Yamamoto, A. A. Kowalska and K. Yakushi, Appl. Phys. Lett. **96**, 122901 (2010).

[204] T. Kakiuchi, Y. Wakabayashi, H. Sawa, T. Takahashi and T. Nakamura, J. Phys. Soc. Jpn. **76**, 113702 (2007).

[205] A. Kobayashi, S. Katayama, K. Noguchi and Y. Suzumura, J. Phys. Soc. Jpn. **69**, 543 (2004).

[206] M. Hirata, K. Ishikawa, K. Miyagawa, M. Tamura, C. Berthier, D. Basko, A. Kobayashi, G. Matsuno and K. Kanoda, Nat. Commun. **7**, 12666 (2016).

[207] H. Kino and H. Fukuyama, J. Phys. Soc. Jpn. **65**, 2158 (1996).

[208] H. Seo, J. Phys. Soc. Jpn **69**, 805 (2000).

[209] Y. Takano, K. Hiraki, H. M. Yamamoto, T. Nakamura and T. Takahashi, J. Phys. Chem. Solids **62**, 393 (2001).

[210] R. Wojciechowsski, K. Yamamoto, K. Yakushi, M. Inokuchi and A. Kawamoto, Phys. Rev. B **67**, 224105 (2003).

[211] T. Ivek, B. Korin-Hamzić, O. Milat, S. Tomić, C. Clauss, N. Drichko, D. Schweitzer and M. Dressel, Phys. Rev. B **83**, 165128 (2011).

[212] Y. Yue, K. Yamamoto, M. Uruichi, C. Nakano, K. Yakushi, S. Yamada, T. Hiejima and A. Kawamoto, Phys. Rev. B **82**, 075134 (2010).

[213] B. Rothaemel, L. Forro, J. Cooper, J. Schilling, M. Weger, P. Bele, H. Brunner, D. Schweitzer and H. Keller, Phys. Rev. B **34**, 704 (1986).

[214] T. Ivek, M. Čulo, M. Kuveždić, E. Tutiš, M. Basletić, B. Mihaljević, E. Tafra, S. Tomić, A. Löhle, M. Dressel, D. Schweitzer, and B. Korin-Hamzić Phys. Rev. B 96, 075141 (2017).

[215] P. Alemany, J.-P. Pouget and E. Canadell, J. Phys.: Condens. Matter **27**, 465702 (2015).

[216] T. Mori, H. Mori and S. Tanaka, Bull. Chem. Soc. Jpn. **72**, 179 (1999).

[217] R. Rousseau, M.-L. Doublet, E. Canadell, R. P. Shibaeva, S. S. Khasanov, L. P. Rozenberg, N. D. Kushch and E. B. Yagubskii, J. Phys. I France, **6**, 1527 (1996).

[218] G. A. Jeffrey, *An Introduction to Hydrogen Bonding* (Oxford University Press, New York, 1997).

[219] M. Dressel, G. Grüner, J.-P. Pouget, A. Breining, and D. Schweitzer, J. de Physique I (France) **4**, 579 (1994).

[220] P. Foury-Leylekian, J.-P. Pouget, Y.-J. Lee, R. Nieminen, P. Ordejón and E. Canadell, Phys. Rev. B **82**, 134116 (2010).

[221] M. Monteverde, M. O. Goerbig, P. Auban-Senzier, F. Navarin, H. Henck, C. Pasquier, C. Mezière, P. Batail, Phys. Rev. B **87**,245110 (2013).

[222] F. Navarin, E. Tisserond, P. Auban-Senzier, C. Mezière, P. Batail, C. Pasquier, M. Monteverde, Physica B, **460**, 257 (2014).

[223] W. Li, E. Uykur, C. A. Kuntscher, and M. Dressel, arXiv:1803.00755v1 [cond-mat.str-el] 2 Mar 2018.

[224] M. Oshima, H. Mori, G. Saito and K. Oshima, Chem. Lett. 1159 (1989).

[225] H. Mori, S. Tanaka, M. Oshima, G. Saito, T. Mori, Y. Maruyama and H. Inokuchi, Bull. Chem. Soc. Jpn. **63**, 2183 (1990).

[226] R. P. Shibaeva and L. P. Rozenberg, Crystallogr. Rep. **39**, 47 (1994).

[227] R. P. Shibaeva, L. P. Rozenberg, N. D. Kushch and E. B. Yagubskii, Crystallogr. Rep. **39**, 747 (1994).

[228] T. Sasaki, N. Toyota, M. Tokumoto, N. Kinoshita and H. Anzai, Solid State Commun. **75**, 93 (1990).

[229] N. Kinoshita, M. Tokumoto and H. Anzai, J. Phys. Soc. Jpn. **60**, 2131 (1991)

[230] N. D. Kushch, L. V. Buravov, M. V. Kartsovnik, V. N. Laukhin, S. I. Pesotskii, R. P. Shibaeva, L. P. Rozemberg, E. B. Yagubskii and A. V. Zvarikina, Synth. Met. **46**, 271 (1992).

[231] H.-H. Wang, K. D. Carlson, U. Geiser, W. K. Kwok, M. D. Vashon, J. E. Thompson, N. F. Larsen, G. D. McCabe, R. S. Hulscher and J. M. Williams, Physica C **166**, 57 (1990).

[232] A.-I. Schegolev, V. N. Laukhin, A. G. Komenko, M. V. Kartsovnik, R. P. Shibaeva, L. P. Rozemberg and A. E. Kovalek, J. Phys. I France, **2**, 2123 (1992).

[233] L. Ducasse and A. Fritsch, Solid State Commun. **91**, 201 (1994)

[234] A. P. Kovalev, M. V. Kartsovnik, R. P. Shibaeva, L. P. Rozenberg, I. F. Schegolev and N. D. Kushch, Solid State Commun. **89**, 575 (1994).

[235] P. Foury-Leylekian, S. Ravy, J. P. Pouget and H. Müller, Synth. Met. **137**, 1271 (2003).

[236] T. Hiejima, S. Yamada, N. Uriuchi and K. Yakushi, Physica B **405**, S153 (2010).

[237] M. Dressel, N. Drichko, J. Schlueter, and J. Merino, Phys. Rev. Lett. **90**, 167002 (2003).

[238] K. Noda, Y. Ihara and A. Kawamoto, Phys. Rev. B **87**, 085105 (2013).

[239] H. Mori, J. Phys. Soc. Jpn. **75**, 051003 (2006)

[240] H. Mori, S. Tanaka and T. Mori, Phys. Rev. B **57**, 12023 (1998).

[241] H. Mori, S. Tanaka and T. Mori, Mol. Cryst. Liq. Cryst. **284**, 15 (1996).

[242] H. Mori, S. Tanaka, T. Mori, A. Kobayashi and H. Kobayashi, Bull. Chem. Soc. Jpn. **71**, 797 (1998).

[243] M. Watanabe, Y. Noda, Y. Nogami and H. Mori, J. Phys. Soc. Jpn. **73**, 116 (2004)

[244] H. Kobayashi, R. Kato, A. Kobayashi, Y. Nishio, K. Kajita and W. Sasaki, Chem. Lett. 789 (1986).

[245] H. Kobayashi, R. Kato, A. Kobayashi, Y. Nishio, K. Kajita and W. Sasaki, Chem. Lett. 833 (1986).

[246] F. Kagawa and H.Oike, Adv. Mater. **29**, 1601979 (2017).

[247] A. Kawamoto, K. Kanoda, K. Miyagawa, Phys. Rev. B **62**, R7679 (2000).

[248] K. Yamamoto, K. Yakushi, K. Miyagawa, K. Kanoda and A. Yamamoto, Phys. Rev. B **65**, 085110 (2002).

[249] T. Takahashi, K. Nogami and K. Yakushi, J. Phys. Soc. Jpn. **75**, 051008 (2006).

[250] Y. Nogami, J.-P. Pouget, M. Watanabe, K. Oshima, H. Mori, S. Tanaka and T. Mori, Synth. Met. **103**, 1911 (1999).

[251] R.-H. McKenzie, J. Merino, J. B. Marston and O.-P. Sushkoy, Phys. Rev. B **64**, 085109 (2001).

[252] R. Torsten Clay, S. Mazumbar and D. K. Campbell, J. Phys, Soc. Jpn. **71**, 1816 (2002).

[253] J. Merino, H. Seo and M. Ogata, Phys. Rev. B **71**, 125111 (2005).

[254] K. Kuroki, Sci. Tecnol. Adv. Mater. **101**, 024312 (2009).

[255] T. Mori, J. Phys. Soc. Jpn. **72**, 1469 (2003).

[256] A. Bondi , J. Phys. Chem. **68**, 441(1964).

[257] S. Alvarez, Dalton Trans. **42**, 8617 (2013).

[258] M. Watanabe, Y. Noda, Y. Nogami and H. Mori, J. Phys. Soc. Jpn., **74**, 2011(2005).

[259] H. Mori, S. Tanaka, T. Mori and Y. Maruyama, Bull. Chem. Soc. Jpn., **68**, 1136 (1995).

[260] http://www.webelements.com

[261] H. Kobayashi, R. Kato, A. Kobayashi, S. Moriyama, Y. Nishio, K. Kajita and W. Sasaki, Chem. Lett. , 2017 (1986).

[262] M. Watanabe, Y. Nogami, K. Oshima, H. Mori, S. Tanaka, J. Phys. Soc. Jpn. **68**, 2654 (1999)

[263] M. Watanabe, Y. Noda, Y. Nogami and H. Mori, Synth. Met. **135-136**, 665 (2003).

[264] The inverse of the half-width at half-maximum, Δq, of the X-ray diffuse scattering leads to a correlation length in the a - 2c and a + 2c directions of $\xi_{||} \approx 15$ Å and of $\xi_{||} \approx 35$ Å in the 3a - 4c and 3a + 4c directions, which respectively amount to about the $a \pm 2c$ and $3a \pm 4c$ periods. Below 120 K, when the q_1' and q_2' short range orders compete in the θ-(Cs, Zn or Co) salts, the transverse correlation $\xi_{\perp} \approx$ 15 Å is comparable to $\xi_{||}$. Note that the values of ξ used here are 3 times smaller than the values quoted in the literature which corresponds to domain lengths defined by $L \approx 3/\Delta q$.

[265] D. Guterding, R. Valentí and H. O. Jeschke, Phys. Rev. B **92**, 081109(R) (2015).

[266] P. Lunkenheimer and A. Loidl, J. Phys.: Condens. Matter **27**, 373001 (2015).

[267] S. Ishihara, J. Phys.: Condens. Matter **26**, 493201(2014).

[268] J. van den Brink and D. I. Khomskii, J. Phys.: Condens. Matter **20**, 434217 (2008).

[269] G. Giovannetti, S. Kumar, J.-P. Pouget, and M. Capone, Phys. Rev. B **85**, 205146 (2012).

[270] G. Giovannetti, R.Nourafkan, G. Kotliar and M. Capone, Phys. Rev. B **91**, 125130 (2015).

[271] W. A. Little, Phys. Rev. **134**, 1416 (1964).

[272] H. Guntfreund and W. A. Little, in: *Highly Conducting One Dimensional Solids*, edited by J. T. Devreese, R. P. Evrard, and V. E. van Doren (Plenum Press, New York, 1979), pp. 305–372.